AD-A193 794 METAL HALIDE OPTICAL GLASSES(U) RENSSELAER POLYTECHNIC 1/2
INST TROY NY C T MOYNIHAN ET AL. JAN 88 RADC-TR-87-279
F19628-83-C-0016

UNCLASSIFIED F/G 11/2 NL

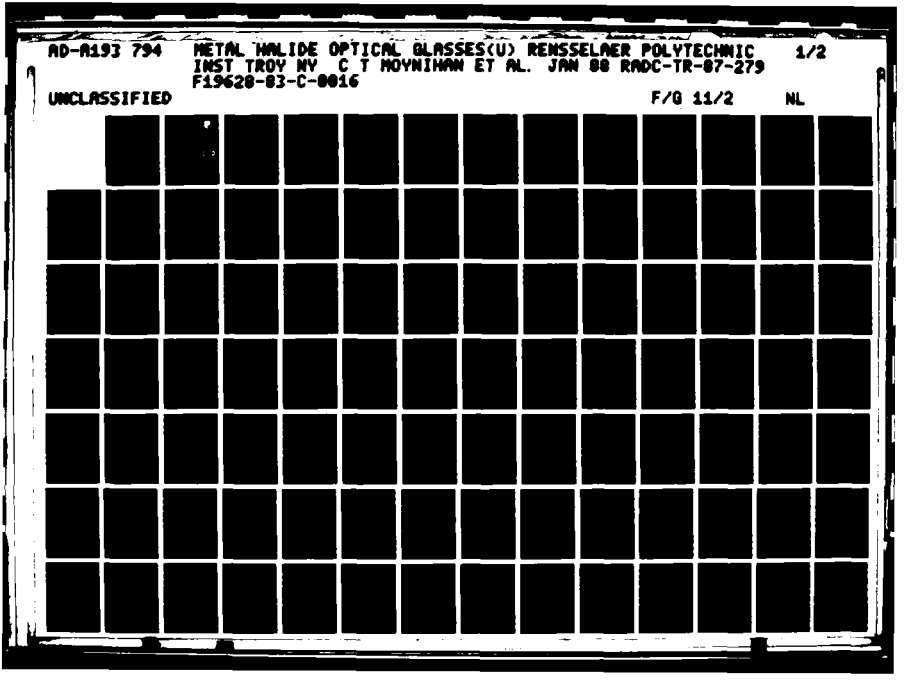

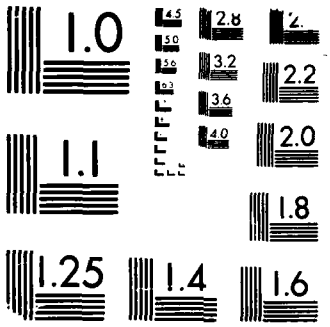

RADC-TR-87-279
Final Technical Report
January 1988

METAL HALIDE OPTICAL GLASSES

Rensselaer Polytechnic Institute

C. T. Moynihan and J. Schroeder

APPROVED FOR PUBLIC RELEASE; DISTRIBUTION UNLIMITED

ROME AIR DEVELOPMENT CENTER
Air Force Systems Command
Griffiss Air Force Base, NY 13441-5700

This report has been reviewed by the RADC Public Affairs Office (PA) and is releasable to the National Technical Information Service (NTIS). At NTIS it will be releasable to the general public, including foreign nations.

RADC-TR-87-279 has been reviewed and is approved for publication.

APPROVED: Alvin J Drehman

ALVIN J. DREHMAN
Project Engineer

APPROVED: Harold Roth

Harold Roth
Director of Solid State Sciences

FOR THE COMMANDER: John A. Ritz

JOHN A. RITZ
Directorate of Plans & Programs

If your address has changed or if you wish to be removed from the RADC mailing list, or if the addressee is no longer employed by your organization, please notify RADC (ESMO) Hanscom AFB MA 01731-5000. This will assist us in maintaining a current mailing list.

Do not return copies of this report unless contractual obligations or notice on a specific document requires that it be returned.

REPORT DOCUMENTATION PAGE

Form Approved
OMB No 0704-0188

1a REPORT SECURITY CLASSIFICATION UNCLASSIFIED	1b RESTRICTIVE MARKINGS N/A
2a. SECURITY CLASSIFICATION AUTHORITY N/A	3. DISTRIBUTION/AVAILABILITY OF REPORT Approved for public release; distribution unlimited.
2b. DECLASSIFICATION/DOWNGRADING SCHEDULE N/A	
4. PERFORMING ORGANIZATION REPORT NUMBER(S) N/A	5. MONITORING ORGANIZATION REPORT NUMBER(S) RADC-TR-87-279
6a. NAME OF PERFORMING ORGANIZATION Rensselaer Polytechnic Institute 6b. OFFICE SYMBOL (If applicable)	7a. NAME OF MONITORING ORGANIZATION Rome Air Development Center (ESMO)
6c. ADDRESS (City, State, and ZIP Code) Troy NY 12180-3590	7b ADDRESS (City, State, and ZIP Code) Hanscom AFB MA 01731-5000
8a. NAME OF FUNDING/SPONSORING ORGANIZATION Rome Air Development Center 8b OFFICE SYMBOL (If applicable) ESMO	9 PROCUREMENT INSTRUMENT IDENTIFICATION NUMBER F19628-83-C-0016
8c. ADDRESS (City, State, and ZIP Code) Hanscom AFB MA 01731-5000	10. SOURCE OF FUNDING NUMBERS PROGRAM ELEMENT NO: 61102F; PROJECT NO: 2306; TASK NO: J1; WORK UNIT ACCESSION NO: 44

11 TITLE (Include Security Classification)
METAL HALIDE OPTICAL GLASSES

12. PERSONAL AUTHOR(S)
C. T. Moynihan, J. Schroeder

13a. TYPE OF REPORT	13b. TIME COVERED	14. DATE OF REPORT (Year, Month, Day)	15. PAGE COUNT
Final	FROM Dec 82 TO Jun 85	January 1988	186

16. SUPPLEMENTARY NOTATION
N/A

17 COSATI CODES			18 SUBJECT TERMS (Continue on reverse if necessary and identify by block number)
FIELD	GROUP	SUB-GROUP	Brillouin Scattering, Dielectric Constant, Chemical Durability, Differential Thermal Analysis, Corrosion, Elastic Constant
11	02		

19 ABSTRACT (Continue on reverse if necessary and identify by block number)

In this report are presented the results of a number of investigations of ZrF_4-based and other heavy metal fluoride glasses. The purpose of these investigations has been primarily to explicate properties and behavior of these glasses relevant to their use as optical transmission media.

Viscosity data covering the range 10^{-1} to 10^{-13} P were collected and analyzed for a ZrF_4-BaF_2-LaF_3-BaF_2(ZBLA) melt. The temperature dependence of viscosity could be described via the four parameter Cohen-Grest equation, allowing estimation of viscosities in temperature ranges where measurement of viscosity was not possible due to rapid crystallization. Characterization of the temperature dependence of viscosity in the region of the glass transition temperature Tg was done for a large number of HMF glasses using a differential scanning calorimetry (DSC) technique. All these materials exhibited a rapid viscosity drop

20 DISTRIBUTION/AVAILABILITY OF ABSTRACT	21 ABSTRACT SECURITY CLASSIFICATION
☒ UNCLASSIFIED/UNLIMITED ☐ SAME AS RPT ☐ DTIC USERS	UNCLASSIFIED
22a NAME OF RESPONSIBLE INDIVIDUAL Alvin J. Drehman	22b TELEPHONE (Include Area Code) (617) 377-4823 22c OFFICE SYMBOL RADC (ESMO)

DD Form 1473, JUN 86 Previous editions are obsolete.

on heating above Tg and became very fluid well below their liquidus temperatures. This is the cause of the relative instability of these melts against devitrication liquidus temperatures T_L were determined for several of HMF glasses by DSC by observing their crystallization and subsequent remelting as they were rate heated above Tg. It was found that the T_l/Tg ratio was approximately constant and equal to about 1.5. DSC measurements of the rate of enthalpy loss due to structural relaxation on annealing at sub-Tg temperatures were carried on for a large number of zrF_4-based glasses. It appeared that drifts due to structural relaxation in properties such as refractive index would not be a problem at ambient temperature over time periods of tens of years.

Rayleigh and Brillouin scattering and index of refraction measurements have been carried out for many HMF glass compositions. These have yielded values of the optical attenuation coefficient, the elastic constants, the Pockel's elastooptic coefficients, the Verdet constant and the stimulated Brillouin scattering threshold. The Rayleigh scattering loss in some ZrF_4-based glasses was found to be as much as four times lower than the loss in high quality SiO_2 glass, while the energy threshold for stimulated Brillouin scattering was sizeably higher.

Corrosion of ZrF_4-based glasses in liquid water was monitored by IR spectroscopy and weight loss measurements. The corrosion mechanism appears to involve rapid formation of a hydrated layer, followed by dissolution of the glass in the liquid water. Addition of AlF_3 to a ZrF_4-BaF_2-LaF_3 glass improves its resistance to corrosion, while additions of alkali fluoride such as LiF and NaF lower the resistance.

Measurements of dielectric constant and of electrical conductivity as a function of temperature were done for a variety of ZrF_4- and HfF_4-based glass compositions. Addition of alkali fluorides lowers the electrical conductivity, and ZrF_4-based glasses containing NaF and/or LiF appear to exhibit a weak mixed alkali effect.

Item 18. SUBJECT TERMS (Continued).

Electrical Conductivity
Flouride Glass
Glass Transition Temperature
Liquidus Temperature
Melting
Pockels' Coefficient
Rayleigh Scattering
Refractive Index
Sound Velocity
Structural Relaxation
Viscosity
Crystallization

TABLE OF CONTENTS

SUMMARY

Heavy metal fluoride (HMF) glasses are a fairly new class of materials which have attracted considerable interest because of their extended range of transparency in the infrared compared to silicate and network oxide glasses. In particular, they show promise as materials for fiber optic waveguides which may exhibit attenuation coefficients in the mid-IR an order of magnitude lower than those of silicate glass fibers. There are, however, a number of problems associated with fabrication of HMF glasses. For example, they are not extremely good glassformers and may partially crystallize on cooling from the melt or on reheating above the glass transition temperature. The presence of crystallites can cause optical losses due to light scattering. In addition, HMF glasses have comparatively poor chemical durability, which can cause mechanical strength problems due to formation and growth of surface flaws.

In this report are presented the results of a number of investigations of ZrF_4-based and other heavy metal fluoride glasses. The purpose of these investigations has been primarily to explicate properties and behavior of these glasses relevant to their use as optical transmission media.

Viscosity data covering the range 10^{-1} to 10^{-13} P were collected and analyzed for a ZrF_4-BaF_2-LaF_3-BaF_2 (ZBLA) melt. The temperature dependence of viscosity could be described via the four parameter Cohen-Grest equation, allowing estimation of viscosities in temperature ranges where measurement of viscosity was not possible due to rapid crystallization. Characterization of the temperature dependence of viscosity in the region of the glass transition temperature Tg was done for a large number of HMF glasses using a differential scanning calorimetry (DSC) technique. All these materials exhibited a rapid viscosity drop on heating above Tg and became very fluid well below their liquidus temperatures. This is the

cause of the relative instability of these melts against devitrification. Liquidus temperatures T_L were determined for several of HMF glasses by DSC by observing their crystallization and subsequent remelting as they were rate heated above Tg. It was found that the T_L/Tg ratio was approximately constant and equal to about 1.5. DSC measurements of the rate of enthalpy loss due to structural relaxation on annealing at sub-Tg temperatures were carried out for a large number of ZrF_4-based glasses. It appeared that drifts due to structural relaxation in properties such as refractive index would not be a problem at ambient temperature over time periods of tens of years.

Raleigh and Brillouin scattering and index of refraction measurements have been carried out for many HMF glass compositions. These have yielded values of the optical attenuation coefficient, the elastic constants, the Pockels' elastooptic coefficients, the Verdet constant and the stimulated Brillouin scattering threshold. The Rayleigh scattering loss in some ZrF_4-based glasses was found to be as much as four times lower than the loss in high quality SiO_2 glass, while the energy threshold for stimulated Brillouin scattering was sizeably higher.

Corrosion of ZrF_4-based glasses in liquid water was monitored by IR spectroscopy and weight loss measurements. The corrosion mechanism appears to involve rapid formation of a hydrated layer, followed by dissolution of the glass in the liquid water. Addition of AlF_3 to a ZrF_4-BaF_2-LaF_3 glass improves its resistance to corrosion, while additions of alkali fluorides such as LiF and NaF lower the resistance.

Measurements of dielectric constant and of electrical conductivity as a function of temperature were done for a variety of ZrF_4- and HfF_4-based glass compositions. Addition of alkali fluorides lowers the electrical conductivity, and ZrF_4-based glasses containing NaF and/or LiF appear to exhibit a weak mixed alkali effect.

CRYSTALLIZATION AND VISCOSITY OF HEAVY METAL FLUORIDE GLASSES

C. T. Moynihan, R. Mossadegh and S. N. Crichton

Materials Engineering Department, Rensselaer Polytechnic Institute
Troy, New York 12180-3590

P. K. Gupta
Owens/Corning Fiberglas
Granville, Ohio 43023

M. G. Drexhage
Rome Air Development Center
Hanscom AFB, Massachusetts 01731

Abstract

Shear viscosity data for a glassforming ZrF_4-BaF_2-LaF_3-AlF_3 composition covering the range from the highly fluid melt down to the glass transition (10^{-1} to 10^{13} P) have been collected from five sources. The viscosity temperature dependence is highly non-Arrhenius and cannot be described by three parameter expressions such as the Fulcher equation. The four parameter Cohen-Grest equation, however, does give a good fit to the data, possibly allowing interpolation in the range of intermediate viscosity important for fiber drawing where data is currently lacking. The viscosity data are compared with crystallization temperatures obtained by DSC during heating and cooling at 10K/min.

Introduction

One of the most serious problems with heavy metal fluoride (HMF) glass-forming melts is their tendency to crystallize, either on initial cooling from the melt, as in casting bulk glass or drawing fibers from a crucible, or on reheating above the glass transition temperature T_g, as in drawing a fiber from a preform.[1-3] The source of this problem lies in their viscosity temperature dependence, as was first pointed out by both Mackenzie and Moynihan at the 1st International Symposium on Halide and Other Non-Oxide Glasses in March, 1982 and subsequently underscored in the published literature.[4-6] The rates of

nucleation and crystallization of a melt are inversely proportional to its shear viscosity. Silicate melts which are good glass formers have high shear viscosities η at their liquidus temperature T_m, and the viscosity increases rapidly with falling temperature. HMF melts, on the other hand, have low viscosities at T_m and remain quite fluid until they are fairly close to T_g, at which point η rises very quickly to values in the vicinity of 10^{13} P. Looking at it from another perspective, on heating above T_g the viscosities of silicate melts remain quite high over a sizeable temperature range, while those of HMF melts fall abruptly, so that well below T_m the melt is sufficiently fluid to crystallize rapidly.

Reliable viscosity data covering the whole temperature range from above T_m down to T_g presently do not exist for any single HMF melt composition. In an earlier paper[7], however, we gleaned from five sources data for a number of ZrF_4-based melts which were close enough in composition that to a first approximation we could ignore small viscosity differences among them. Taken together, these data did span the T_m to T_g range. In that paper we compared the viscosity temperature dependence of the collection of melts with that predicted from two theoretically based models and with the crystallization behavior measured by differential scanning calorimetry (DSC). The present paper is an update of the earlier study[7] in which we replace viscosity data estimated from DSC relaxational measurements with actual beam bending viscosity results obtained in one of our laboratories and compare the viscosity temperature dependence with that predicted from four theoretically based models. As will be noted below, some of the conclusions of the earlier study[7] are modified in the present paper.

Viscosity temperature dependence

The melts whose viscosities are considered here all contain 56-60 mol% ZrF_4, 30-36 mol% BaF_2 and 7-10 mol% MF_3 (M = La and/or Al). They will be referred to collectively as a "ZBLA melt". Their exact batch compositions are given in

Table 1, along with the sources of the data, the temperature and viscosity range covered by each study, and the viscosity measurement technique. The last data set (Ref. 11) contains viscosity vs. temperature curves measured for three different specimens, one of which was from a different batch from the other two.

Table 1. Compositions, experimental ranges, measurement techniques and data sources for ZBLA melt viscosities

Composition (mol%)	Range T(K)	Range log η (P)	Method	Ref.
$60ZrF_4$-$30BaF_2$-$10LaF_3$	783-1116	-0.7 to 0.6	rotational	4
$60ZrF_4$-$30BaF_2$-$10AlF_3$	994-1160	-0.8 to -0.5	rotational	4
$57ZrF_4$-$36BaF_2$-$3LaF_3$-$4AlF_3$	760-976	-0.5 to 0.6	rotational	8
$60ZrF_4$-$33BaF_2$-$4LaF_3$-$3AlF_3$	583-609	7.9 to 11.4	penetrometer	9
$56ZrF_4$-$34BaF_2$-$6LaF_3$-$4AlF_3$	576-613	8.3 to 12.4	beam bending	10
$58ZrF_4$-$33BaF_2$-$5LaF_3$-$4AlF_3$	578-598	9.7 to 13.3	beam bending	11

All of the viscosity data from the sources in Table 1 are shown in Figure 1 as a plot of log η (P) vs. T(K) and in Figures 2 and 3 in the form of Arrhenius plots of log η (P) vs. 1/T(K). The first three sets of data in Table 1 are for the high temperature, low viscosity range and are in gratifyingly good agreement with one another. The last three sets of data in Table 1, for the low temperature, high viscosity range in Figures 1 to 3, show more scatter, but are still confined to a fairly narrow band. Note that there is a large range of viscosity, roughly 10^1-10^8 P, where there are no data, in part because the melts tend to crystallize readily in this region.

As is usual for glassforming melts, the plots of Figures 2 and 3 are curved, and the viscosity temperature dependence is highly non-Arrhenius in character. The most commonly used expression which allows for behavior of this sort is the well known Fulcher equation:

$$\log \eta = A + B/(T-T_0) \qquad (1)$$

where A, B and T_0 are constants. One theoretical justification[12] of Eq. (1) assumes that the viscosity depends exponentially on the inverse of the free volume V_f and that this in turn is a linear function of $(T-T_0)$. T_0 is thus interpreted as the temperature at which free volume would vanish at equilibrium. A non-linear least squares fit of the ZBLA melt data to the Fulcher equation was carried out by us. The fit parameters are given in Table 2, along with the standard deviation of log η from the best fit curve, and the solid line in Figure 2 was calculated from these. The Fulcher equation fit is not within experimental error; the experimental viscosity data appear to exhibit a much sharper "bend" between the high and low temperature regions than can be accommodated by Eq. (1). This is not surprising. It has been found previously[13-15] for a large number of liquids (organics, network oxides, fused salts) that the simple Fulcher equation cannot give a good fit to viscosity data which extend over 13-15 orders of magnitude. Fulcher equation fits over this range[13,14] had the appearance of Figure 2. What is inevitably found in these other systems[13-16] is that the curvature of the Arrhenius plot (in terms of Eq. (1)) is larger at high temperature than at low temperatures, so that a Fulcher fit to the high temperature data grossly overestimates the low temperature viscosity. Hu and Mackenzie[4] observed this for HMF melts; Fulcher fits to their high temperature viscosities did not accurately predict T_g.

Table 2. Parameters from least squares fits of viscosity (P) vs. temperature (K) data for ZBLA melt to Eqs. (1) to (4)

Expression	A	B	C	T_o	Std. Dev. log η
Fulcher, Eq. (1)	-3.11	1148	-	507.8	0.37
Adam-Gibbs, Eq. (2)	-2.58	1240	-	504.7	0.36
Sturm, Eq. (3)	-5.46	5.549	-	558.5	0.52
Cohen-Grest, Eq. (4)	-1.27	269.5	2.50	635.2	0.24

Two other three parameter viscosity equations were tested against the data of Figure 1-the Adam-Gibbs equation[17] and the Sturm equation.[18] The Adam-Gibbs equation, in its simplest form, is:

$$\log \eta = A + B/T \ln(T/T_o) \qquad (2)$$

while the Sturm equation is:

$$\log \eta = A - B \ln[1 - (T_o/T)] \qquad (3)$$

A, B and T_o are constants in each expression. T_o is interpreted as the temperature at which in Eq. (2) the configurational entropy and in Eq. (3) the free volume would vanish at equilibrium. The parameters obtained from a non-linear least squares fit of the ZBLA melt data to Eqs. (2) and (3) are given in Table 2, and the corresponding viscosity curves are shown in Figure 2. The fit obtained from the Adam-Gibbs equation is indistinguishable from that obtained with the Fulcher equation, but the fit obtained from the Sturm equation is markedly worse. It appears that none of the simple three parameter viscosity vs. temperature equations can give a good fit to HMF melt data.

Cohen and Grest[15,16,19] have developed a "new" free volume model for molecular transport, which leads to the expression:

$$\log \eta = A + 2B/\{T-T_0 + [(T-T_0)^2 + 4CT]^{1/2} \qquad (4)$$

where A, B, C and T_0 are constants. Unlike the corresponding parameters in Eqs. (1)-(3), T_0 in Eq. (4) no longer has a simple, conceptual interpretation. The fundamental thrust of Cohen and Grest's expression is that at high temperature the free volume is linear in $(T-T_0)$, as implied by the Fulcher equation, but at low temperatures it changes more slowly (as $T^{1/2}$ near T_0). This makes Arrhenius plots less curved at low temperature than they are at high temperature, which replicates experimentally observed behavior. Cohen and Grest[15,16] found that their Eq. (2) could fit within experimental error viscosity data extending over 13-15 orders of magnitude for six different systems.

We have fit the ZBLA melt data to Eq. (4); the least squares fit parameters are given in Table 2 and the corresponding viscosity plots are shown as solid lines both in Figures 1 and 3. It appears that the Cohen-Grest equation can fit the data within experimental error. This is contrary to the conclusion of our previous study[7], where a good fit with the Cohen-Grest equation was not obtained. Unfortunately, in that study a constraint in the non-linear least squares procedure had been placed on the T_0 parameter to prevent it from becoming larger than Tg (=587K). When that constraint was removed, Eq. (4) was found to give an excellent fit to the data set of our previous study. Our best fit T_0 value (Table 2) for Eq. (4) for the ZBLA melt lies somewhat above Tg, as was found by Cohen and Grest[16] for six other glassforming melts.

One of our initial hopes in this study was to be able to splice together smoothly the high temperature and low temperature viscosity data of Figures 1 to 3 using expressions such as Eqs. (1) to (4), which have some sort of theo-

retical basis and are well established empirically. This would provide a valuable analytical tool for interpolating viscosity/temperature values in ranges where data are missing and are likely to be hard to obtain for HMF melts, e.g., the 10^3-10^5 P range of importance for fiber drawing from preforms or from the melt.[2,3] It would appear that we may tentatively accept the fits obtained with the Cohen-Grest equation for this purpose, but with sizeable reservations, since the region (10^1-10^8 P) of missing data in Figures 1 and 3 in which interpolation must be performed is very large.

As shown in Figure 3, the ZBLA melt exhibits approximately an Arrhenius viscosity temperature dependence (log η is roughly linear in 1/T) in the high viscosity region. Judging from results available so far[1,9-11], this sort of behavior is likely to be typical of other ZrF_4-based compositions as well. Departure from Arrhenius behavior (curvature in the log η vs. 1/T plot) appears to set in around 10^8 P in Figure 4. This suggests that one should view with caution estimates of temperature for viscosities in the 10^3-10^5 P fiber drawing range which have been obtained via extrapolation of log η vs. 1/T data in the viscosity range above 10^7 P, as was done by Tokiwa and coworkers.[1-3] What is needed as a guide is a set of more complete viscosity/temperature curves for typical HMF melts. Prospects of obtaining this in the face of the ease with which these systems devitrify are discussed in the next section.

Crystallization and viscosity measurements

Shown in Figure 4 are DSC scans done on a Perkin-Elmer Model DSC-4 of a ZBLA glass encapsulated in a gold pan during heating at 10 K/min from 450 to 950 K and during subsequent cooling at the same rate. The specimen was from the same piece of glass (ZBLA 7/31/84) described by Drexhage[20], i.e., a crystal-free specimen with low light scattering, prepared from high purity chemicals batched in a dry box and melted under reactive atmosphere in a modified crystal

growth furnace. On heating the sample first passes through the glass transition at Tg (587 K). It then begins to crystallize roughly at a temperature T_{XH} (663 K). Crystallization is essentially complete by about 700 K; the main phases formed on crystallization are β - $BaZrF_6$ and β - $BaZr_2F_{10}$.[21] On further heating the sample undergoes a metastable-stable β - $BaZrF_6 \rightarrow$ α - $BaZrF_6$ solid-solid transition at about 750 K[21] and then begins to remelt. The melting endotherm is complex, since the crystallized glass contains a number of phases, and melting is not complete until T_M (873 K). On subsequent cooling at 10 K/min the melt supercools to nearly 150°C below T_M before crystallization (into so far unidentified phases) commences at T_{XC} (726 K). [Note from the results of Ref. 20 that on cooling on the DSC at a somewhat higher rate, 100 K/min, this specimen does not crystallize and reforms a glass.]

Crystallization of a melt requires a nucleation step, followed by growth of the nuclei into macroscopic crystals. Since nucleation rates and crystal growth velocities generally have different temperature dependences and reach their maximum values at different degrees of supercooling, the net rate of crystallization of a melt at a given temperature depends on its thermal history below T_M. Nonetheless, in a rough, empirical fashion we can take the interval (T_{XC}-T_{XH}) measured for moderate (several K/min) heating and cooling rates as an indicator of the temperature range in which processing steps or physical property measurements on an HMF melt, unless they are carried out very rapidly, will be difficult or impossible due to devitrification.

The characteristic temperatures Tg, T_{XH}, T_{XC}, and T_M from the DSC scans have been indicated on the ZBLA melt viscosity plot in Figure 1. The temperature region (T_{XC}-T_{XH}) where viscosity measurements should be impossible for this melt seems very roughly to correspond to the range $10^{1.5}$-$10^{3.5}$ P, only about two orders of magnitude. The rotational viscosity measurements of Ref. 8 did in fact extend

well into the supercooled region, to within about 35 K of T_{XC}, and to a viscosity of $10^{0.6}$ P, within an order of magnitude of the estimated viscosity at T_{XC}. It should be possible to extend this high temperature branch of the viscosity curve to somewhat lower temperatures and higher viscosities, perhaps to 10^{1} P, without crystallizing the melt by taking rotational viscometer readings continually while slowly cooling the melt. The above estimate of $10^{3.5}$ P for the viscosity at the low temperature end of the "inaccessible" region is probably overoptimistic. Both Tokiwa et al.[1] and Wilson and Poole[22] have noted that small amounts of crystallization, when measured by very sensitive techniques such as light scattering or high sensitivity DSC, occur on reheating a HMF glass at temperatures somewhat lower than the onset of the large crystallization endotherm in Figure 4. Using a parallel plate viscometer and carrying out measurements while heating 10 K/min, however, Wilson and Poole were able to measure viscosities down to about $10^{5.5}$ P before crystallization set in a LiF-containing ZrF_4-based melt. In Figures 1 to 3 the low temperature data extend to only 10^{8} P on the low viscosity end. It should be possible to extend measurements down to at least 10^{6} P without crystallizing the melt if one starts the measurements at the lower temperature end with a quenched melt. Viscosity measurement techniques appropriate for the 10^{6}-10^{8} P range are parallel plate viscometry[6,22,23] and rotational viscometry in the decay mode using a very small spindle.[24,25]

The HMF composition, ZBLA, considered here as an example is only a moderately good glass-former as these systems go. We have suggested here that the viscosity data gap for ZBLA should be able to be narrowed to about 10^{1}-10^{6} P. Other HMF melts, particularly those containing alkali fluorides[1-3,9], are much less susceptible to devitrification, and somewhat narrower viscosity data gaps should be realizable with these. Hopefully attention will be given in the near future to this important experimental undertaking of generating com-

plete viscosity/temperature curves for HMF melts.

References

1. Tokiwa, H., Mimura, Y., Shinbori, O., and Nakai, T., IEEE J. Lightwave Technol, LT-3, p. 569 (1985).

2. Tokiwa, H., Mimura, Y., Shinbori, O., and Nakai, T., IEEE J. Lightwave Tech., LT-3, p. 574 (1985).

3. Tokiwa, H., Mimura, Y., Nakai, T., and Shinbori, O., Electron. Lett., 21, p. 1131 (1985).

4. Hu, H. and Mackenzie, J. D., J. Non-Cryst. Solids, 54, p. 241 (1983).

5. Moynihan, C. T., Gavin, D. L., Chung, K.-H., Bruce, A. J., Drexhage, M. G., and El Bayoumi, O. H., Glastechn. Ber., 56K, p. 862 (1983).

6. Tran, D. C., Ginther, R. J., and Sigel, G. H., Jr., Mat. Res. Bull. 17, p. 1177 (1982).

7. Moynihan, C. T., Mossadegh, R., Gupta, P. K., and Drexhage, M. G., Materials Science Forum, 6, p. 655 (1985).

8. Loretz, T. J., Annual Tech. Rept., AFSC/USAF Contract No. F19628-81-C-0073, Galileo Electro-Optics Corp., Sturbridge, MA, 16 Dec. 1982.

9. Mimura, Y., Tokiwa, H., and Shinbori, O., Electron Lett., 20, p. 100 (1984).

10. Shelby, J. E., Pantano, C. G., and Tesar, A. A., J. Am. Ceram. Soc., 67, p. C-164 (1984).

11. Crichton, S. N., Mossadegh, R., Schroeder, J., and Moynihan, C. T., unpublished data.

12. Cohen, M. H. and Turnbull, D., J. Chem. Phys., 31, p. 1164 (1959).

13. Macedo, P. B. and Napolitano, A., J. Chem. Phys., 49, p. 1887 (1968).

14. Tweer, H., Laberge, N., and Macedo, P. B., J. Am. Ceram. Soc., 54, p. 121 (1971).

15. Grest, G. S. and Cohen, M. H., in Advances in Chemical Physics, Vol. 48, I. Prigogine and S. A. Rice, Eds., Wiley, New York, 1981, p. 455.

16. Cohen, M. H. and Grest, G. S., Phys. Rev. B, 20, p. 1077 (1979).

17. Adam, G. and Gibbs, J. H., J. Chem. Phys., 43, p. 139 (1965).

18. Sturm, K. G., Glastechn. Ber., 53, p. 63 (1980).

19. Cohen, M. H. and Grest, G. S., J. Non-Cryst. Solids, 61&62, p. 749 (1984).

20. Drexhage, M. G., Materials Science Forum, 5, p. 1 (1985).

21. Bansal, N. P., Doremus, R. H., Bruce, A. J., and Moynihan, C. T., Mat. Res. Bull. 19, p. 577 (1984).

22. Wilson, S. J. and Poole, D., Materials Science Forum, 6, p. 665 (1985).

23. Fontana, E. H., Bull. Am. Ceram. Soc., 49, p. 594 (1970).

24. Weiler, R., Blaser, S. and Macedo, P. B., J. Phys. Chem., 73, p. 4147 (1969).

25. Ambrus, J. H., Moynihan, C. T., and Macedo, P. B., J. Electrochem. Soc., 119, p. 192 (1972).

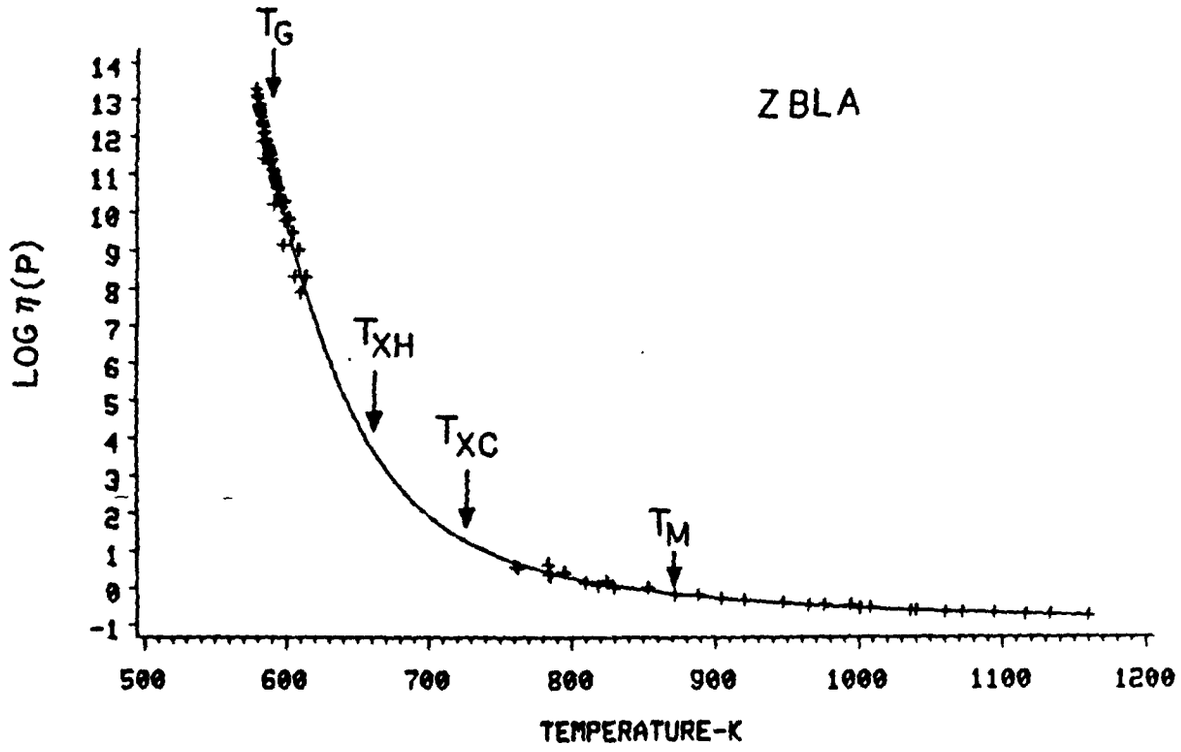

Figure 1. Logarithm of viscosity versus temperature for ZBLA melt. Solid line is best fit to Cohen-Grest equation.

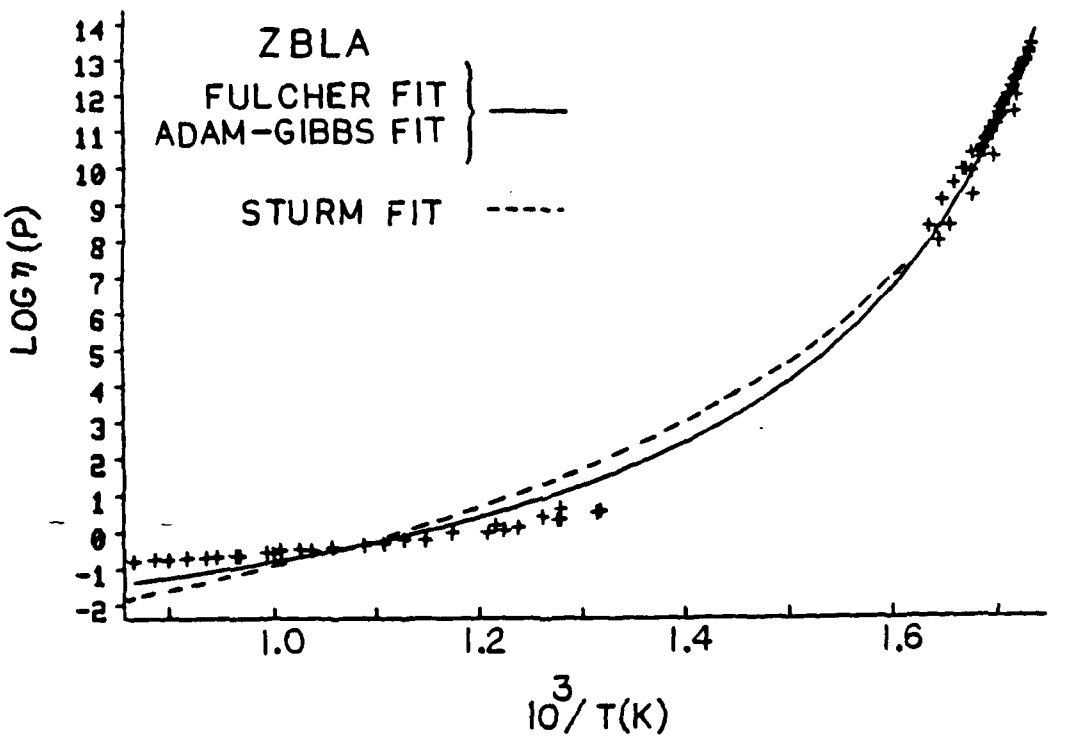

Figure 2. Arrhenius plot and best fits to Fulcher, Adam-Gibbs and Sturm equations for ZBLA melt.

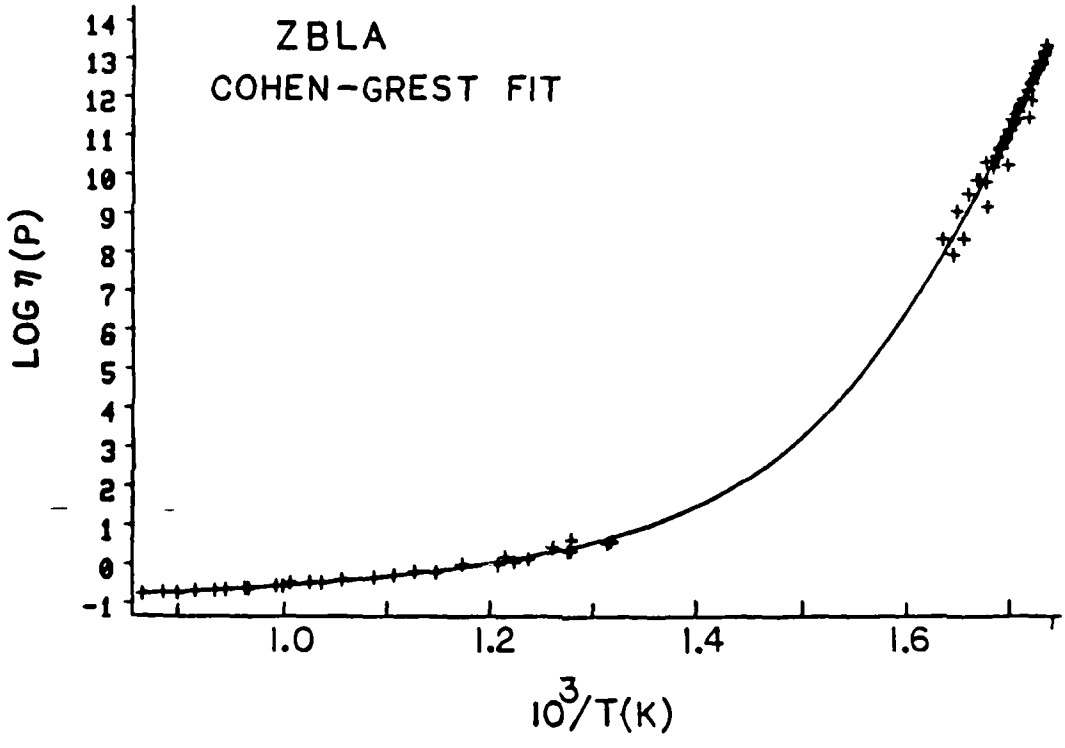

Figure 3. Arrhenius plot and best fit to Cohen-Grest equation for ZBLA melt.

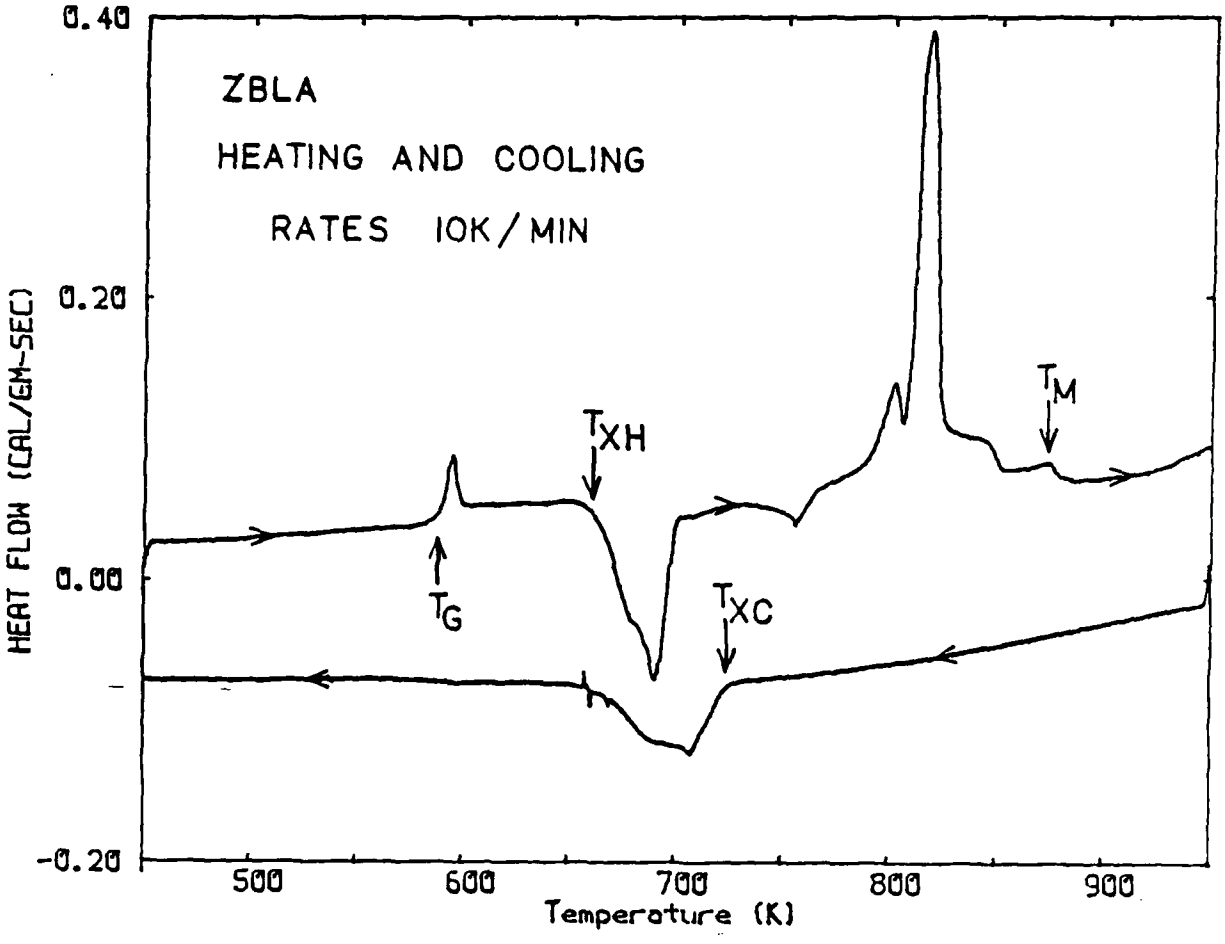

Figure 4. DSC scans during heating at 10 K/min (upper curve) and subsequent cooling at 10 K/min (lower curve) of 57 ZrF_4-36 BaF_2-3 LaF_3-4 AlF_3 glass encapsulated in gold sample pan.

ACTIVATION ENERGY FOR VISCOUS FLOW IN THE GLASS TRANSITION REGION OF ZrF_4- AND HfF_4-BASED HEAVY METAL FLUORIDE GLASSES

A. J. Bruce, D. L. Gavin and C. T. Moynihan
Materials Engineering Department
Rensselaer Polytechnic Institute
Troy, NY 12180-3590

and

M. G. Drexhage
Solid State Sciences Division
Rome Air Development Center
Hanscom AFB, MA 01731

Introduction

Heavy metal fluoride glasses (HMFG) have transmission windows which can be extended from the near UV to the mid IR range.[1] Particularly because of their transparency in IR, they are potentially useful materials for a wide range of optical devices including IR lenses, windows, laser hosts and optical wave guides.[2] However, a severe restriction to their utilization has been imposed by their strong tendency to crystallize both on quenching and on subsequent reheating above the glass transition temperature T_g.[3] This instability is due to the viscosity-temperature curves of the HMFG above T_g. Data from several sources[4,5] indicate that the viscosity-temperature curves for HMFG are highly

non-Arrhenian, the Arrhenius plots being relatively flat near the liquidus temperature T_ℓ and with low viscosities persisting close to T_g. These factors indicate that there must be a region immediately above T_g where the viscosity decreases very rapidly with increasing temperature. In this region viscosity dependent phenomena, such as the rate of diffusion controlled crystallization, will exhibit the same marked temperature dependence as the viscosity. In such a system glass formation from the melt can often be achieved only by rapid cooling, and the working viscosity range ($\sim 10^{11}$-10^4 Pa·s) is confined to a narrow temperature regime.

To improve on the glass forming ability of these systems and at the same time extend their working temperature ranges it is necessary to reduce the temperature dependence (i.e., the activation energy) of the viscosity above the glass transition region, so that the melt remains highly viscous over a larger temperature range. Such improvements have been made on a phenomenological basis by adding various components to the parent HMFG compositions.[3,5,6] However, to assess these improvements more fully, and also to obtain a basis for a structural interpretation of the phenomenon, a more rigorous investigation is required.

Moynihan et al.[7-9] have previously reported a differential scanning calorimetric (DSC) technique for measuring the activation energy ΔH^* for enthalpy relaxation

in the glass transition range. This activation energy is virtually the same as that for viscous flow[7-10] and can therefore be used to obtain viscosity-temperature data in the same range. When considering glass forming ability and resistance to crystallization, viscosity-temperature data should strictly be obtained over the complete range between T_g and T_ℓ. However, because HMFG crystallize readily at temperatures relatively close to T_g, it seems reasonable that the compositional trends observed in the ΔH^* values near T_g will also apply in somewhat higher temperature regimes and that they can be used as a basis for assessing relative glass forming ability in a series of compositionally similar glasses. The lower the ΔH^* values the greater the glass forming ability. It will be noted later that this assumption is supported by the good correlation observed between the ΔH^* values near T_g and activation energies E_c obtained at higher temperatures from crystal growth studies for several ZrF_4-based glasses.[11-13]

In a previous publication[14] we reported some of our early data on the ΔH^* values for HMFG and showed that a good correlation existed between better glass forming ability and smaller ΔH^*. In this paper a more comprehensive set of ΔH^* values will be presented for ZrF_4- and HfF_4-based glasses, which systems seem likely to provide the first generation of HMFG optical components.

Experimental

The HMFG's were synthesized using procedures described previously.[6,15] Qualitative scans on a DSC* at 10 K/min heating rate were used to determine the glass transition temperature and the temperature of extrapolated onset of crystallization T_x. Heat capacities C_p were measured using DSC's† equipped with computer data acquisition systems.≠ The samples used for DSC measurements were in bulk form and typically between 40-50 mg in mass. These were enclosed in non-hermetically sealed aluminum DSC pans, and a constant flow of dry nitrogen (25 cm^3/min) was maintained in the DSC cavity during the measurements. Single crystal Al_2O_3 and high purity indium were used as heat flow and temperature calibration standards respectively.

Following the procedure outlined in Ref. 7, a glass sample was heated in the DSC to a maximum temperature far enough above T_g to exhibit the equilibrium liquid C_p (but not high enough for significant crystallization to take place) and then cooled at rates between 0.31 and 80 K/min to 140 K below the maximum temperature (far enough below T_g that the glass transition did not contribute significantly to C_p). Following each cool C_p of the sample was measured while reheating at 10 K/min over the same temperature range. To maximize precision the sample was not removed from the

---

* Model DSC-4, Perkin-Elmer Corp., Norwalk, CT or Model 990, DuPont Co., Wilmington, DE.
† Models DSC-2 or DSC-4, Perkin-Elmer Corp., Norwalk, CT.
≠ Laboratory Microsystems, Troy, NY.

DSC cavity between the heating and cooling cycles. C_p values were calculated at 0.2 K intervals using the computer software.[≠]

An equation for the temperature dependent glass heat capacity C_{pg} was obtained by a linear least squares fit of the C_p values over a temperature range well below T_g [$\sim(T_g-100)$ to (T_g-50)K]. The equilibrium liquid heat capacity C_{pe} was taken as the average C_p value in a temperature region just above the hysteresis peak [$\sim(T_g+25)$ to (T_g+30)K].

The limiting fictive temperature T_f[7,9,10] attained on cooling was calculated from each reheating scan from the expression

$$T_f = T^* + \int_{T^*}^{T<<T_g} [(C_p-C_{pg})/(C_{pe}-C_{pg})]\, dT \qquad (1)$$

where T^*, C_{pg} and C_{pe} are defined schematically in Fig. 2.

Results and Discussion

1. Phenomenological Glass Forming Ability

The batch compositions of the HMFG studied are listed in Table I. Roman numerals (I, II and III) distinguish different melts containing the same components and sometimes with the same batch composition. The "base" glasses (ZB and HB) were very difficult to fabricate into crystal-free pieces more than 1 mm in thickness, while some of the multi-component "modified" glasses (e.g., ZBLAN) could easily be cast into pieces several mm thick.

The difference between the crystallization and glass transition temperatures (T_x-T_g), as defined in Fig. 1, or better, this quantity normalized by dividing by T_g (in Kelvin), is considered to be a measure of glass forming ability.[13,16] However, it should be emphasized that the T_x values can be considerably depressed if the glasses contain nucleating heterogeneities.[17] Therefore it should not automatically be assumed that glasses exhibiting low values of the stability parameters $(T_x-T_g)/T_g$ have the most temperature dependent viscosities. Values of T_g and of $(T_x-T_g)/T_g$ are listed in Table II for all the glasses investigated.

2. Activation Energy and Width of the Glass Transition Region

Heat capacities measured for a ZBL glass after cooling at three different rates are shown in Fig. 2. The increase in the heat capacity hysteresis peak with decreasing cooling rate is a manifestation of a corresponding reduction in limiting fictive temperature T_f.

The dependence of the limiting fictive temperature on cooling rate q is given by

$$d\ln|q|/d\,(1/T_f) = -\Delta H^*/R \qquad (2)$$

where ΔH^* is the activation energy for the structural enthalpy relaxation which is again generally found to be the same as the shear viscosity activation energy.[7-10] Typical plots

of log |q| versus $1/T_f$ for ZB-II, ZBL, ZBLA, ZBLAN and ZBLALi glasses are presented in Fig. 3. These plots are linear within experimental error, indicating that ΔH^* is roughly temperature independent over the limited temperature range investigated. This was found to be the case for all the glasses studied. The ΔH^* values obtained via Eq. (2) are presented in Table II. Some of the ΔH^* determinations were carried out in duplicate on specimens from the same melt and/or on specimens of the same batch composition from different melts; agreement between duplicate measurements is generally within ±5%.

It should be noted that the ΔH^* values for the HMFG are extremely large in comparison to other inorganic glass forming systems (cf. Table III). Indeed, the values for ZB-III are, to our knowledge, the highest ever reported.

The large ΔH^* values for the HMFG are also reflected in the sharpness of their glass transitions, as measured, for example, by the difference (T_2-T_1) shown in Fig. 2 for the C_p curve measured during heating at a rate equal to the prior cooling rate. For instance, for the ZBL glass of Fig. 2 (T_2-T_1) is 14 K, compared to a (T_2-T_1) value of 35 K for the network oxide glass B_2O_3, which has a much lower ΔH^* than, but has T_g in the same range as, the ZBL glass.[19] For glasses with a given ratio of prior cooling rate to heating rate, the <u>shape</u> of the C_p heating curve in the transition region is controlled by three parameters:[9,19]

the activation energy ΔH^*, a non-linearity parameter (denoted as $\underline{x}$ in Refs. 9 and 19) and a parameter characterizing the width of the distribution of structural relaxation times (denoted as $\underline{\beta}$ in Refs. 9 and 19). For such C_p curves of glasses with the same β and x parameters it then follows from the analysis of Refs. 9 and 19 that the quantity $(\Delta H^*/R)\cdot\Delta(1/T)$ should be constant, where $\Delta(1/T) = 1/T_1 - 1/T_2$.

Values of $(\Delta H^*/R)\cdot\Delta(1/T)$ are listed in Table II for the ZrF_4- and HfF_4-based glasses. Almost all of these values fall in the range 6 to 8, the mean is 7.3±0.8, and there are no trends in $(\Delta H^*/R)\cdot\Delta(1/T)$ with changing ΔH^*. Hence this parameter is nearly constant within experimental error for this family of similar glasses. Values of $(\Delta \bar{H}^*/R)\cdot\bar{\Delta}(1/T)$ given in Table III for the network oxide glasses and for As_2Se_3 (also a covalent network glass) are also nearly all the same and lie in the range roughly 4 to 5 with a mean of 4.8±0.5. $(\Delta H^*/R)\cdot\Delta(1/T)$ for the ionic glass $40Ca(NO_3)_2$-$60KNO_3$ is quite large compared to the other entries in Tables II and III; this is no doubt a reflection of the fact that the β and x parameters for $40Ca(NO_3)_2$-$60KNO_3$ are rather low compared to other inorganic glasses[21], both of which factors tend to stretch out the transition region. If we use a global value of about 6 for $(\Delta H^*/R)\cdot\Delta(1/T)$ for the HMFG and inorganic network glasses, it appears that one can make a rough estimate of

ΔH^* for these materials simply from a qualitative DSC or DTA scan through the transition region and (see below) determine very quickly whether the viscosity-temperature curve of the glass is such as to cause problems with devitrification and narrowness of working range and whether or not a change in composition (with concommitant change in ΔH^*) has alleviated any such problems.

3. Viscosity-Temperature Dependence

The high ΔH^* values for the HMFG indicate that their viscosities decrease rapidly with increasing temperature at and just above T_g. This is illustrated in Fig. 4, where the logarithm of viscosity (η) has been plotted in the manner of Uhlmann[22] and Angell[23] against a reduced temperature T_g/T for a number of glasses including ZB-I and ZBLA-I. The high temperature data for the HMFG were obtained by rotational viscometry[4,24], while the low temperature data were obtained from Eq. (2) by setting T_g equal to T_f for 2.5 K/min rate cooled samples and defining T_g as an isoviscous point ($\eta = 10^{12}$ Pa·s).

Hu and Mackenzie[4] were able to fit their high temperature data for molten ZB I, II ($BaZr_2F_{10}$) to a Fulcher equation of the form

$$\ell n\eta = A + B/(T-T_o) \qquad (3)$$

However, the Fulcher equation cannot fit the HMFG viscosity over the whole temperature range from high temperatures down to T_g[4], as has also been found for the $Ca(NO_3)_2$-KNO_3 melt[30]

and for o-terphenyl[22], whose curves in Fig. 4 parallel those for the HMFG. The HMFG data in Fig. 4 were therefore connected by visually drawn lines rather than by calculated ones. Since the viscosity curves for HMFG are more akin to those for molten salt, metallic and organic glass forming systems than to those for network oxide glasses, they fall into Angell's category[31] of "fragile" liquids, which exhibit highly non-Arrhenian viscosity-temperature behavior, as opposed to "strong" liquids such as SiO_2, whose viscosity-temperature behavior is Arrhenian over a wide viscosity range.

4. Compositional Trends in ΔH^* and Melt Covalency

The decreases in ΔH^* in Table II with changing composition correlate well with the resistance of the melts to devitrification. In particular, HMFG glasses with low ΔH^* are those with the highest values of $(T_x-T_g)/T_x$ and which can most readily be cast into thick pieces without devitrification. For example, for the ZrF_4-based glasses, changing the composition from 50 ZrF_4-50 BaF_2 (ZB III), which lies at the edge of the glass forming region of the binary glasses, to 65 ZrF_4-35 BaF_2 (ZB I, II), which lies near the center of that region, reduces ΔH^* by about 20%. Adding a few mol % of LaF_3 alone or in combination with AlF_3 or PbF_2 to the ZB I, II composition gives glasses whose ΔH^* is even further reduced (by roughly 30-40% relative to ZB III). The largest reductions in ΔH^* (roughly 50% relative to ZB III) are achieved by additions of considerable amounts ($\sim$20 mol %) of alkali fluoride to the

ZBL or ZBLA compositions. Experimentally the ZBLALi or ZBLAN glasses are more resistant to devitrification than the corresponding ZBLLi or ZBLN glasses, although this does not appear to be manifested in corresponding differences in ΔH^*.

In the HfF_4-based glasses a much narrower composition range has been explored than with the ZrF_4-based glasses, but, within experimental error, the trends in ΔH^* appear to be consistent with those of the ZrF_4-based systems. In particular, the multicomponent HBLAPbCs composition, which is the best glass-former in the HfF_4-based group, has a sizably lower ΔH^* than the other HfF_4-based compositions.

Because of the non-Arrhenian viscosity-temperature dependence of the HMFG melts, viscous flow activation energies and related quantities measured in temperature ranges of lower viscosity above the transition region will be lower than the ΔH^* values reported in Table II, but the compositional trends should be the same. A good example is the result of Mimura et al.[32], who found that ΔH^* for viscous flow measured by a penetrometer in the range 10^7-10^{10} Pa·s dropped from 860 kJ/mol for a composition close to ZBLA to 750 kJ/mol for a composition close to ZBLAN. The same result is found from activation energies E_c for crystal growth well above the transition region.[11-13] E_c decreased from roughly 370 kJ/mol for ZB I, II to 320 kJ/mol for ZBL I, II to 190 kJ/mol for ZBLALi and 200 kJ/mol for ZBLALiPb. It should be pointed

out that these E_c values also pertain only to limited temperature ranges and, unlike for the ΔH^* values of Table II, these regions need not have identical viscosity regimes. Indeed, we have observed in some of our investigations that the plots from whence the E_c values are calculated can be nonlinear and, as might be expected, the E_c values decrease somewhat with increasing temperature. Therefore, it is not possible at present to compare E_c values for different glasses at isoviscous points (e.g., the fiber drawing point $\eta \sim 10^3$-10^4 Pa·s) and additional viscometry data is required to complement the crystallization studies. This being the case, the ΔH^* values of Table II are perhaps the best available indication of relative stability for these glasses.

As pointed out in our earlier publication[14], a first indication of relative E_c values can be obtained by observing how rapidly the crystallization peaks develop during constant heating rate DSC scans (cf. Fig. 1). More gradual onsets of crystallization are consistent with a lower temperature dependence of the crystal growth rate and lower E_c values.

In order to establish a more quantitative basis for interpreting the compositional influence on the ΔH^* values, it is desirable to have some understanding of the glass structure and of the role played by each component in the glass in determining whether glass formation occurs. A few papers on these subjects, of which most of the conclusions are based on x-ray diffraction, vibrational spectroscopy

and molecular dynamics simulation studies of the glass and on analogies drawn between the structures of glasses and crystals, have been written about the ZrF_4- and HfF_4-based HMFG.[1,3,33-39] Poulain's paper[38] is of particular interest. He suggests, among other things, that the HMFG can be viewed fruitfully as a collection of cations inserted into a variety of sites in a disordered, non-close-packed F^- ion sublattice. Glass formation is favored by the presence of high (but not too high) field cations both energetically (the large cation-anion attractive energies immobilize the local structure) and structurally (the high fluoride to metal ion ratio favors an F^- sublattice with a large number of cation sites).

Taking our cue from Poulain[38], we sought some correlations between ΔH^* and the ionic radii and charges and relative number of fluoride ions of the glass constituents. According to Poulain's energy criterion, glass formation ought to depend on the mean cation-anion coulombic attractive energy, which can be parameterized by the quantity $\sum x_i z_i z_F/(r_i + r_F)$, where x_i is the cation fraction of cation i, z_i and z_F the charges on cation i and fluoride anion, and r_i and r_F the corresponding ionic radii. A plot of ΔH^* values from Table II versus $\sum x_i z_i z_F/(r_i + r_F)$ (ionic radii of 6-fold coordination taken from Ahrens[40]) is shown in Fig. 5A; it appears to be devoid of correlations. A similar plot, inspired by Poulain's structural criterion, of ΔH^* versus the ratio (F/M) of the total number of F^- ions to total number of cations in the glass

was likewise devoid of correlations.

We considered a large number of possible correlations of this general type; the best was the following. The electrostatic field strength z_i/r_i^2 is a measure of the polarizing power of a cation. The mean field strength of the cations in the glass per fluoride ion then gives a measure of the average covalency C_{AV} of the glass:

$$C_{AV} = \sum x_i (z_i/r_i^2)/(F/M) \qquad (4)$$

A plot of ΔH^* from Table II versus C_{AV} is shown in Fig. 5B. There is sizable scatter about the linear least squares correlation line. Much of this is probably due to uncertainties in the C_{AV} values arising, first, from small differences between the batch compositions (used in calculating C_{AV}) and the actual glass compositions and, second and probably more important, from uncertainties in the cationic radii.[40,41] Granted this, there does seem to be a (roughly linear) correlation such that ΔH^* decreases with increasing C_{AV}. A possible qualitative interpretation of this might be that an increase in average covalency would make the binding energy of the glass quasi-lattice stronger and increase the directionality of the bonds. This in turn would lead to a decrease in the thermal disruption of the glass structure with increasing temperature, leading in turn to a lower viscosity-temperature coefficient, i.e., lower ΔH^*. Possibly contrary to this speculation, however, is the

fact that $\Delta\bar{C}_p$ for these glasses does not show much composition dependence, as noted in the following section.

There are no significant differences between the ΔH^* values for high sodium and lithium content glasses in Table II. This would seem to oppose the suggestion of Lecoq and Poulain[42] that sodium and lithium ions perform different structural roles in HMFG.

5. Heat Capacities of the HMFG Glasses

In an earlier paper[43] we reported C_p data from 250K to above T_g for four ZrF_4- and HfF_4-based compositions (ZBL, ZBLA, HBL II and HBLA). Our present study covers a much narrower range near T_g, and the C_p data are summarized in Table IV. All C_p values in Table IV represent averages over the eight DSC scans (for eight prior cooling rates) done on each glass. The glass heat capacities C_{pg} (see Fig. 2) for the range roughly T_g-100K to T_g-50K are presented as linear equations of the form:

$$C_{pg}\,(J/g\cdot K) = A + BT(K) \qquad (5)$$

The equilibrium liquid heat capacities C_{pe} (see Fig. 2) for the range $T_g + 25K$ to $T_g + 30K$ were considered temperature independent. Both the C_{pg} and C_{pe} data in Table II are in excellent agreement (within a few percent) with our previous results[43] for the compositions common to both studies.

Also listed in Table IV are $\bar{C}_{pg}$ and $\Delta\bar{C}_p$, respectively the glass heat capacity just below T_g and the difference

between the liquid and glass heat capacities at T_g per mole of atoms:

$$\bar{C}_{pg} = MC_{pg}$$
$$\Delta\bar{C}_p = M(C_{pe}-C_{pg})$$

where M (given in Table IV) is the average atomic weight of the glass calculated from the batch composition in Table I. As found previously[43], the $\bar{C}_{pg}$ values near T_g are essentially the same for all the glasses (mean value 24.8 ± 0.6 J/mol K) and very close to the Dulong-Petit limit of 3R (24.9 J/mol K) for the vibrational heat capacity of solids. Likewise, $\Delta\bar{C}_p$ is the same for all the glasses within experimental error (mean value 13.9 ± 0.7 J/mol K).

As noted before[43], $\Delta\bar{C}_p$ for the HMFG is much larger than $\Delta\bar{C}_p$ for typical network oxide glasses (5 to 8 J/mol K) and comparable to $\Delta\bar{C}_p$ observed for chalcogenide glasses. $\Delta\bar{C}_p$ is usually considered to reflect the energy required to effect changes in the liquid structure above T_g.[23,31] The large values of $\Delta\bar{C}_p$ for the HMFG thus presumably indicate that substantial changes in the melt structure occur in the temperature range just above T_g, which is in line with their extraordinarily large viscosity temperature dependences as manifested in the ΔH^* values near T_g. On the other hand, the systematic variations of ΔH^* with composition do not seem to be reflected in corresponding variations in $\Delta\bar{C}_p$.

Concluding Remarks

The phenomenological ease of glass formation for a range of ZrF_4- and HfF_4-based glasses have been found to correlate very well with decreasing ΔH^* values in the glass transition region. These ΔH^* values are therefore good indicators of the relative stability of these glasses. On the basis of our measurements we conclude that the ZBLALi and ZBLAN compositions are among the best glass formers studied to date. These glasses are already being used for optical fiber fabrication.[5,32,44] Models for the compositional effects on ΔH^* await the further elucidation of the HMFG structures, although a first approximation of the ΔH^* values, for ZrF_4- and HfF_4-based glasses at least, can be made on the basis of the calculated average covalency (C_{AV}) of the glasses.

Acknowledgement

The authors are grateful to Drs. D. C. Tran and G. H. Sigel, Jr., of the Naval Research Laboratory for supplying the ZBLALi and ZBLALiPb samples.

References

1. M. Poulain, M. Chanthanasinh and J. Lucas, "New Fluoride Glasses", Mater. Res. Bull., 12 151-56 (1977).

2. C. H. L. Goodman, "Devices and Materials for 4μm Band Fibre-Optical Communication", IEEE J. Sol. State Electron. Dev., 2 129-37 (1978).

3. A. Lecoq and M. Poulain, "Phenomenological Study of the Stabilizing Role of Aluminum in Zirconium Tetrafluoride Glasses", Verres Refract., 34 [3] 333-42 (1980).

4. H. Hu and J. D. Mackenzie, "Viscosity of Molten Fluorozirconates", J. Non-Cryst. Solids, 54 [3] 241-51 (1983).

5. D. C. Tran, R. J. Ginther and G. H. Sigel, "Fluorozirconate Glasses with Improved Viscosity Behavior for Fiber Drawing", Mater. Res. Bull., 17 1177-84 (1982).

6. K-H. Chung, "Synthesis and Characterization of Infrared Transmitting Fluoride Glasses", Ph.D. Thesis, Catholic University of America, 1982, pp. 69-86.

7. C. T. Moynihan, A. J. Easteal, M. A. DeBolt and J. Tucker, "Dependence of the Fictive Temperature of Glass on Cooling Rate", J. Am. Ceram. Soc., 59 [1-2] 12-16 (1976).

8. C. T. Moynihan, A. J. Easteal, J. Wilder and J. Tucker, "Dependence of the Glass Transition Temperature on Heating and Cooling Rate", J. Phys. Chem., 78 [26] 2673-77 (1974).

9. C. T. Moynihan, P. B. Macedo, C. J. Montrose, P. K. Gupta, M. A. DeBolt, J. F. Dill, B. E. Dom, P. W. Drake, A. J. Easteal, P. B. Elterman, R. P. Moeller, H. Sasabe and J. A. Wilder, "Structural Relaxation in Vitreous Materials", Ann. N.Y. Acad. Sci., 279 15-35 (1976).

10. H. Sasabe, M. A. DeBolt, P. B. Macedo and C. T. Moynihan, "Structural Relaxation in an Alkali-Lime-Silicate Glass", Proc. XIth Intl. Congress on Glass, Vol. I, Prague, 1977, pp. 339-48.

11. N. P. Bansal, R. H. Doremus, A. J. Bruce and C. T. Moynihan, "Kinetics of Crystallization of ZrF_4-BaF_2-LaF_3 Glass by Differential Scanning Calorimetry", J. Am. Ceram. Soc., 66 [4] 233-38 (1983).

12. N. P. Bansal, A. J. Bruce, R. H. Doremus and C. T. Moynihan, "Crystallization of Heavy Metal Fluoride Glasses", Proc. SPIE, in press.

13. N. P. Bansal, A. J. Bruce, R. H. Doremus and C. T. Moynihan, "The Influence of Glass Composition on the Crystal Growth Kinetics of Heavy Metal Fluoride Glasses", J. Non-Cryst. Solids, to be published.

14. C. T. Moynihan, D. L. Gavin, K-H. Chung, A. J. Bruce, M. G. Drexhage and O. H. El Bayoumi, "Viscous Flow Activation Energy and Devitrification of Heavy Metal Fluoride Glasses", Glastech. Ber., 56K 862-67 (1983).

15. M. G. Drexhage, O. H. El Bayoumi, C. T. Moynihan, A. J. Bruce, K-H. Chung, D. L. Gavin and T. J. Loretz, "Preparation and Properties of Heavy-Metal Fluoride Glasses Containing Ytterbium or Lutetium", J. Am. Ceram. Soc., 65 [10] C-168 - C-171 (1982).

16. E. I. Cooper and C. A. Angell, "Far-IR Transmitting Cadmium Iodide-Based Glasses", Paper No. 8, Extended Abstracts, 2nd Intl. Symposium on Halide Glasses, Troy, NY, 1983.

17. A. J. Bruce, C. T. Moynihan, M. G. Drexhage and O. H. El Bayoumi, "DSC Study of Nucleation and Crystallization of Heavy Metal Fluoride Glasses", Paper No. 7, Extended Abstracts, 2nd Intl. Symposium on Halide Glasses, Troy, NY, 1983.

18. A. J. Easteal, J. A. Wilder, R. K. Mohr and C. T. Moynihan, "Heat Capacity and Structural Relaxation of Enthalpy in As_2Se_3 Glass", J. Am. Ceram. Soc., 60 [3-4] 134-38 (1977).

19. M. A. DeBolt, A. J. Easteal, P. B. Macedo and C. T. Moynihan, "Analysis of Structural Relaxation in Glass Using Rate Heating Data", J. Am. Ceram. Soc., 59 [1-2] 16-21 (1976).

20. C. T. Moynihan, A. J. Easteal, D. C. Tran, J. A. Wilder and E. P. Donovan, "Heat Capacity and Structural Relaxation of Mixed-Alkali Glasses", J. Am. Ceram. Soc., 59 [3-4] 137-40 (1976).

21. C. T. Moynihan, H. Sasabe and J. Tucker; pp. 182-94 in Molten Salts. Edited by J. P. Pemsler et al., Electrochemical Society, Princeton, NJ, 1976.

22. W. T. Laughlin and D. R. Uhlmann, "Viscous Flow in Simple Organic Liquids", J. Phys. Chem., 76 [16] 2317-25 (1972).

23. C. A. Angell and W. Sichina, "Thermodynamics of the Glass Transition: Empirical Aspects", Ann. N.Y. Acad. Sci., 279 53-57 (1976).

24. J. T. Loretz, J. L. Mansfield, A. W. Mustico, J. J. Jalbert and M. G. Drexhage, "Fabrication Methods for Fluoride Glasses", Extended Abstracts, 1st Intl. Symposium on Halide and Nonoxide Glasses, Cambridge, England, 1982.

25. E. H. Fontana and W. A. Plummer, "A Study of the Viscosity-Temperature Relationships in the GeO_2 and SiO_2 Systems", Phys. Chem. Glasses, 7 [4] 139-46 (1966).

26. A. Napolitano and E. G. Hawkins, "Viscosity of a Standard Soda-Lime-Silica Glass", J. Res. Natl. Bur. Stand., 68A 439-48 (1964).

27. A. Napolitano, J. H. Simmons, D. H. Blackburn and R. E. Chidester, "Analysis of Low Temperature Viscosity Data for Three NBS Standard Glasses", J. Res. Natl. Bur. Stand., 78A 323-29 (1974).

28. H. S. Chen and D. Turnbull, "Evidence of a Glass-Liquid Transition in a Gold-Germanium-Silicon Alloy", J. Chem. Phys., 48 2560-71 (1968).

29. R. Weiler, S. Blaser and P. B. Macedo, "Viscosity of a Vitreous Potassium Nitrate-Calcium Nitrate Mixture", J. Phys. Chem., 73 [12] 4147-51 (1969).

30. H. Tweer, N. Laberge and P. B. Macedo, "Inadequacies of Viscosity Theories for a KNO_3-$Ca(NO_3)_2$ Melt", J. Am. Ceram. Soc., 54 [2] 121-23 (1971).

31. C. A. Angell, "Strong and Fragile Liquids", Proc. Workship on Relaxation Processes, Blacksburg, VA, July, 1983, to be published.

32. Y. Mimura, H. Tokiwa and O. Shinbori, "Fabrication of Fluoride Glass Fibres by the Improved Crucible Technique", Electronics Lett., 20 [2] 100-01 (1984).

33. M. Poulain and J. Lucas, "A New Class of Materials: Zirconium Tetrafluoride Glasses", Verres Refract., 32 [4] 505-13 (1978).

34. J. Lucas, M. Chanthanasinh, M. Poulain, P. Brun and M. J. Weber, "Preparation and Optical Properties of Neodymium Fluorozirconate Glasses", J. Non-Cryst. Solids, 27 273-83 (1978).

35. R. Almeida and J. D. Mackenzie, "Vibrational Spectra and Structure of Fluoro-Zirconate Glasses", J. Chem. Phys., 74 5954-61 (1981).

36. R. Coupe, D. Louer, J. Lucas and A. J. Leonard, "X-Ray Scattering Studies of Glasses in the System ZrF_4-BaF_2", J. Am. Ceram. Soc., 66 [7] 523-29 (1983).

37. J. Lucas, C. A. Angell and S. Tamaddon, "Fluoride Bridging Modes in Fluorozirconate Glasses by X-Ray and Computer Simulation Studies", to be published.

38. M. Poulain, "Glass Formation in Ionic Systems", Nature, 293 [5830] 279-80 (1981).

39. C. M. Baldwin and J. D. Mackenzie, "Fundamental Condition for Glass Formation in Fluoride Systems", J. Am. Ceram. Soc., 62 [9-10] 537-38 (1979).

40. L. H. Ahrens, "The Use of Ionization Potentials I; Ionic Radii of the Elements", Geochim. Cosmochim. Acta, 2 155-69 (1952).

41. R. D. Shannon and C. T.Prewitt, "Effective Ionic Radii in Oxides and Fluorides", Acta Cryst., B25 925-46 (1969).

42. A. Lecoq and M. Poulain, "Lanthanum Fluorozirconate Glasses", J. Non-Cryst. Solids, 34 101-10 (1979).

43. D. L. Gavin, K-H. Chung, A. J. Bruce, C. T. Moynihan, M. G. Drexhage and O. H. El Bayoumi, "Heat Capacities of Heavy Metal Fluoride Glasses", J. Am. Ceram. Soc., 65 [11] C-182 - C-183 (1982).

44. K. Ohsawa, T. Shibata, K. Nakamura and S. Yoshida, "Fluorozirconate Glasses for I.R. Transmitting Optical Fibers", 1st Intl. Symposium on Halide and Nonoxide Glasses, Cambridge, England, 1982.

TABLE I

BATCH COMPOSITIONS OF HEAVY METAL FLUORIDE GLASSES

Glass	Composition (mol %)
ZB I, II	65 ZrF_4-35 BaF_2
ZB III	50 ZrF_4-50 BaF_2
ZBL I, II	62 ZrF_4-33 BaF_2-5 LaF_3
ZBLA I, II	58 ZrF_4-33 BaF_2-5 LaF_3-4 AlF_3
ZBLPb	58.9 ZrF_4-31.35 BaF_2-4.75 LaF_3-5.00 PbF_2
ZBLN	58 ZrF_4-15 BaF_2-6 LaF_3-21 NaF
ZBLLi	58 ZrF_4-15 BaF_2-6 LaF_3-21 LiF
ZBLAN I, II, III	55.8 ZrF_4-14.4 BaF_2-5.8 LaF_3-3.8 AlF_3-20.2 NaF
ZBLALi	50.7 ZrF_4-20.7 BaF_2-5.2 LaF_3-3.2 AlF_3-20.2 LiF
ZBLALiPb	49.8 ZrF_4-17.0 BaF_2-5.0 LaF_3-3.1 AlF_3-20.0 LiF-4.1 PbF_2
HB I, II	65 HfF_4-35 BaF_2
HBL I	62 HfF_4-33 BaF_2-5 LaF_3
HBL II	70 HfF_4-20 BaF_2-10 LaF_3
HBL III	60 HfF_4-25 BaF_2-15 LaF_3
HBLA	58 HfF_4-33 BaF_2-5 LaF_3-4 AlF_3
HBLAPbCs	62 HfF_4-15 BaF_2-5 LaF_3-2 AlF_3-10 PbF_2-6 CsF

TABLE II

STRUCTURAL RELAXATION ACTIVATION ENERGIES AND
OTHER CHARACTERISTIC PARAMETERS FOR
ZrF_4- and HfF_4-BASED GLASSES

Glass	ΔH^*/kJ mol^{-1}	T_g/K	$(T_x-T_g)/T_g$	$(\Delta H/R)\cdot\Delta(1/T)$
ZB-I	1600	570	0.08	7.0
ZB-II	1580	566	0.10	6.4
ZB-III	2170, 1900	594	0.08	8.5, 7.8
ZBL-I	1480, 1520	573, 574	0.14	7.8, 7.3
ZBL-II	1370, 1510	573, 575	0.13	7.5, 7.1
ZBLA-I	1270	582	0.16	7.4
ZBLA-II	1400, 1380	585	0.16	8.1, 7.4
ZBLPb	1250	575	0.12	6.0
ZBLN	1020	515	0.17	8.1
ZBLLi	990	514	0.22	7.3
ZBLAN-I	1020	536	0.24	7.0
ZBLAN-II	1000	537	0.22	7.6
ZBLAN-III	910, 960	535, 537	0.24	7.1, 7.5
ZBLALi	1120	523	0.23	7.3
ZBLALiPb	1040	513	0.21	8.1
HB-I	1350	576	0.11	5.8
HB-II	1380	584	0.12	6.2
HBL-I	1420, 1500	595, 598	0.13, 0.14	6.8, 7.0
HBL-II	1470	602	0.14	9.4
HBL-III	1520	608	0.14	7.8
HBLA	1300	598	0.17	6.5
HBLAPbCs	1150, 1090	574, 570	0.17	8.2, 6.9

TABLE III

CHARACTERISTIC TEMPERATURES AND ACTIVATION ENERGIES IN THE GLASS TRANSITION REGION FOR VARIOUS GLASSES COOLED AND REHEATED AT EQUAL RATES (10 or 20 K/min)

Glass	T_g(K)	ΔH^*(kJ/mol)	$(\Delta H^*/R)\cdot\Delta(1/T)$	Ref.
As_2Se_3	454	340	4.7	9,18
B_2O_3	557	380	4.9	19
25 Na_2O-75 SiO_2	757	410	4.0	20
NBS 710 (alkali lime silicate)	838	610	5.2	10
BSC (alkali borosilicate)	844	620	5.3	7
40 $Ca(NO_3)_2$-60 KNO_3	336	590	11.9	7,21

TABLE IV

HEAT CAPACITY DATA FOR ZrF_4- AND HfF_4-BASED GLASSES

Composition	M(g/mol)	glass				-liquid-	
		Temp. Range (K)	A (J/g•K)	10^4B (J/g•K^2)	$\bar{C}_{pg}$ at T_g-25K (J/mol•K)	C_{pe} (J/g•K)	$\Delta\bar{C}_p$ at T_g (J/mol•K)
ZB II	39.55	470-520	0.505	2.30	24.9	0.992	14.1
ZBL I	39.94	470-520	0.554	1.06	24.5	0.963	13.9
ZBLA I	39.53	490-540	0.551	1.21	24.4	0.982	14.3
ZBLA II	39.53	490-540	0.483	2.51	24.6	0.989	14.2
ZBLPb	41.18	470-520	0.386	4.39	25.8	0.969	13.6
ZBLN	35.88	410-460	0.528	3.01	24.2	1.066	13.7
ZBLLi	35.04	410-460	0.619	1.46	24.2	1.097	14.1
ZBLAN I	35.25	440-490	0.600	1.42	23.9	1.045	13.0
ZBLAN II	35.25	440-490	0.559	2.51	24.2	1.092	14.2
ZBLALi	35.73	430-480	0.611	1.51	24.5	1.096	14.5
ZBLALiPb	36.49	420-470	0.573	2.05	24.6	1.036	13.1
HB I	52.74	480-530	0.368	1.97	25.1	0.774	15.4
HB II	52.74	480-530	0.365	2.09	25.4	0.765	14.7
HBL I	52.55	490-540	0.325	2.93	25.9	0.747	13.0
HBL II	51.73	490-540	0.363	2.22	25.4	0.750	13.1
HBLA	51.44	490-540	0.408	1.42	25.2	0.762	13.8
HBLAPbCs	53.93	470-520	0.409	0.75	24.3	0.715	14.2

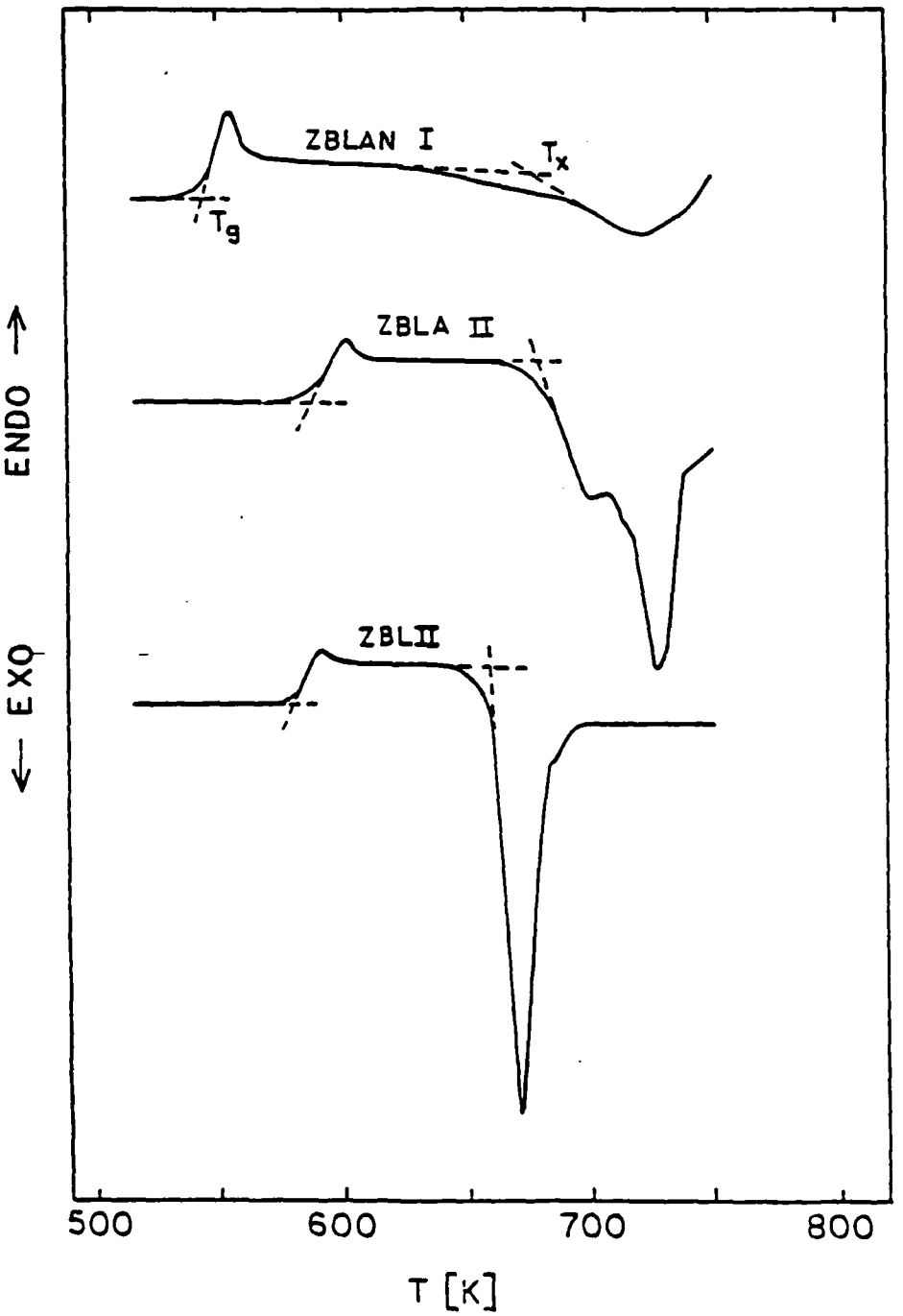

Fig. 1 DSC scans of ZBL, ZBLA and ZBLAN at a heating rate of 10 K/min showing the glass transition and crystallization peaks.

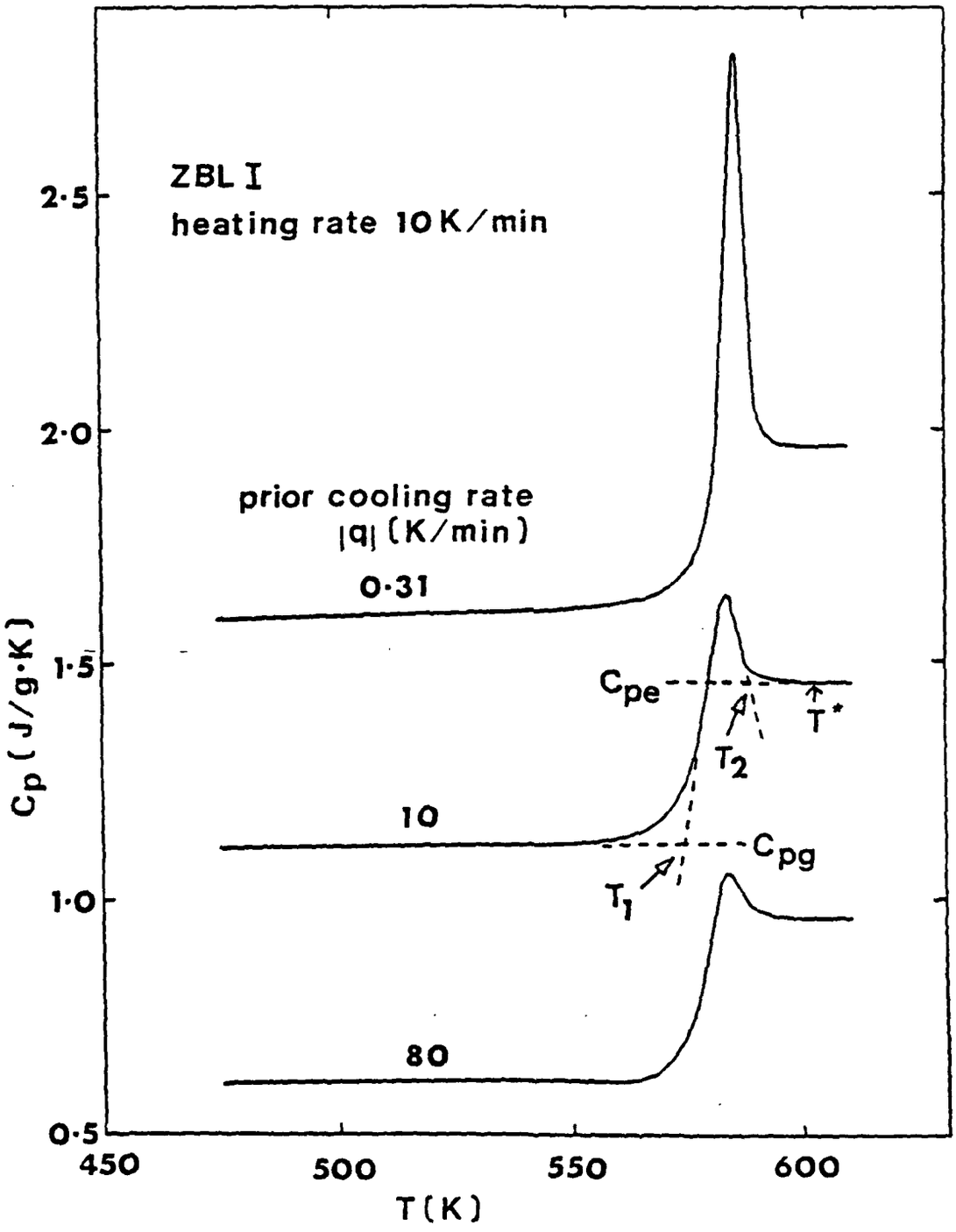

Fig. 2 Heat capacities of ZBL I glass measured at a heating rate of 10 K/min after cooling at -0.31, -10 and -80 K/min. The results for the cooling rates of -10 and -0.31 K/min have been displaced upwards by 0.5 and 1.0 J/g·K respectively for clarity.

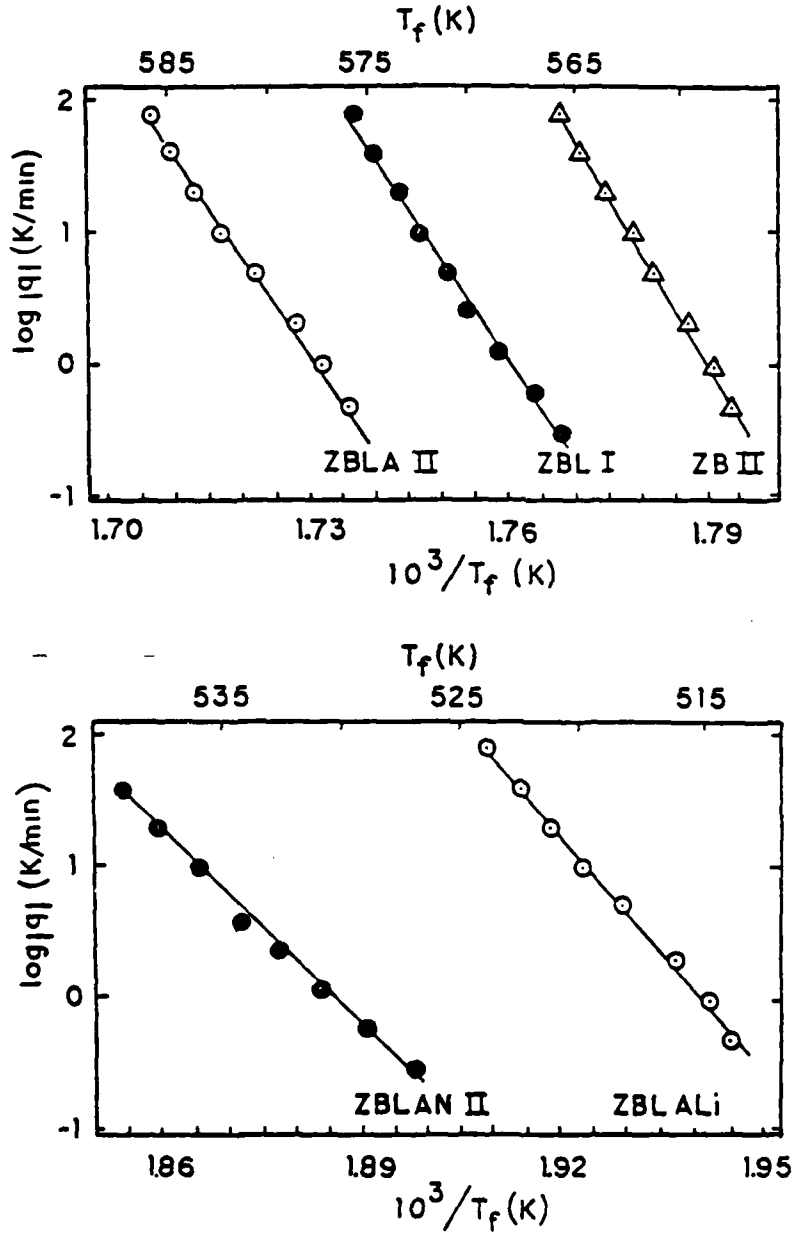

Fig. 3 Arrhenius plots of log |q| versus $1/T_f$ for ZB II, ZBL, ZBLA, ZBLAN and ZBLALi glasses.

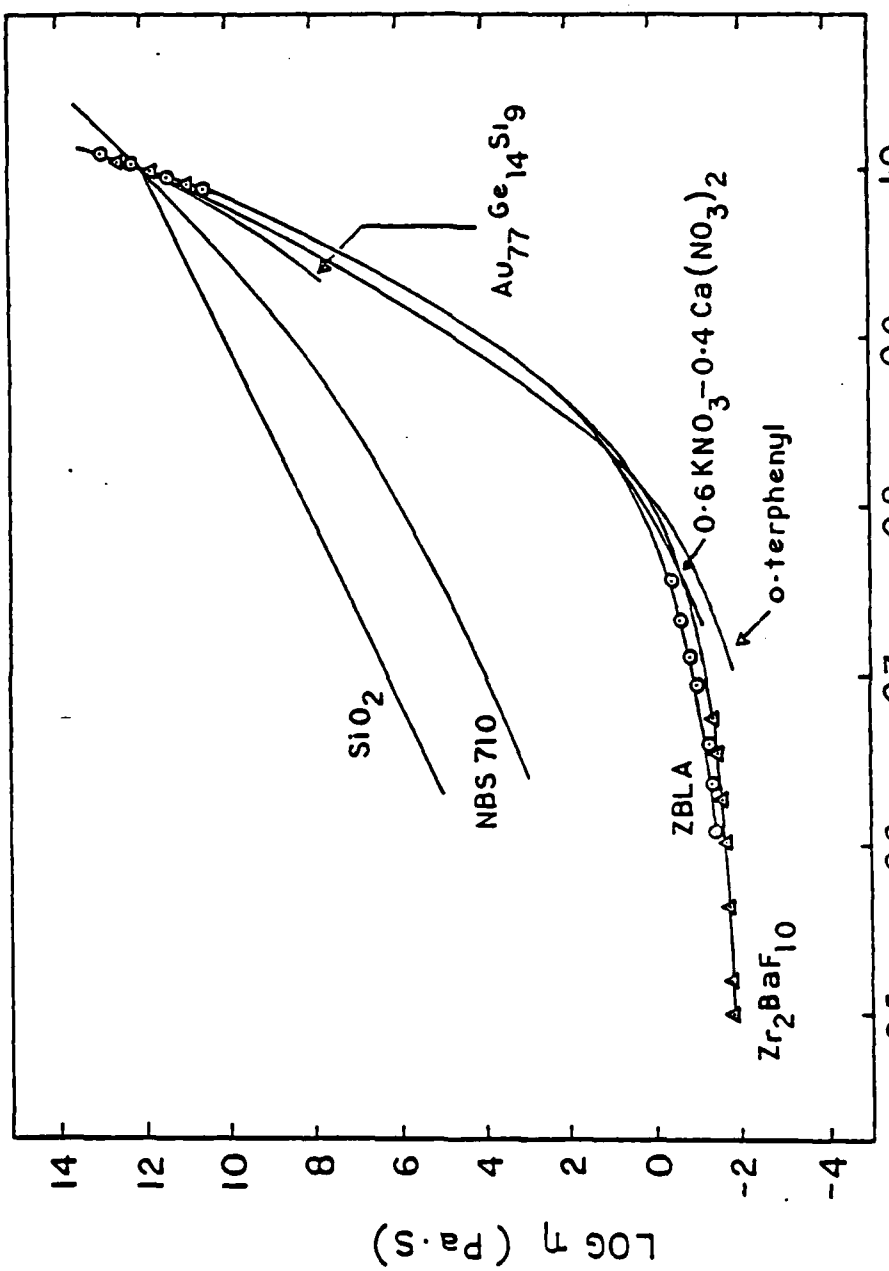

Fig. 4 Arrhenius plots of logarithm of viscosity versus reduced inverse temperature T_g/T for SiO_2 [25], NBS 710 [26,27], $Au_{77}Ge_{14}Si_9$ [28], $40\,Ca(NO_3)_2$-$60\,KNO_3$ [29,30], o-terphenyl [22], ZBLA [24] and ZBLA-1 [24] glasses.

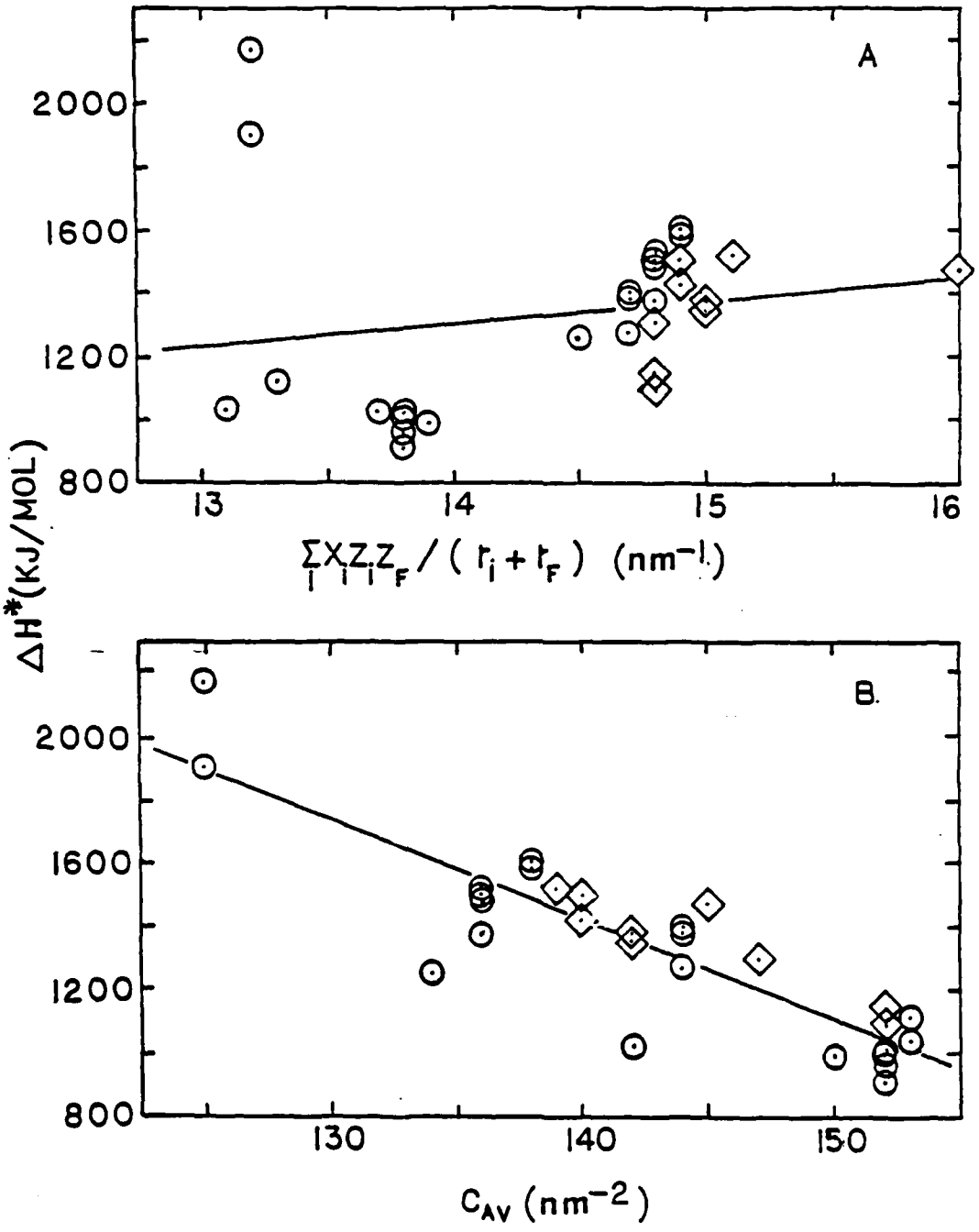

Fig. 5 Plots of ΔH* versus (A) mean cation-anion attractive potential energy and (B) average covalency parameter for ZrF_4-based (⊙) and HfF_4-based (◇) glasses. Solid lines are linear least squares correlation lines.

DSC STUDIES OF MELTING BEHAVIOR OF HEAVY METAL FLUORIDE GLASS COMPOSITIONS

R. Mossadegh and C. T. Moynihan
Rensselaer Polytechnic Institute
Troy, New York, 12181

A. J. Bruce
AT&T Bell Laboratories
Murray Hill, New Jersey 07974

M. G. Drexhage
Rome Air Development Center
Hanscom AFB, MA 01731

ABSTRACT

Differential scanning calorimetry (DSC) studies of a number of heavy metal fluoride glasses have been carried out while heating from below the glass transition up to 950K. The glasses first crystallize and then remelt. The final stage of melting is generally marked by a small, high temperature endotherm, whose location allows assignment of a liquidus temperature T_L to the glass composition. The ratio T_L/T_g of the liquidus to the glass transition temperature is roughly constant and equal to about 1.5 for a wide variety of glass compositions.

Introduction

Numerous studies have now been carried out of crystallization of heavy metal fluoride (HMF) glass forming compositions (see, for example, Refs. 1-5). Since these are multicomponent systems, the crystallization behavior is complex and involves the appearance at various temperatures of a large number of different crystalline phases, many of which are metastable. These phases appear and disappear at temperatures below the liquidus curves, and to date there appears to be some confusion in the assignment of equilibrium liquidus temperatures to HMF melts. Knowledge of the liquidus temperature is clearly important in these systems because it marks the minimum temperature at which crystal-free melts can be obtained.

Our knowledge to date of melting temperatures of HMF systems is derived from DSC or DTA studies of the remelting of crystallized glasses (see, for example, Refs. 1,3,5-7). Typically the "melting" or "fusion" point of the system has been taken either at the onset or at the peak of the main melting endotherm, in spite of clear evidence in the DSC or DTA traces of smaller higher temperature events which must be associated with the completion of the melting process. In this paper we report careful DSC studies of remelting of a number of HMF compositions in order to clarify the assignment of liquidus temperatures.

Experimental Procedures

Glass samples used in this study were synthesized both in our own laboratories and elsewhere using standard procedures (8,9). Compositions are given in Table I and include examples from the more widely studied ZrF_4- and HfF_4- based glasses as well as representatives from other HMF glassforming families.

Differential scanning calorimetry (DSC) measurements were carried out at heating rates of 10 or 20 K/min using a Perkin-Elmer Model DSC-4 modified to operate at temperatures above 600°C and equipped with a Laboratory Microsystems data acquisition system. The glass samples were encapsulated in gold DSC pans. Temperature and heat flow calibrations were done using appropriate standards.

Results and Discussion

Sequential DSC Heating Scans of ZBLA Glass

Typical DSC scans (specific heat versus temperature) are shown in Fig. 1 for ZBLA glass. The scans were done at a 10K/min heating rate and extend from well below the glass transition region up to 925K.

The initial scan in Fig. 1 shows, in order of increasing temperature, the glass transition at T_g, a series of exotherms due to crystallization and metastable-to-stable solid-solid (SS) transitions (2) and, finally, a series of melting endotherms. In previous studies characteristic temperatures have been

assigned to the main melting endotherm - the "fusion" temperature T_F for the onset of this endotherm and T_M for its maximum. Two smaller endotherms occurring above T_M are also evident in Fig. 1. We have designated the temperature at which the last of these terminates as T_L and believe that this corresponds to the liquids temperature of the system, i.e., the temperature at which the last crystals disappear and a single liquid phase is obtained. Although these small, high temperature endotherms are evident in a number of analogous DSC scans published in the literature (e.g., Refs. 3,6, and 7), they have generally not been commented on and their significance seems to have been overlooked. In the first rescan of Fig. 1, taken after fast cooling of the sample on the DSC, the magnitude of the specific heat change at T_g, ΔCp, is the same as in the initial scan, indicating within experimental precision that the sample has completely vitrified on cooling. (Note that the difference in the specific heat overshoot at T_g for the initial scan is much larger than for the two rescans. This is an effect of structural relaxation (10) and is due to the fact that the initial scan was for a well annealed glass, while the rescans are for rapidly cooled glasses.) However, in the first rescan the crystallization and SS transformation exotherms are somewhat altered from those of the initial scan, e.g., the 750K endotherm is missing in the first rescan. The initial

melting endotherms are also somewhat different between the initial scan and the first rescan, although the minor endotherms appear to be unaltered between the two scans. The second rescan in Fig. 1, however, closely replicates the first rescan.

The differences between the initial scan and the first rescan are probably not surprising. The first crystallization phases to appear on reheating of HMF glasses have always been found to be metastable (1-5). Consequently a wide variety of crystallization paths are available to these materials, and the exact route followed will depend on the conditions. In the present case, after the initial scan the nucleation kinetics may be changed for the rescan because the sample has melted and wetted the gold DSC pan surface and/or because the melt surface may have been altered slightly by decomposition (see below).

After the second rescan of Fig. 1, the sample was recooled at 100K/min, removed from the DSC and inspected under a low power polarizing microscope. The bulk of the sample was glassy with no crystals in evidence. However, a few, very small black spots, due perhaps to reduced ZrF_4 (11), were discernible at the interface between the bottom of the glass samples and the gold DSC pan surface.

In principle an enthalpy balance requires that the area under the low temperature crystallizationand SS transition exotherms should match the area under the high temperature melting endotherms. An attempt to test this is shown in the second rescan of Fig. 1. The zero heat flow line (the dashed line) has been drawn to connect the DSC scan between two temperature regimes where the sample is entirely liquid. The shaded areas above and below this line match approximately, but not exactly. We believe this to be mostly due to the experimental problem of specifying the zero heat flow line in the face of curvature of the DSC baseline over large temperature regimes. Attempts to resolve areas under individual peaks in the DSC scans are even more frought with error because of effective baseline changes due to specific heat changes in passing from liquid to crystal and vice versa.

Sequential DSC Heating Scans of ZBLAN Glass

Figure 2 shows a series of DSC scans for ZBLAN glass analogous to those of Fig. 1. As in expected from the stability of this composition against devitrification (12-14), crystallization was incomplete during the inital scan. This is indicated by the small area of the crystallization exotherm for the

initial scan compared to those for the two rescans. Nucleation and crystallization of ZBLAN glass is facilitated during the rescans, probably for the reasons given in the previous section. In Fig. 2 we have associated the liquidus temperature T_L with the small high temperature endotherm which appears in all three plots. The specific heat change ΔCp at T_g is the same for all three scans of Fig. 2, indicating that the ZBLAN melt can be quenched completely to a glass during 100K/min cooling on the DSC. Examination of the rapidly cooled ZBLAN DSC sample following the second rescan revealed a crystal-free glass in the bulk, but a very thin, slightly cloudy layer on the surface.

Test for Completion of Melting at T_L

We carried out some additional experiments on ZBLA and ZBLAN glasses to verify our hypothesis that the actual liquidus temperature corresponds to T_L and that melting is not complete at T_M. The results are shown in Figs. 3 and 4. In the initial scan in Fig. 3 the as-formed ZBLA glass was heated to a temperature of 830K, just above T_M, held isothermally for 3 min and then cooled at 100K/min to below T_g. It was then rescanned at 10K/min to 950K. The rescan shows no glass transition or crystallization or SS transition exotherms, but only melting endotherms. This, in conjunction with the results of Fig. 1, shows that just above T_M the ZBLA glass was not completely melted and contained sufficient crystalline material to cause

nucleation and complete crystallization on recooling to below T_g.

The initial scan for ZBLAN glass in Fig. 4 was terminated just above T_M at 750K, the sample held isothermally for 3 min and then cooled at 100K/min to below T_g. In this case it appears that the crystals remaining just above T_M induced about one third of the sample to crystallize on cooling, since ΔCp for the first rescan in Fig. 4 is only about two thirds of ΔCp for the initial scan and the area under the crystallization exotherms for the first rescan is markedly smaller than the area under the melting endotherms. T_g for the first rescan in Fig. 4 is noticeably lower than T_g for the initial scan, indicating that the residual glass and the crystals at the start of the first rescan are both different in composition from the initial bulk glass. Since addition of NaF to ZrF_4based glasses lowers T_g, the residual glass and the crystals at the start of the first rescan are presumably respectively enriched and depleted in NaF. This is not inconsistent with the results of Parker et al. (5), who found that barium fluorozirconates were the first phases to crystallize on heating of ZrF_4-BaF_2-NaF glasses. The first rescan in Fig. 4 took the ZBLAN sample to above T_L, after which it was recooled at 100K/min and given a second rescan to 950K. As expected, the second rescan in Fig. 4 is virtually identical to the first and second rescans in Fig. 2.

Liquidus Temperature Correlations for HMF Melts

In Fig. 5 are shown DSC scans at a 20K/min heating rate for four additional HMF glasses, including two examples (BZnYbT and PGMYA) from compositions not based on ZrF_4. Note that a normalized T/T_g temperature scale has been used in Fig. 5 and that the liquidus temperatures T_L are indicated. In Table 2 are listed the characteristic temperatures T_g, T_M and T_L along with the T_M/T_g and T_L/T_g ratios for all twelve of the compositions investigated.

In ten of the systems studied here the liquidus temperature T_L was found to lie somewhat above the main melting endotherm which has its peak at T_M. The only exceptions were the ZBLLi and ZBLALi(I) compositions, where melting appeared to be complete after the main endotherm, i.e., T_M and T_L are virtually the same. In all cases, however, the majority of melting was complete at T_M. This suggests that all of these glass-forming compositions lie close to eutectic points in the multicomponent phase diagrams, in line with the general expectation that the better glass forming compositions in any system are those which sit near minima on the liquidus surface.

As shown in Table 2, the ratios T_M/T_g and T_L/T_g are roughly constant -- 1.4 and 1.5 respectively -- for all the HMF compositions. While this correlation is strictly empirical, it may prove useful in estimating liquidus temperatures from T_g values for these materials and hence in determining minimum temperatures for obtaining crystal-free melts.

REFERENCES

1. Y. Kawamoto and F. Sakaguchi, Bull. Chem. Soc. Jpn. 56, 2138 (1983).

2. N. P. Bansal, R. H. Doremus, A. J. Bruce and C. T. Moynihan, Mat. Res. Bull. 19, 577 (1984).

3. G. F. Neilson, G. L. Smith and M. C. Weinberg, Mat. Res. Bull. 19, 279 (1984).

4. G. Lu, C. F. Fisher, M. J. Burk and D. C. Tran, Bull Am. Ceram. Soc. 63, 1416 (1984).

5. J. M. Parker, G. N. Ainsworth, A.B. Seddon and A. Clare, Phys. Chem. Glasses, in press.

6. S. Takahashi, S. Shibata, T. Kanamori, S. Mitachi and T. Manabe, in Advances in Ceramics, Vol. 2, B. Bendow and S. S. Mitra, Eds., American Ceramic Society, Inc., Columbus, OH, 1981, pp. 74-82.

7. M. Poulain, M. Chanthanasinh and J. Lucas, Mat. Res. Bull. 12, 151 (1977).

8. M. G. Drexhage, in Treatise on Materials Science and Technology, Vol. 26, M. Tomozawa and R. H. Doremus, Eds., Academic Press, New York, 1985, pp. 151-243.

9. M. J. Suscavage, J. J. Hutta, M.G. Drexhage, N. Perazzo R. Mossadegh and C. T. Moynihan, Mater. Sci. Forum 5, 35 (1985).

10. C. T. Moynihan, A. J. Bruce, D. L. Gavin, S. R. Loehr, S. M. Opalka and M. G. Drexhage, Polymer Engin. and Sci. 24, 1117 (1984).

11. M. Robinson, R. C. Pastor, R.R. Turk, D. P. Devor and M. Braunstein, Mat. Res. Bull. 15, 735 (1980).

12. K. Ohsawa and T. Shibata, J. Lightwave Tech. LT-2, 602 (1984).

13. Y. Mimura, H. Tokiwa and O. Shinbori, Electron. Lett. 20, 100 (1984).

14. L. E. Busse, G. Lu, D. C. Tran and G. H. Sigel, Jr., Mater. Sci. Forum 5, 219 (1985).

TABLE I

Composition of HMF Glasses

Glass	Composition (mol %)
ZB	$65ZrF_4 - 35BaF_2$
ZBL	$62ZrF_4 - 33BaF_2 - 5LaF_3$
ZBLA	$57ZrF_4 - 36BaF_2 - 3LaF_3 - 4AlF_3$
ZBLN	$58ZrF_4 - 15BaF_2 - 6LaF_3 - 21NaF$
ZBLLi	$58ZrF_4 - 15BaF_2 - 6LaF_3 - 21LiF$
ZBLAN	$56ZrF_4 - 14BaF_2 - 6LaF_3 - 4AlF_3 - 20NaF$
ZBLALi (I)	$53ZrF_4 - 19BaF_2 - 5LaF_3 - 3AlF_3 - 20LiF$
ZBLALi (II)	$56ZrF_4 - 14BaF_2 - 6LaF_3 - 4AlF_3 - 20LiF$
HB	$65HfF_4 - 35BaF_2$
HBL	$62HfF_4 - 33BaF_2 - 5LaF_3$
BZnYbT	$19BaF_2 - 27ZnF_2 - 27YbF_3 - 27ThF_4$
PGYMA	$35PbF_2 - 24MnF_2 - 34GaF_3 - 5YF_3 - 2AlF_3$

TABLE II

Characteristic Temperatures of HMF Glasses

Glass	T_g(K)	T_M(K)	T_L(K)	T_M/T_g	T_L/T_g
ZB	570	798	860	1.40	1.51
ZBL	580	820	883	1.41	1.52
ZBLA	587	815	872	1.39	1.49
ZBLN	535	735	821	1.37	1.53
ZBLLi	515	815	815	1.58	1.58
ZBLAN	541	730	882	1.35	1.63
ZBLALi (I)	530	815	820	1.54	1.55
ZBLALi (II)	525	810	887	1.54	1.69
HB	580	825	880	1.42	1.52
HBL	605	832	920	1.38	1.52
BZnYbT	623	910	973	1.46	1.56
PMGYA	546	799	857	1.46	1.57
			ave	1.44	1.56
				±0.08	±0.06

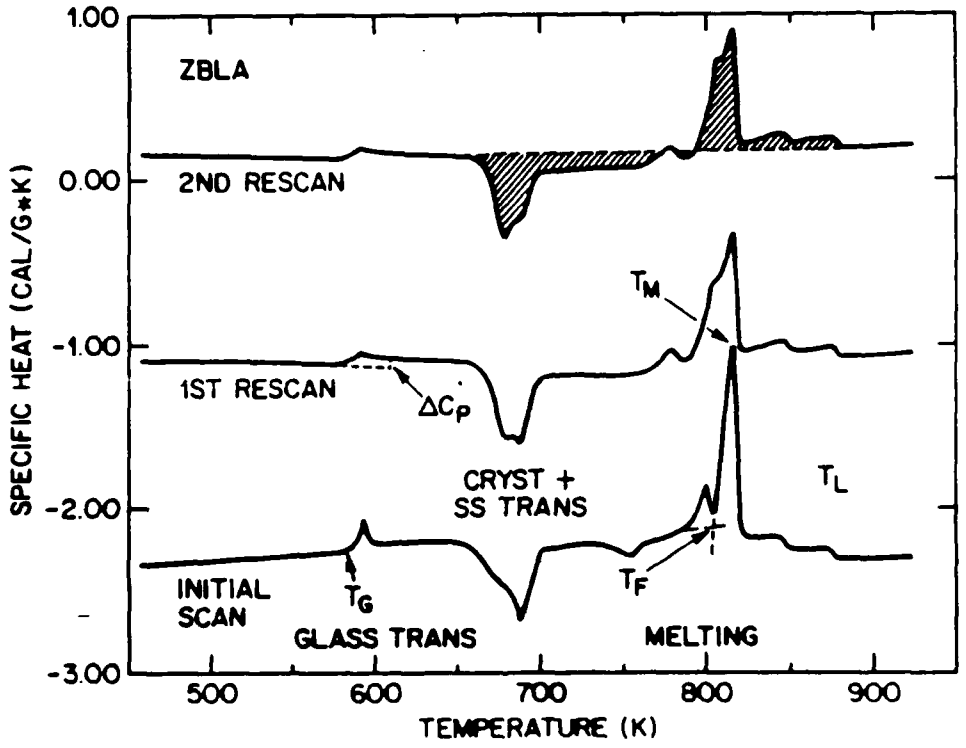

Fig. 1.

DSC scans of ZBLA glass at a 10K/min heating rate. The specific heat scale is correct for the 2nd rescan; the other two scans have been displaced downward for clarity. The initial scan was done on the as-formed glass; the rescans were obtained after cooling the sample at 100K/min to below T_g.

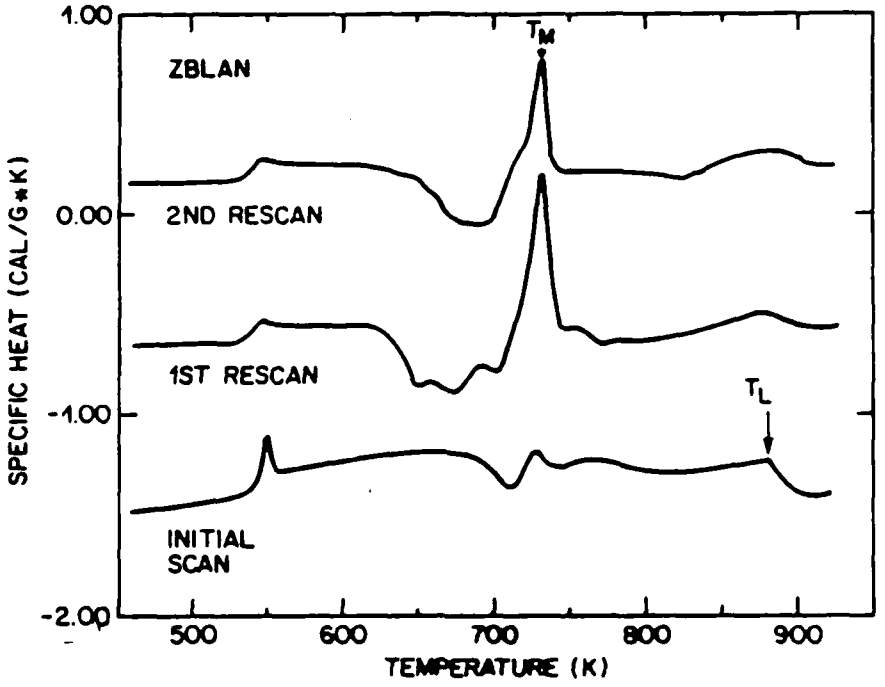

Fig. 2.

DSC scans of ZBLAN glass at 10K/min heating rate. Comments in caption to Fig. 1 apply to this figure.

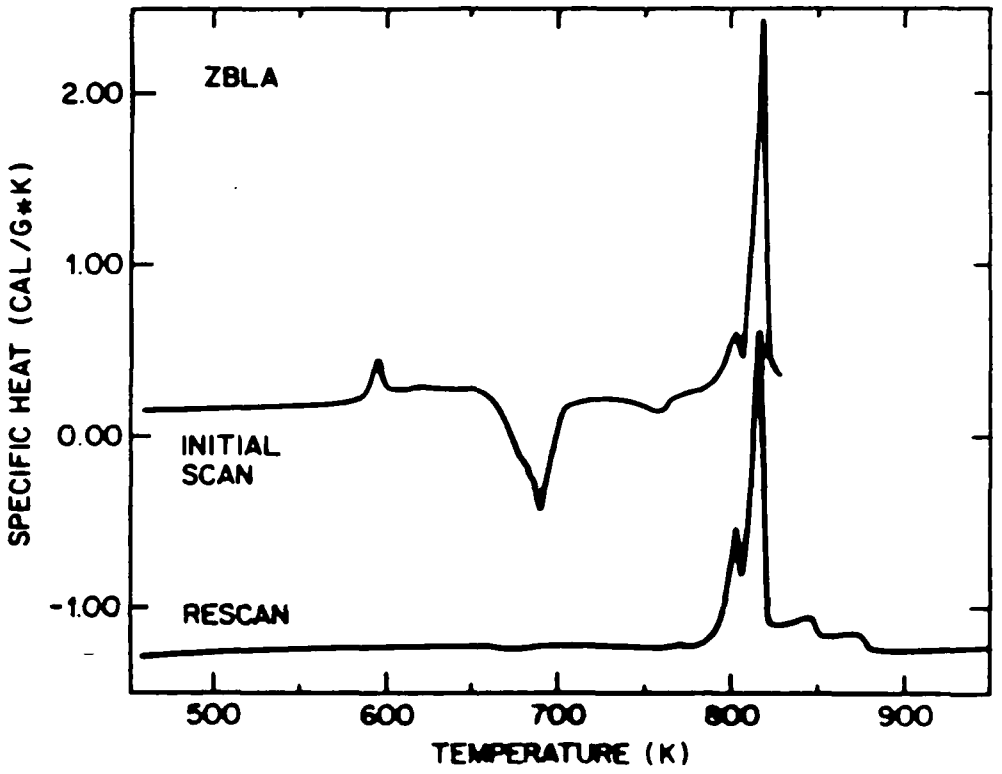

Fig. 3.

DSC scans of ZBLA glass at 10K/min heating rate. The initial scan on the as-formed glass was stopped just above T_M at 830K. After holding for 3 min at 830K, the sample was cooled at 100K/min and then rescanned up to 950K. Specific heat scale is correct for initial scan.

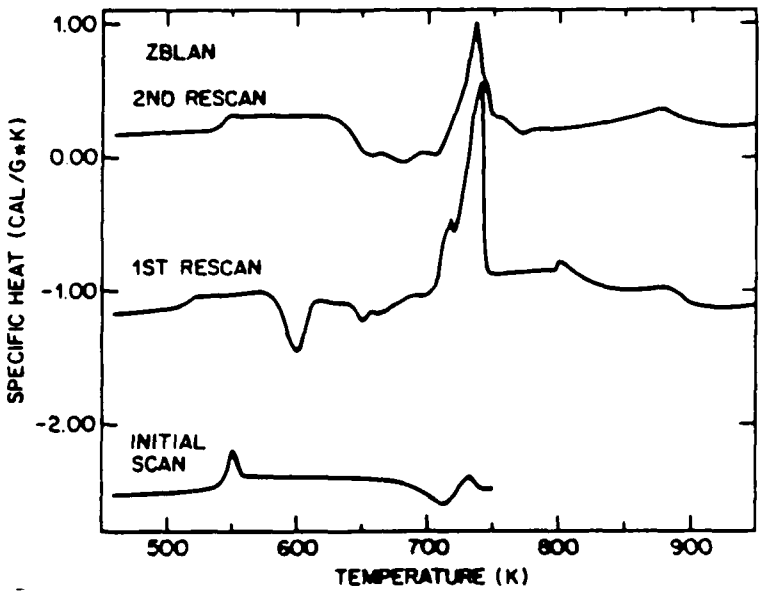

Fig. 4

DSC scans of ZBLAN glass at 10K/min. The initial scan on the as-formed glass was stopped at 750K. After holding for 3 min at 750K, the sample was cooled at 100K/min and then rescanned up to 950K. The second rescan was carried out after 100K/min cooling from 950K. Specific heat scale is correct for second rescan.

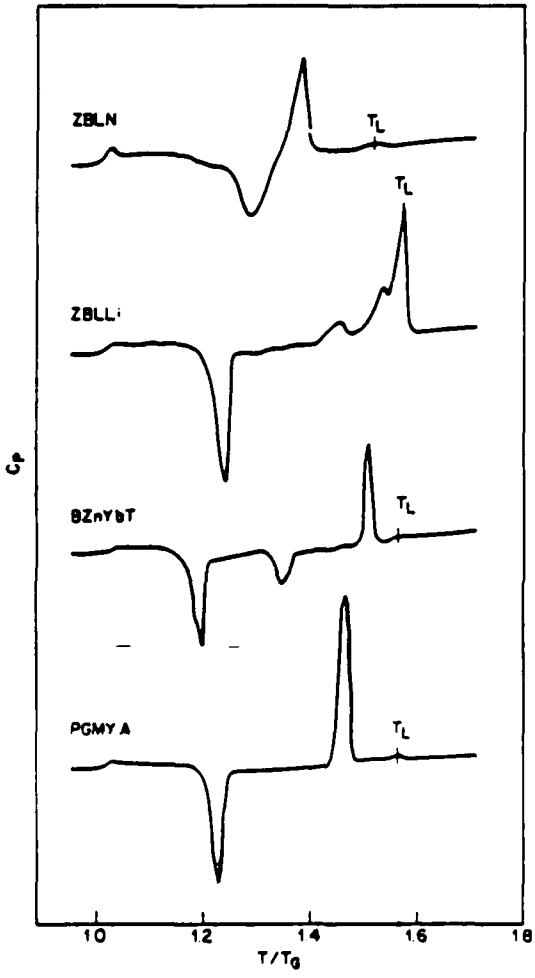

Fig. 5

DSC scans at 20K/min heating rate for several HMF glasses plotted on a normalized T/T_g temperature scale (6).

STRUCTURAL RELAXATION IN FLUORIDE GLASSES

C. T. Moynihan, S. M. Opalka, R. Mossadegh, S. N. Crichton
and A. J. Bruce
Center for Glass Science and Technology
Materials Engineering Department
Rensselaer Polytechnic Institute
Troy, NY 12180-3590, USA

ABSTRACT

Structural relaxation studies during annealing of a series of ZrF_4-based glasses below the glass transition temperature have been carried out. Indications are that no property changes due to structural relaxation are likely to occur at ambient temperature over periods of tens of years. Some of the lower Tg glasses, however, did exhibit detectable structural relaxation on annealing at temperatures as low as 100°C over roughly a one year time period.

1. INTRODUCTION

Heavy metal fluoride glasses (HMFG) are a fairly new class of materials which are currently receiving much attention because of potential uses as optical materials in the mid-IR. (1,2). Depending on composition, their IR transparency extends out to 6-9 μm, much further than silicate glasses, whose IR transparency stops at around 2-3 μm. The most widely characterized of the HMFG are those whose main component is ZrF_4. ZrF_4-based HMFG compositions, which are typical for these materials and which were characterized in this study, are listed in Table I, along with their glass transition temperatures Tg measured by differential scanning calorimetry (DSC) at a 10 K/min heating rate.

Table I. HMFG compositions (mol%) and glass transition temperatures.

Glass	ZrF_4	BaF_2	LaF_3	AlF_3	NaF	LiF	PbF_2	Tg(K)
ZBL	62	33	5	-	--	--	--	574
ZBLA	58	33	5	4	--	--	--	584
ZBLAN	56	14	6	4	20	--	--	536
ZBLALi	51	21	5	3	--	20	--	523
ZBLALiPb	50	17	5	3	--	20	4	513

Tg's for these glasses are fairly low - 240 to 311°C - with the alkali fluoride containing glasses having the lower Tg's. There thus exists the possibility that at ambient temperatures structural relaxation or physical aging of these glasses might cause their properties to drift over long periods of time. (See Refs. 3-10 for some recent articles on structural relaxation in glasses.) Slight changes in, for instance, refractive index over a period of years could lead to unacceptable changes in optical properties of extremely long fiber optic waveguides made from these materials. Such considerations prompted our studies of sub-Tg structural relaxation in HMFG.

2. SUB-Tg ANNEALING EXPERIMENTS

Our experimental approach has been described in detail in a report of some early results (9) and is illustrated schematically in Fig. 1. Briefly, samples of the glasses were rated cooled on the DSC at 10 or 100 K/min from above to well below the glass transition region. The samples were then annealed isothermally at temperature T_A well below Tg for times t_A ranging up to over one year. Following the isothermal anneal, the specific heats Cp were measured on the DSC at 10 K/min while reheating through the glass transition region. During this reheat the glass regains any enthalpy lost due to the earlier sub-Tg anneal, so that the Cp curves measured during reheating can be used to monitor the progress of enthalpy changes due to structural relaxation during sub-Tg annealing.

Typical DSC results are shown in Figs. 2 and 3. Figure 2 is characteristic of anneals carried out at temperatures a moderate distance (10-60 K) below Tg. The effect of annealing is to increase the magnitude of the Cp maximum in the main glass transition region and shift it to higher temperature. Figure 3 is characteristic of anneals carried out a fairly

large distance (100-140 K) below Tg. Here the effect of annealing shows up as an increase in Cp or even a small, extra Cp peak in the sub-Tg region just below the main glass transition region. Both of these results are in accord with predictions of the standard Tool-Narayanaswamy kinetic model for structural relaxation (3-10), which assumes that the relaxation process is non-linear and is controlled by a monotonic, single-peaked spectrum of relaxation times. The appearance of two peaks in the Cp reheating curve does not require a double-peaked spectrum of relaxation times and does not imply that there are two distinct relaxation mechanisms in the glass (6,7).

For purposes of analysis it is convenient to express the changes in enthalpy due to structural relaxation in terms of the time dependence of the fictive temperature T_f. T_f may be thought of as a measure of the average configurational enthalpy of the glass and is defined such that $T = T_f$ for a glass in the equilibrium state at temperature T (see Fig. 1). T_f is calculated from the experimental Cp data obtained during reheating via the following expression (3):

$$T_f = T^* + \int_{T^*}^{T<<Tg} [(Cp-Cpg)/(Cpe-Cpg)]dT \qquad (1)$$

where T* is a temperature above the glass transition region and Cpg and Cpe are respectively the glass and equilibrium liquid heat capacities. This calculation is illustrated in Fig. 4 for a ZBLA glass sample. T_f in this case is the fictive temperature reached by the glass immediately after cooling at 100 K/min through the transition region and would correspond to T_{fo} in Fig. 1.

3. RESULTS OF SUB-Tg ANNEALING EXPERIMENTS

Figure 5 shows typical results for ZBLA glass for the evolution of T_f with time during sub-Tg annealing at several temperatures T_A. Note from Fig. 4 that the initial fictive temperature at time t=0 obtained immediately after rate cooling through the glass transition region is approximately equal to Tg. For the sub-Tg anneal at the highest temperature the sample comes to equilibrium ($T_f = T_A = 575$ K) within one day. For annealing at the next two lower temperatures ($T_A = 472$ and 524 K) relaxation is slower but appreciable over a one year time period. However, the samples are still very far

from equilibrium after one year. At the lowest temperature (T_A = 376 K) some 210 K below Tg no detectable relaxation has occurred in nearly two years. Similar results are shown in Fig. 6 for ZBLALiPb glass. Note that with this glass a small but detectable change in T_f does occur on annealing for several months or longer at 376 K, as is also indicated directly in Fig. 3 by the effect of annealing on the Cp curves. Figure 7 compares the rates of sub-Tg relaxation following a 100 K/min cool of all five glasses of Table I at a common temperature T_A = 472 K. As expected, the glasses with the lowest Tg relax most rapidly.

4. ANALYSIS OF SUB-Tg RELAXATION CURVES

The Tool-Narayanaswamy model (3-10) for structural relaxation during isothermal annealing at temperature T_A gives for the time dependence of fictive temperature:

$$T_f(t) = T_A + \sum_{i=1}^{n} g_i[T_{fi}(0) - T_A]\exp[-\int_0^t dt/\tau_i(t)] \quad (2)$$

where the relaxation process is assumed to involve n relaxing order parameters, the contribution of each of which is governed by a weighting coefficient g_i and a relaxation time τ_i. A fictive temperature $T_{fi}(t)$ is associated with each of the order parameters, and the experimental fictive temperature $T_f(t)$ is the weighted average of these:

$$T_f(t) = \sum_{i=1}^{n} g_i\, T_{fi}(t) \quad (3)$$

$T_{fi}(0)$ in Eq. (2) is the initial fictive temperature (i.e., immediately after rate cooling) associated with the ith order parameter. The relaxation is non-linear, so that the relaxation times depend both on actual temperature T and average fictive temperature $T_f(t)$:

$$\tau_i(t) = A_i \exp[x\Delta H^*/RT + (1-x)\Delta H^*/RT_f(t)] \quad (4)$$

where A_i is a pre-exponential constant, ΔH^* the activation energy for structural relaxation, $x(0 \leq x \leq 1)$ the non-linearity parameter and R the ideal gas constant.

The activation energy ΔH^* can be determined from the dependence of the fictive temperature T_{fo} obtained immediately after rate cooling the glass on the cooling rate q (3,11):

$$d\ell n|q|/d(1/T_{fo}) = -\Delta H^*/R \qquad (5)$$

This is illustrated in Fig. 8 for ZBLA glass. In Table II are listed the structural relaxation activation energies obtained in this fashion for the glass samples of the present study. ΔH^* is generally found to be the same or very nearly the same as the activation energy ΔH^*_η for shear viscosity in the glass transition region (3). We have also listed in Table II values of ΔH^*_η obtained from beam bending measurements in our laboratory for two of the glasses. The agreement between ΔH^* and ΔH^*_η is within or nearly within experimental error. An apparent large discrepancy between ΔH^* and ΔH^*_η for ZBLA glass reported by Shelby et al. (12) has been found probably to be due to differences between their viscosity samples and our DSC samples (13). It has been suggested (11,14) that the decrease in ΔH^* or ΔH^*_η that occurs when alkali fluoride is incorporated into ZrF_4-based glasses is largely responsible for the improved stability of the alkali fluoride-containing compositions against devitrification.

ΔH^* for the HMFG is extremely large, so that at equilibrium ($T_f = T$) the relaxation times would change by an order of magnitude roughly every 5 K. That extensive relaxation can be observed in these glasses very far below Tg thus indicates that the relaxation is highly non-linear, i.e., that the relaxation times depend very strongly on T_f and that x in Eq. (4) is relatively small. (Hodge (7) has noted and rationalized a correlation between large ΔH^* and small x.) This high degree of non-linearity is apparent in the data of Figs. 5, 6 and 7. For example, during the ZBLA glass anneal at 524 K shown in Fig. 5 the relaxation is initially fairly rapid, and T_f drops about 6 K in the first day. Once this has occurred, however, the relaxation times via Eq. (4) are greatly increased, and a subsequent 6 K drop in T_f takes much longer - about 30 days.

A fit of the data in Figs. 5 and 6 along with analogous data for relaxation of ZBLA and ZBLALiPb glasses initially cooled at 10 K/min to Eq. (2) was carried out. The (g_i,τ_i) pairs in Eq. (2) were chosen to correspond to the well known KWW or stretched exponential relaxation function $\exp[-(t/\tau_0)^\beta]$ (8,15). Hence a fit to Eq. (2) requires the use of four adjustable parameters - β, A_0, ΔH^* and x. The last three of these determine the value of KWW relaxation time τ_0 for non-linear relaxation (4-6):

Table II. Activation energies ΔH^* for structural relaxation obtained from Eq. (5) and activation energies ΔH^*_η for viscous flow in the glass transition region.

Glass	ΔH^*(kJ/mol)	ΔH^*_η(kJ/mol)
ZBL	1430	-
ZBLA	1400	1150
ZBLAN	930	870
ZBLALi	1100	-
ZBLALiPb	1030	-

$$\tau_o(t) = A_o \exp[x\Delta H^*/RT + (1-x)\Delta H^*/RT_f(t)] \qquad (6)$$

The values of A_o and ΔH^* are fixed by the slope and intercept of the best fit line through the $\ell n|q|$ vs. $1/T_{fo}$ plot (4,5) (see Fig. 8), so that to fit data such as that in Figs. 5 and 6 one need only iterate on two parameters, x and β.

The fit to the sub-Tg annealing T_f vs. t data for ZBLA and ZBLALiPb glasses was carried out using procedures similar to those employed previously (4-6,8). The structural relaxation parameters are listed in Table III, and the solid curves in Figs. 5 and 6 were calculated from these parameters via Eq. (2). (That β and x are the same for the ZBLA and ZBLALiPb glasses may be fortuitous). Hodge (7) has compared the relaxation parameters A_o, ΔH^*, β and x for a variety of polymeric, organic and inorganic glasses and showed that there appear to be correlations among them, e.g., a high ΔH^* is generally associated with low values of ℓnA_o, β and x. Interestingly, the values of the relaxation parameters for the HMFG glasses in Table III fall fairly closely on Hodge's correlation lines.

The best fits to the data using the Tool-Narayanaswamy model are in general not within experimental error, as is particularly clear from Fig. 5 in which a wide range of sub-Tg annealing temperatures is covered. This is not surprising. Scherer (16), for instance, has recently analyzed sub-Tg annealing data for a soda-lime silicate glass and found that structural relaxation rates for rapidly cooled specimens at temperatures far below Tg were considerably faster than were predicted from fits to data at higher temperatures closer to Tg. Improvements in the semi-empirical Tool-Narayanaswamy model to allow accurate modelling and prediction of rates of structural relaxation

Table III. Best fit structural relaxation kinetic parameters for T_f vs. t curves obtained during sub-Tg annealing of ZBLA and ZBLALiPb glasses following rate cools at 10 and 100 K/min.

Glass	A_0(s)	ΔH^*(kJ/mol)	β	x
ZBLA	4.1×10^{-124}	1400	0.54	0.28
ZBLALiPb	2.8×10^{-103}	1030	0.54	0.28

over a wide range of times and temperatures is a currently active research area both at our laboratory and elsewhere.

5. CONCLUSIONS

In this study we have investigated the change in enthalpy H of HMFG during sub-Tg annealing. Of interest for fiber optic applications are changes in index of refraction. Refractive index n, which generally correlates linearly with density, does not and is not expected to relax at exactly the same rate as enthalpy (4,5,8). However, judging from results on oxide glasses (4,5,8), differences in the rates of relaxation of H and π appear to be relatively small - no more than a factor of 2 in the relaxation times. Hence one may conclude that any substantial drifts in enthalpy due to structural relaxation will be accompanied by substantial drifts in refractive index.

Lacking at the moment a good kinetic model for extrapolating rates of structural relaxation to low temperatures and long times, we can only make qualitative predictions based on the actual data of rates of drift of properties at use temperatures envisioned for HMFG. Inspection of the data for annealing at 376 K (= 103°C) indicates only minor structural relaxation over times of the order of a year for the lowest Tg, fastest relaxing glass - ZBLALiPb (see Figs. 3 and 6). Indications are thus that negligible long term structural relaxation and change of properties at ambient temperature are expected for any of the glasses of the present study. Given that more rapidly quenched glasses, e.g., optical fibers, relax more quickly than slowly cooled glasses (9,16), however, some of the low Tg HMFG might show some perceptible long term property drifts if use temperatures range up to the 100°C region. Likewise, IR transmitting glasses with substantially lower

Tg's ($\leq$ about 200°C) than those considered here are very apt to suffer from long term ambient temperature structural relaxation.

REFERENCES

1. Drexhage, M. G., in "Treatise on Materials Science and Technology", Vol. 26, M. Tomozawa and R. H. Doremus, Eds., Academic Press, New York, 1985, pp. 151-243.
2. Tran, D. C., Sigel, G. H. and Bendow, B., J. Lightwave Tech. LT-2, 566 (1984).
3. Moynihan, C. T., Easteal, A. J., DeBolt, M. A. and Tucker, J., J. Am. Ceram. Soc. 59, 12 (1976).
4. DeBolt, M. A., Easteal, A. J., Macedo, P. B. and Moynihan, C. T., J. Am. Ceram. Soc. 59, 16 (1976).
5. Moynihan, C. T. et al., Ann. NY Acad. Sci. 279, 15 (1976).
6. Hodge, I. M. and Berens, A. R., Macromolecules 15, 762 (1982).
7. Hodge, I. M., Macromolecules 16, 898 (1983).
8. Scherer, G. W., J. Am. Ceram. Soc. 67, 504 (1984).
9. Moynihan, C. T., Bruce, A. J., Gavin, D. L., Loehr, S. R., Opalka, S. M. and Drexhage, M. G., Polym. Engin. and Sci. 24, 1117 (1984).
10. Rekhson, S. M., J. Non-Cryst. Solids 73, 151 (1985).
11. Moynihan, C. T., Gavin, D. L., Chung, K.-H., Bruce, A. J., Drexhage, M. G. and El Bayoumi, O. H., Glastechn. Ber. 56K, 862 (1983).
12. Shelby, J. E., Pantano, C. G., and Tesar, A. A., J. Am. Ceram. Soc. 67, C-164 (1984).
13. Shelby, J. E., private communication.
14. Bansal, N. P., Bruce, A. J., Doremus, R. H. and Moynihan, C. T., J. Non-Cryst. Solids 70, 379 (1985).
15. Moynihan, C. T., Boesch, L. P. and Laberge, N. L., Phys. Chem. Glasses 14, 122 (1973).
16. Scherer, G. W., unpublished manuscript.

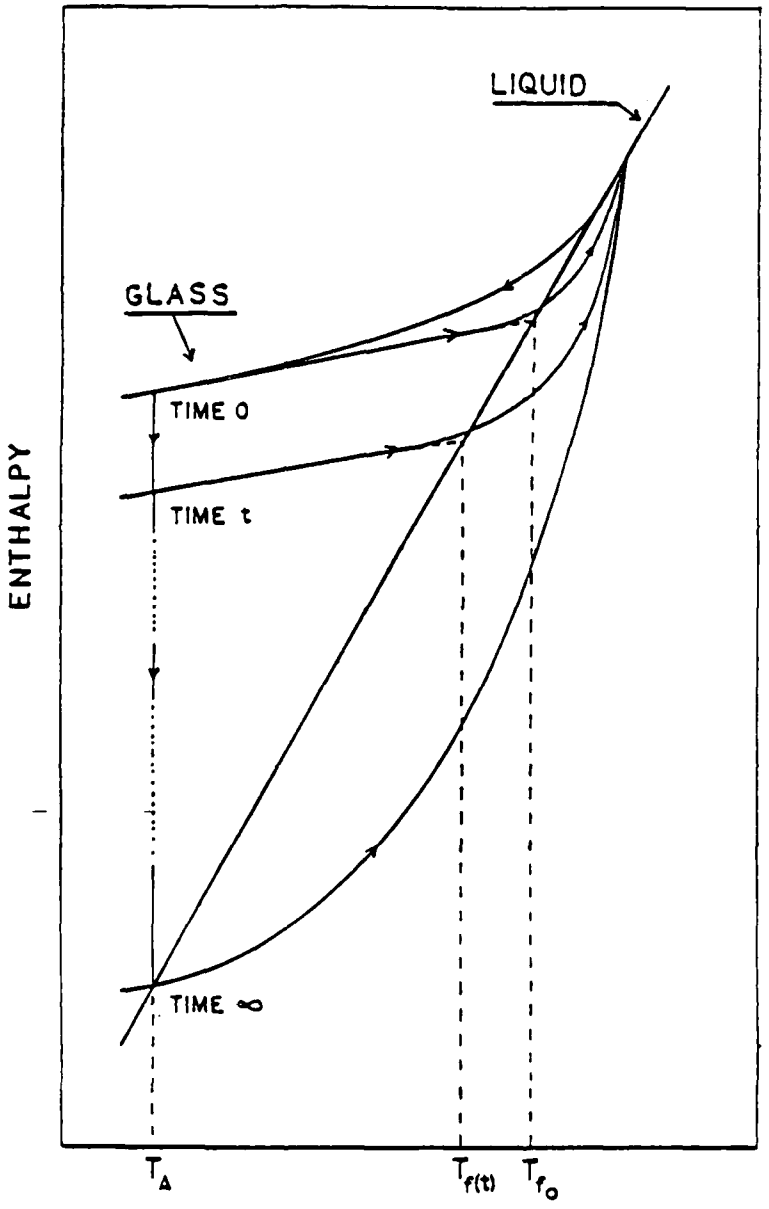

Figure 1. Schematic representation of the variation of enthalpy and fictive temperature during rate cooling through the glass transition region, sub-Tg annealing and rate heating through the glass transition region.

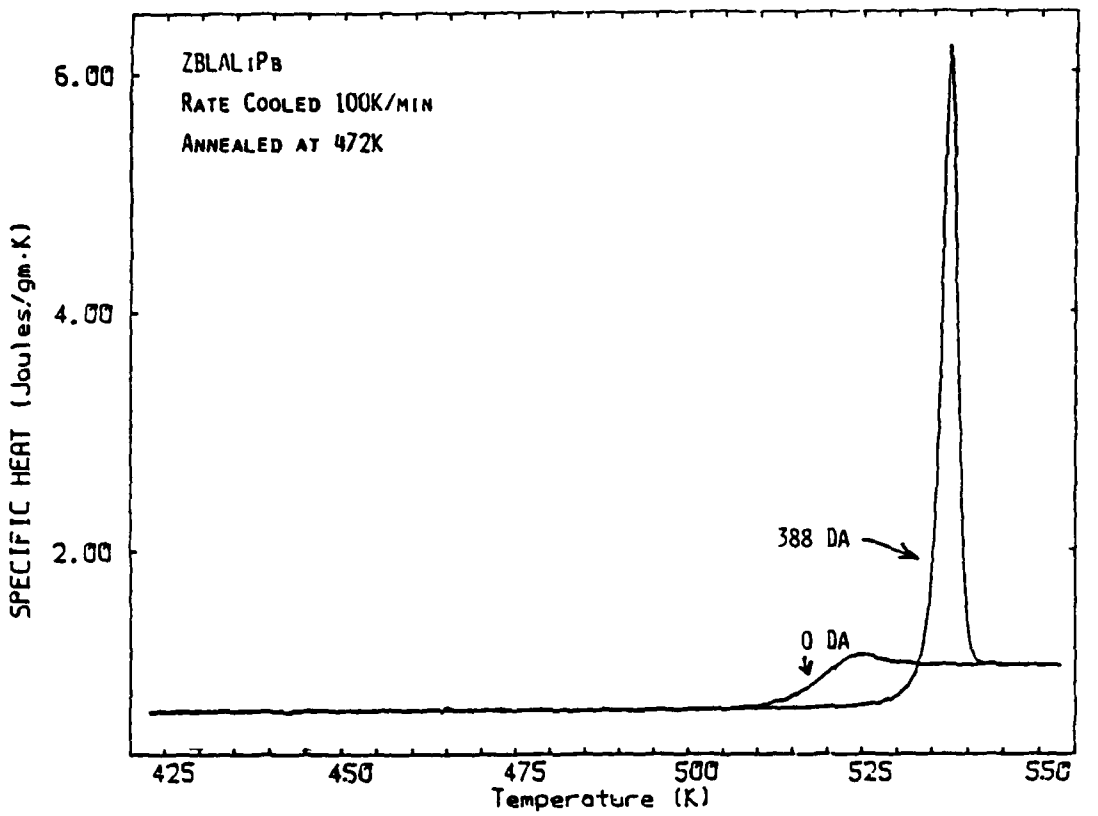

Figure 2. Specific heat measured at 10 K/min heating rate for ZBLALiPb glass following rate cool and sub-Tg anneal for times shown in figure.

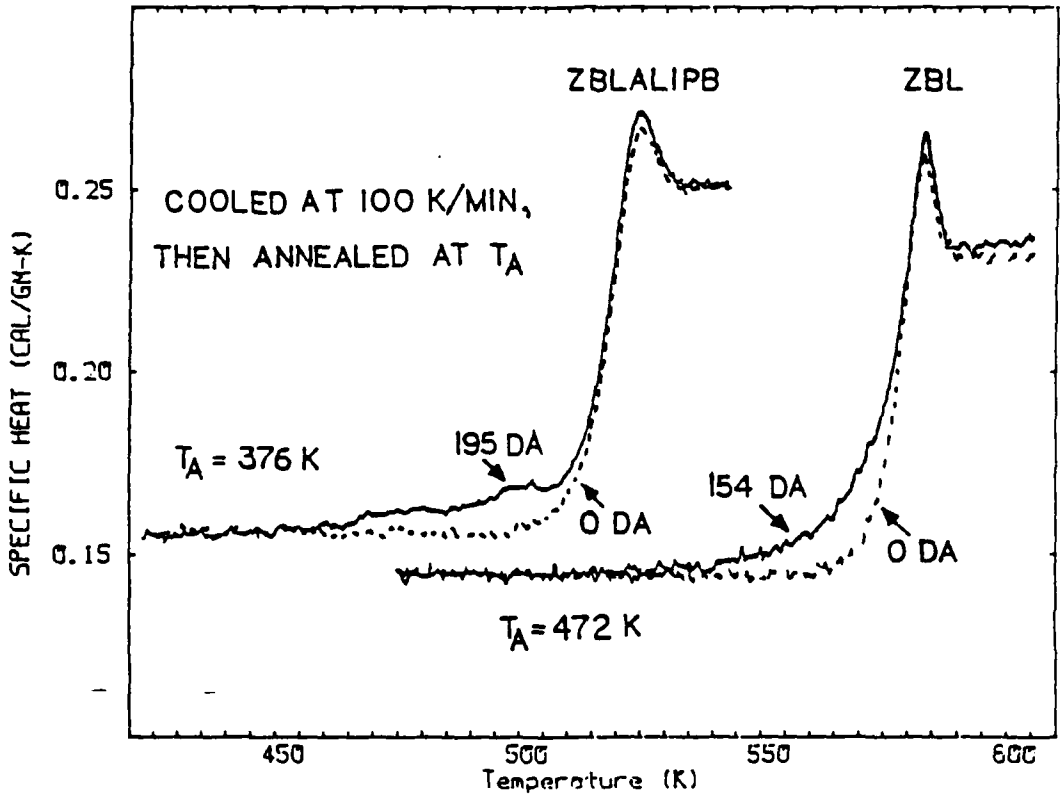

Figure 3. Specific heat measured at 10 K/min heating rate for ZBL and ZBLALiPb glasses following rate cool and sub-Tg anneal for times shown in figure.

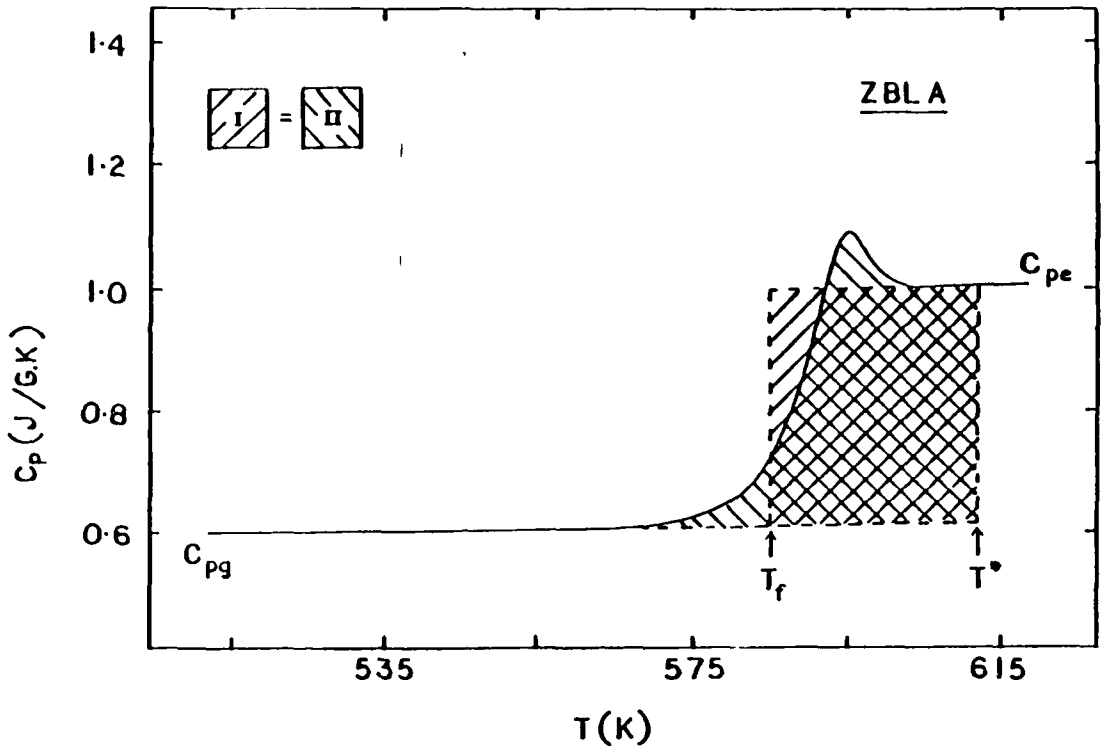

Figure 4. Illustration of fictive temperature calculation for ZBLA glass heat capacity data measured at a 10 K/min heating rate immediately following a 100 K/min rate cool through the transition region.

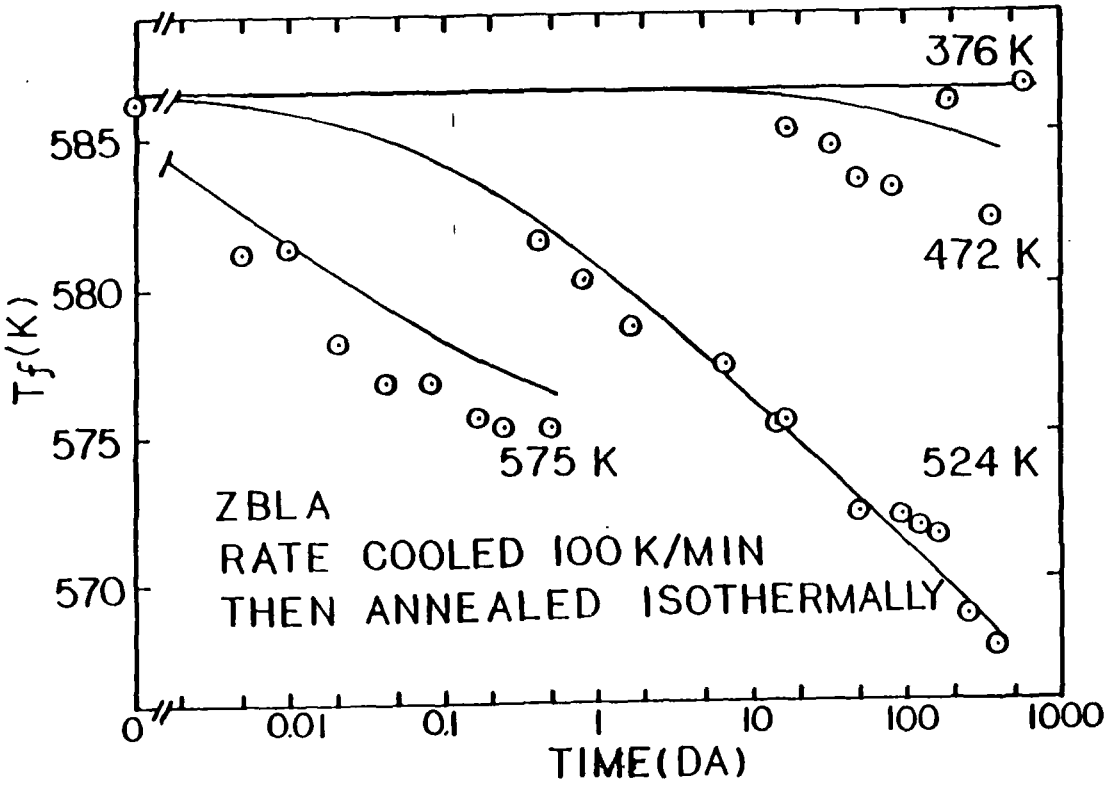

Figure 5. Evolution of fictive temperature of ZBLA glass during sub-Tg annealing following a rate cool at 100 K/min. Solid lines are calculated from parameters in Table III as described in text.

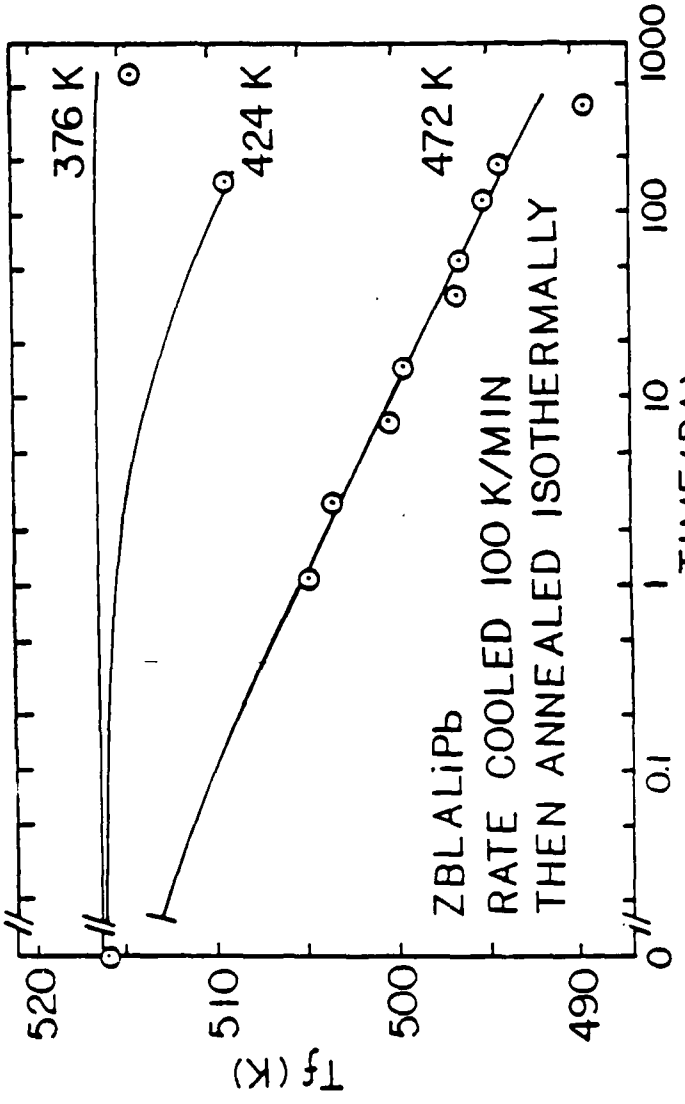

Figure 6. Evolution of fictive temperature of ZBLALiPb glass during sub-Tg annealing following a rate cool at 100 K/min. Solid lines are calculated from parameters in Table III as described in text.

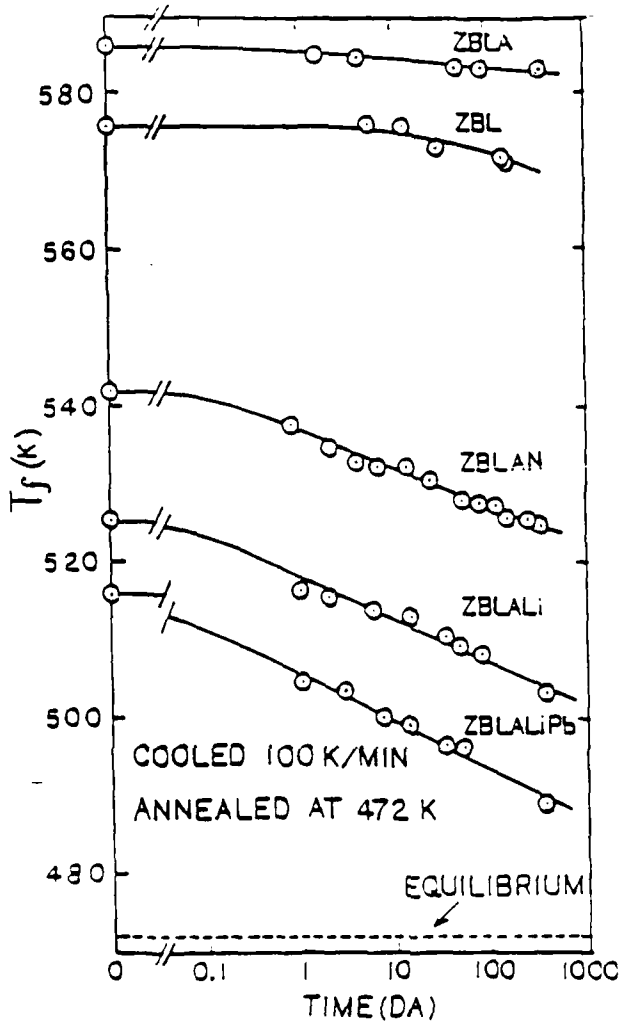

Figure 7. Evolution of fictive temperature of five glasses during sub-Tg annealing at 472 K following a rate cool. Solid lines are smooth curves drawn through the data points.

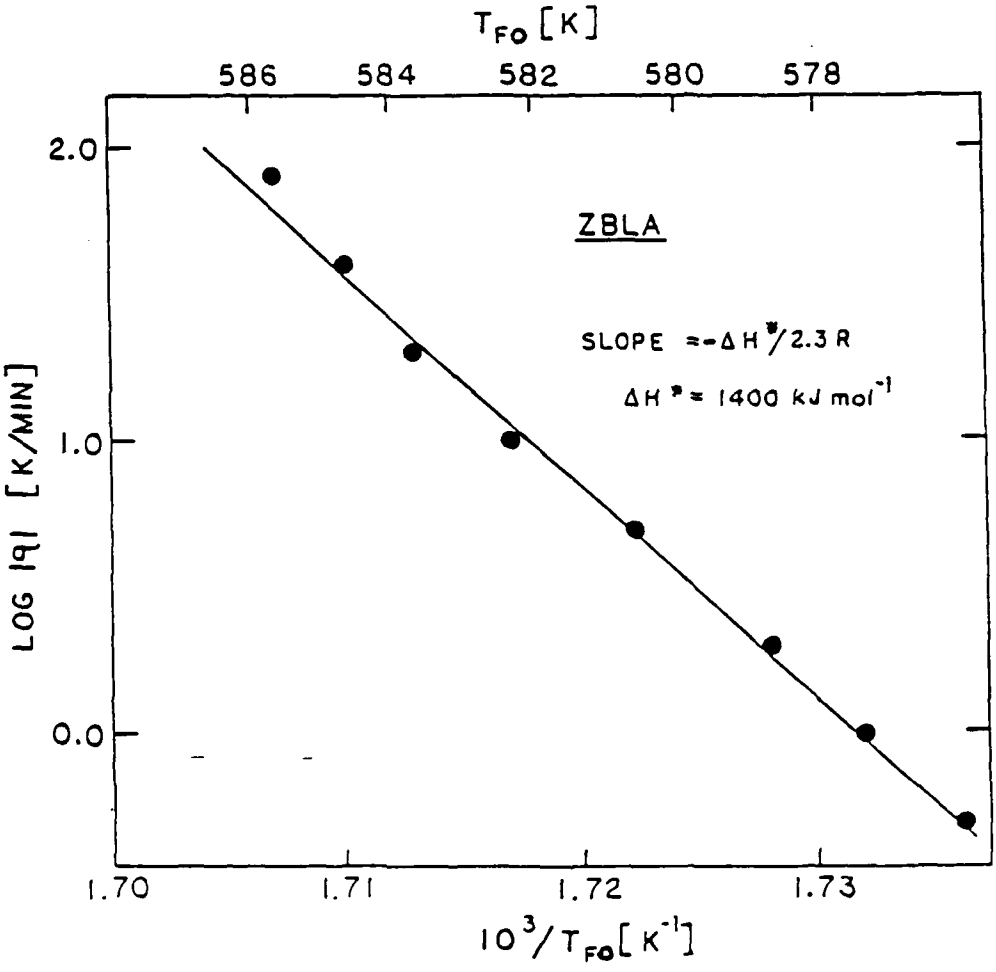

Figure 8. Logarithm of cooling rate |q| vs. reciprocal of fictive temperature T_{fo} for ZBLA glass.

RAYLEIGH AND BRILLOUIN SCATTERING IN HEAVY METAL FLUORIDE GLASSES

John Schroeder, Marsha Fox-Bilmont , Brian G. Pazol ,
Veneta Tsoukala
Physics Department, Rensselaer Polytechnic Institute,
Troy, New York 12181

Martin G. Drexhage, Osama H. El-Bayoumi
Rome Air Development Center, Hanscom Air Force Base, Massachusetts
01754

ABSTRACT

Heavy metal fluoride glasses are a recently synthesized class of non-oxide amorphous materials whose molecular structure, morphology and optical behavior is at variance from the more common and conventional oxide based glasses. This study will treat two specific classes of fluoride glasses; namely the fluorozirconates and fluorohafnates where the network formers are ZrF_4 and HfF_4, respectively, with modifiers being BaF_2 and fluorides of rare earths, group-III elements or alkalis. These glasses exhibit high transparency over a frequency range spanning the mid IR to the near UV. The primary goal of this study is to focus on the intrinsic Rayleigh scattering of these glasses. The principles of quasi-elastic and inelastic light scattering in glasses will be presented and discussed in great detail. The application of Rayleigh and Brillouin light scattering to various heavy metal fluoride glasses has resulted in valuable information on understanding the possible scattering mechanisms in these glasses. In addition, Brillouin scattering measurements allowed the calculation of the elastic and elastooptic (Pockels') coefficient of the same fluoride glasses. The full implications that the scattering behavior has on the possible fiber optic waveguide application of heavy metal fluoride glasses will be discussed. The physical significance of the elastic constants and elastooptic coefficients will also be considered on the basis of existing theoretical models.

INTRODUCTION

Heavy metal fluoride glasses are a recently synthesized class of non-oxide amorphous materials whose molecular structure, morphology and optical behavior is at variance from the more common and conventional oxide based glasses.[1] The compositional flexibility of these heavy metal fluoride glasses is such that glasses with a broad range of optical transmission, refractive index and magnetooptic characteristics can be produced.

Considerable work has been devoted recently in the preparation and characterization of these multicomponent heavy metal fluoride glasses, especially fluorozirconates[2] and fluorohafnates[3] where the network formers are ZrF_4 and HfF_4, respectively, with modifiers being BaF_2 and fluorides of rare earths, group-III elements or alkalis. These glasses exhibit high transparency over a frequency range spanning the mid IR to the near UV. This property alone makes them possible candidates for a wide variety of applications ranging from laser windows, infra-red transmitting windows to infra-red fiber optics.

Attenuation of light in a glass is brought about by several mechanisms. Fortunately, the different mechanisms may be isolated since they are not of equal magnitude at the same wavelength of the exciting light. Rayleigh scattering seems to dominate below 2000 nm. At longer wavelengths, absorption features, for example those of the OH^- ion dominate, and beyond 5000 nm multi-phonon absorption is many orders of magnitude larger than the Rayleigh scattering or the OH^- absorption. Hence, it is most important to understand the basic Rayleigh scattering

behavior of a glass if we wish to make predictions about its attenuation up to about 6000 nm and be able to reduce the scattering losses such that a fluoride glass could be employed as a suitable material for fiber optic applications.

THEORETICAL BACKGROUND

Rayleigh scattering in dense disordered materials is brought about due to microscopic fluctuations in the dielectric susceptibility about its equilibrium value. Consequently, the intenstiy of the scattered light is given by $I(\theta) \alpha \langle \delta \varepsilon_K^2 \rangle$ where $\langle \delta \varepsilon_K^2 \rangle$ is the k-th component of the mean square fluctuations of the dielectric constant. For a multi-component liquid it follows that the fluctuations in the dielectric susceptibility about its equilibrium value have the form,[4,5]

$$\langle \delta \varepsilon_k^2 \rangle = \left(\frac{\partial \varepsilon}{\partial \rho}\right)^2_{T,\{c\}} \left(\frac{\partial \rho}{\partial S}\right)_{P,\{c\}} \langle \delta S_{red}^2 \rangle + \left(\frac{\partial \varepsilon}{\partial \rho}\right)^2_{T,\{c\}} \left(\frac{\partial \rho}{\partial P}\right)_{S,\{c\}} \langle \delta P^2 \rangle + \sum_{j=1}^{n-1} \sum_{k=1}^{n-1} \left(\frac{\partial \varepsilon}{\partial c_j}\right)_{T,P,\{c'\}} \left(\frac{\partial \varepsilon}{\partial c_k}\right)_{T,P,\{c'\}} \langle \delta c_j \delta c_k \rangle \quad (1)$$

Where $\langle \delta P^2 \rangle$ represent pressure fluctuations which manifest themselves in sound waves. These are propagating fluctuations and they result in the inelastic scattering or Brillouin lines. $\langle \delta S_{red}^2 \rangle$ and $\langle \delta c_j \delta c_k \rangle$ are entropy fluctuations and concentrations fluctuations, respectively, with the former being caused by thermal diffusion and the later by mass diffusion. Both are diffusive modes, consequently they are non-propagating and will be found as quasi-elastic scattering or the Rayleigh line.

For a binary or pseudo-binary liquid the above equation for the fluctuations in the dielectric susceptibility reduces to the form[5]

$$\langle \delta\epsilon_k^2 \rangle \alpha \left(\frac{\partial \epsilon}{\partial \rho}\right)^2_{C,T} \langle \delta\rho_k^2 \rangle + \left(\frac{\partial \epsilon}{\partial c}\right)^2_{P,T} \langle \delta c_k^2 \rangle \qquad (2)$$

where we have contributions only from density and concentration fluctuations, respectively. The scattered intensity that one measures in a Rayleigh-Brillouin experiment is proportional to the mean square fluctuation in the dielectric susceptibility (i.e. $I(\theta) \alpha I_o < \delta\epsilon^2_K >$) and to carry over this formalism to a metastable high viscosity liquid one must introduce several additional parameters. Configurational temperatures that reflect the thermodynamic state of the system when structural rearrangement of the molecular configuration is no longer possible; namely, fictive temperatures, for both density fluctuation and concentration fluctuations; and compressibilities at very low frequencies and at very high frequencies are required. Once these concepts are introduced in equation (2), we may define a normalized intensity ratio, the Landau-Placzek ratio in the following way,[5]

$$R_\rho \equiv \frac{I_R(\rho)}{2I_B} = \frac{T_f}{T}(\rho\, V_L^2\, K_{T,o}(T_f) - 1) \qquad (3)$$

which is valid for Rayleigh scattering by density fluctuations only; and

$$R_c \equiv \frac{I_R(c)}{2I_B} = \frac{T_f'}{T} \frac{(\partial\epsilon/\partial c)^2_{P,T}}{(\rho \frac{\partial \epsilon}{\partial \rho})^2_{T,c}} \left(\frac{V}{N'}\right) \rho\, V_L^2 \left(\frac{\partial \mu}{\partial c}\right)^{-1}_{P,T} \qquad (4)$$

which represents the concentration fluctuations in the Rayleigh line.[5] Usually the total Landau-Placzek ratio is measured and the most

important quantities that appear in equations (3) and (4) are the fictive temperature for density fluctuations, T_f; the fictive temperature for concentration fluctuations T_f'; the isothermal compressibility at T_f, namely $K_{T,o}(T_f)$; and the derivative of the chemical potential with respect to the concentration, $(\partial\mu/\partial c)_{p,T}$.

The basic question that must now be addressed is how does one minimize the four basic quantities as given in equation (2) where the entire scattering problem is described by four basic parameters; namely, the mean square fluctuations of density and concentration, and the gradients of the dielectric susceptibility with respect to density and also concentration.

The Landau-Placzek ratio as defined in equations (4) and (5) involves Rayleigh scattered intensities and Brillouin scattered components. In Brillouin scattering for a given incident and scattered light direction in an isotropic solid, four possible scattered light components exist; namely, VV, VH, HV and HH. Here V denotes polarization perpendicular to the scattering plane and H polarization parallel to the scattering plane. For the case of 90° scattering, which is what is used in this work, the following equations give the Brillouin scattering cross section for scattering in glasses:[6]

$$\left(\frac{d\sigma}{d\Omega}\right)_{VV} = \varepsilon_o^4 \left(\frac{\omega_o}{c}\right)^4 \frac{VkT}{32\pi^2} \frac{P_{12}^2}{C_{11}} \tag{5}$$

$$\left(\frac{d\sigma}{d\Omega}\right)_{HH} = \varepsilon_o^4 \left(\frac{\omega_o}{c}\right)^4 \frac{VkT}{32\pi^2} \frac{P_{44}^2}{C_{11}} \tag{6}$$

$$\left(\frac{d\sigma}{d\Omega}\right)_{VH} = \varepsilon_o^4 \left(\frac{\omega_o}{c}\right)^4 \frac{VkT}{32\pi^2} \frac{P_{44}^2}{2c_{44}} \tag{7}$$

$$\left(\frac{d\sigma}{d\Omega}\right)_{HV} = \varepsilon_o^4 \left(\frac{\omega_o}{c}\right)^4 \frac{VkT}{32\pi^2} \frac{P_{44}^2}{2c_{44}} \tag{8}$$

Hence, the choice of polarization for the incident light and scattered light selects specific acoustic modes. The two sets of material constants, the elastic constants C_{ij} and the Pockels' elastooptic coefficients P_{ij} determine the Brillouin spectrum. P^2_{ij} determines the intensity of each line and C_{ij} the extent of the shift with respect to frequency from the incident light frequency.

From the Brillouin line shifts that are measured the sound velocity at hypersonic frequencies may be calculated and this is done with the Brillouin equation[7] in the form:

$$\frac{\Delta\nu}{\nu_o} = \pm 2\frac{n}{c} V(\omega_\mu, \hat{l}_k) \sin\frac{\phi}{2} \tag{9}$$

where V is the phase velocity, n and c the refractive index and speed of light, respectively and φ the scattering angle. For a glass the velocity is independent of the direction of propagation and only one longitudinal and one transverse acoustic branch exist. From equation (9) it is evident that measurement of the Brillouin shifts allows the calculation of the sound velocity provided that the refractive index of the material is known. By measuring the Brillouin intensities at the various polarization states the Pockels' elastooptic coefficients may also be determined. For a glass only P_{11}, P_{44} and P_{12} will be non-zero and $P_{11} = 2P_{44} + P_{12}$. Thus, a combination of Rayleigh and Brillouin scattering measurements and ultra-sonic sound velocity measurements allow one to fully predict the light scattering behavior of an isotropic glass by using equations (3) and (4).

EXPERIMENTAL ASPECTS

Raw materials were either obtained in anhydrous form or by fluoridation of the appropriate oxides. The anhydrous materials were further purified by sublimation to greater than 99.999% purity. The fluoridation was done via reaction with ammonium bifluoride. The starting materials were placed in a platinum or carbon crucible after being well mixed and were heated to ~ 900°C for several hours to insure complete melting. For some of them a reactive gas atmosphere such as CCl_4 was used in conjunction with an inert gas (N_2) to remove any OH^- present. Melting was accomplished for some of the samples by resistance heated furnaces and for others by RF-induction heated furnaces. After solidification the glasses were annealed. More details about the techniques used for the preparation of glasses can be found elsewhere.[8] Finally, the resulting samples with diameters of 1.5-3.5 cm and thicknesses of 1.0-2.0 cm were polished to obtain optically smooth surfaces.

The experimental apparatus used for Rayleigh-Brillouin scattering measurements will be found in figure 1. The exciting source is a single-mode Argon-ion laser operating at 488 nm coupled to a stabilized multi-pass high contrast Fabry-Perot interferometer with a photon counting detection system and associated data handling electronics. The entire Fabry-Perot is contained in a thermally stabilized box and the whole system (laser, interferometer, detector and optics) is mounted on a vibration isolated optical table. The detector consists of an ITT-FW 130 photo-multiplier tube with a photo-cathode that is cooled to -20°C. The dark count of this photo-multiplier tube in the cooled state is

persistently about 0.4 counts/sec and it has a quantum efficiency of 10% at 488 nm. The current generated by the photo-multiplier is shaped, amplified, discriminated and converted to counts/sec and the data of subsequent scans are stored in a 1024 channel multi-channel analyzer of the Burleigh DAS-1 system. This Burleigh DAS-1 system scans the Fabry-Perot and assures long-term stability of the interferometer by providing servo-control for the piezo-electric stacks of the Fabry-Perot. The scattering experiments reported here were done in a three-pass mode with mirrors of 93% reflectivity resulting in a finesse of about 80, a contrast of about 10^8 and the overall measured transmission was about 0.40. The high contrast of about 10^8 was especially important in being able to measure the transverse Brillouin lines in some of the strong scattering Heavy Metal Fluoride Glasses. The auxiliary parameters of refractive index and density were independently measured in ~~our~~ laboratory. The refractive index was measured by determining the angle of minimum deviation of a sample that had been immersed in some well characterized index matching oil (i.e. parafin oil, cyclo-hexane etc.), and from the measured angle the refractive index of the sample is calculated. The density was determined by an Archimedean technique where cyclo-hexane was the working fluid.

For the measurement all samples were immersed in water-free parafin oil in a glass scattering cell to minimize any parasitic scattering and also to protect the delicate surfaces from water vapor attack.

The primary quantities that are measured in this study are the Landau-Placzek ratio (a normalized Rayleigh intensity), the Brillouin intensities and the shift of the Brillouin lines.

RESULTS

Table IIa shows the results of the scattering loss measurements made at 488 nm, in terms of the Landau-Placzek ratio, for the Heavy Metal Fluoride Glasses. The Landau-Placzek ratio of SiO_2 is also given for comparison purposes.

One should note that some of the fluoride glasses show a scattering loss that is about equal or even less than the pure SiO_2 sample. For some of the fluoride glass samples the scattering loss in dB/km is also given.

The scattering loss in dB/km is calculated from a combination of Rayleigh and Brillouin data by the following scheme. The Brillouin scattering loss α_B is given by,[9]

$$\alpha_B = \frac{8\pi^3}{3} \frac{kT}{\lambda_o^4} (n^4 P_{12})^2 \frac{1}{\rho V_{L,\infty}^2} \tag{10}$$

and the Rayleigh scattering loss becomes

$$\alpha_S = \alpha_B (R_{L.P.} + 1) \tag{11}$$

where n, P_{12}, ρ, $V_{L,\infty}$, λ_o and T are refractive index, Pockels' coefficient, density, longitudinal velocity, laser wavelength and lattice temperature, respectively. To express the Rayleigh attenuation in dB/km one simply multiplies α_S by (-4.34×10^5).

In Figures (2) and (3) the Landau-Placzek ratio of the various samples is given as a function of either rare-earth dopant concentration (Figure 2) or concentration of Thorium-Fluoride (Figure 3). Both of these figures portray the large variations that exist in the Rayleigh scattering of the Heavy Metal Fluoride Glasses quite strongly. In each figure SiO_2 is given as the lower limit and note should be made that several of Heavy Metal Fluoride Glasses do approach this lower limit. Specifically, the glasses ZBLA-139, ZBrAEu-147, and HBLA-153 show this behavior. In the thoriated glasses as given by Figure (3) only one glass tends to approach the limit and that is BMDNT-357.

From the basic measurements of Brillouin shifts the sound velocities, longitudinal and transverse, are calculated and in turn give the elastic constants. The Brillouin shifts also allow the determining of Poisson's ratio by use of the following equation:

$$\sigma = \frac{(\Delta\nu_B^L)^2 - 2(\Delta\nu_B^T)^2}{2[(\Delta\nu_B^L)^2-(\Delta\nu_B^T)^2]} \qquad (12)$$

where $\Delta\nu_B^L$ and $\Delta\nu_B^T$ are the longitudinal and transverse Brillouin shifts, respectively. Table IIb and Table IIc summarize the elastic properties of some of the fluoride glass samples. In addition Table IIb contains some Verdet constants calculated from Faraday rotation measurements at two wavelengths. Table IIc gives Poisson's ratio for several of the

AD-A193 794 METAL HALIDE OPTICAL GLASSES(U) RENSSELAER POLYTECHNIC 2/2
INST TROY NY C T MOYNIHAN ET AL. JAN 88 RADC-TR-87-279
F19628-83-C-0016

UNCLASSIFIED F/G 11/2 NL

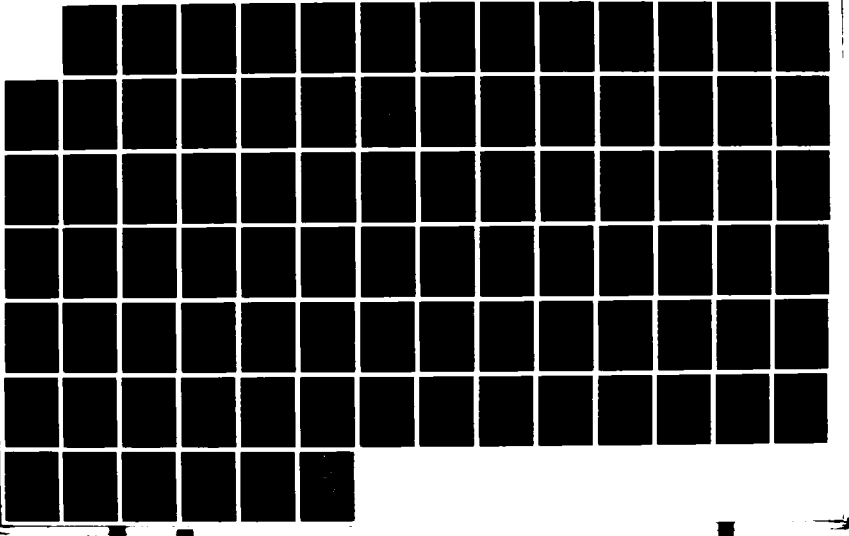

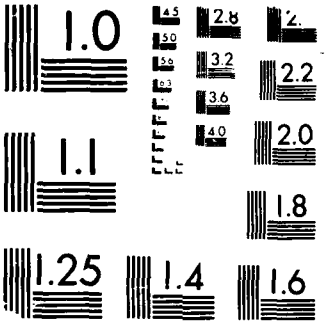

MICROCOPY RESOLUTION TEST CHART

fluoride glass samples and the measured value of Poisson's ratio of $\sigma = 0.30$ indicates that these glasses have a much more elastic structure (softer lattice) than the pure SiO_2 sample. The sound velocities also give an indication that in the fluoride glasses we are dealing with a less rigid lattice than in a typical silicate glass. The elastic constants of the fluoride glasses are of comparable size to the SiO_2 sample C_{11} and that is primarily caused by the much greater densities of the fluoride compared to the silicate glass.

The Brillouin intensities at the various polarization selections and Brillouin shifts coupled with the auxiliary parameters of density and refractive index give the Pockels' elastooptic coefficients for these glasses. The Pockels' coefficients are determined for Heavy Metal Fluoride Glasses with respect to the SiO_2 glass by the following equations:[6]

$$P_{12} = \left[\frac{I_B(VV)}{I_B(VV)_o}\right]^{1/2} \left[\frac{\Delta\nu_B^L}{\Delta\nu_B^L(o)}\right] \left[\frac{n(o)}{n}\right]^5 \left[\frac{\rho}{\rho(o)}\right]^{1/2} P_{12}(o) \qquad (13)$$

and

$$P_{44} = \pm P_{12} \left(\frac{V_{T,\infty}}{V_{L,\infty}}\right)\left[2\,\frac{I_B(VH)}{I_B(VV)}\right]^{1/2} \qquad (14)$$

In the above equations $I_B(VV)_o$, $\Delta\nu_B^L(o)$, $n(o)$, $\rho(o)$, $P_{12}(o)$ refer to the Brillouin intensity, Brillouin shift, refractive index, density and

Pockels' coefficient of SiO_2, while the same quantities without the zero designator refer to the actual sample parameters. In equation (14) $V_{T,\infty}$, $V_{L,\infty}$ are the transverse and longitudinal sound velocities, and (VH) and (VV) are the different polarization modes, as discussed in a previous section.

The Pockels' elastooptic coefficients are summarized in Figure 4. Here the P_{12} of the fluoride glasses show at most a linear dependence with refractive index. This is in contrast to a binary sodium-silicate glass that shows a higher order functional dependence of P_{12} on a refractive index. P_{44} changes extremely slowly as the refractive index changes, again atypical when compared with a silicate glass.[6]

The results of Figures (2) and (3) and also Table IIa show that a rather large variation in the Rayleigh scattering does exist between the various samples. The question that comes up is whether we are seeing a consistent effect or an effect due to the thermal history, or both. To examine this question more precisely Table III is given, where only one particular sample type (ZBLA) is examined for its light scattering behavior. On the basis of Table III it seems that the initial melting technique does play a dominant role in determining the amount of Rayleigh scattering in every sample.

DISCUSSION

The results presented above show that the Landau-Placzek ratio and in turn the scattering losses vary quite non-linearly with changes in compositions and several of Heavy Metal Fluoride Glasses exhibit less Rayleigh scattering than the best available SiO_2 glass. Let us first

examine the effect of concentration fluctuations on the Landau-Placzek ratio. From equation (4) the contribution to the Rayleigh scattering intensity can be written as

$$R_{L.P.}(c) \propto \left(\frac{\partial \varepsilon}{\partial c}\right)^2_{P,T} \langle \delta c_k^2 \rangle \qquad (15)$$

On the basis of measured values of the refractive index as a function of concentration noting that $\varepsilon = n^2$ for a transparent isotropic solid, it can be asserted that ε is at most a slowly varying monotonic function with concentration thereby $(\partial\varepsilon/\partial c)$ must also change slowly with concentration. In the Heavy Metal Fluoride Glasses it has not been established that any metastable liquid-liquid immiscibility domes exist at elevated temperatures, consequently any anomalous scattering due to the disappearance of $(\partial\mu/\partial c)$ may not be a predominant factor. Unless immiscibility domes can be found, the scattering intensity due to pure concentration fluctuations is expected to be small.

It is to be noted that the general bonding picture for fluoride glasses does not allow for a metastable immiscibility dome since covalent or mixed ionic and covalent bonding is required. The fluoride glasses seem to be mostly ionic bonded solids as one may ascertain from the measured Poisson's ratio data.

The Rayleigh scattering that is observed in some of the fluoride glass samples, at least the ones that show the lowest scattering, may solely be attributed to density fluctuation scattering. From equation (3) the contribution to the Rayleigh scattering intensity from

microscopic density fluctuations is given by,

$$R_{L.P.}(\rho) \propto T_f \, K_{T,o}(T_f) \qquad (16)$$

If we compare oxide glasses to fluoride glasses one sees that although the compressibility is greater for the fluoride glass than the oxide glass the configurational temperature, T_f, is much smaller for the fluoride glass with respect to the oxide glass. Consequently, the scattering that some of fluoride glasses exhibit is only goverened by the magnitude of the microscopic density fluctuations, at least for these fluoride glasses that are comparable in Landau-Placzek ratio values to the best silicate glasses.

So the question remains to what mechanism may we attribute the large changes of the Landau-Placzek ratio with concentration and also thermal history. It has been observed in some of our work that the scattering increases with long time annealing of samples held just at the glass transition temperature. These particular glasses also showed an increase in the depolarized scattering. Density fluctuations (and/or concentration fluctuations) in an isotropic medium can produce only diagonal elements in the polarizability tensor, consequently the scattered light is in the same direction as the incident light. However, in a glass where one has non-spherical molecules (or molecular groups) the scattering behavior can show considerable depolarization of the scattered light indicating the presence of off-diagonal elements in the polarizability tensor.[10,11] Thus, the depolarized scattering increase is certainly evidence that the isotropic system is slowly

changing to a anisotropic system and one possibility could be nucleation and growth and eventual devitrification. If devitrification has started the crystal grains will act as additional scattering centers and if they become very dense then multiple scattering will set in. In some of these large magnitude scattering samples multiple scattering does seem to be the predominant extrinsic scattering mechanism.

Hence, the scattering in fluoride glasses with low intrinsic Rayleigh scattering losses is predominantly determined by a mechanism based on microscopic density fluctuations where scaling may be used to predict the intrinsic loss behavior at the infra-red wavelengths.[12] On the basis of the λ^{-4} scaling, some of the heavy metal fluoride glasses with low Rayleigh scattering losses are prime optical wave guide material for the near infra-red regime.[13]

The samples that show a large quasi-elastic scattering, most likely Mie scattering and/or multiple scattering, do not obey the λ^{-4} scaling. Multiple scattering or stochastic scattering follows a wavelength dependence of λ^{-n} where $n < 4$.[18] Consequently, their scattering behavior will be much worse at the infra-red wavelengths than those that obey normal Rayleigh scattering.

Up to now the question of intrinsic Rayleigh scattering has been addressed by measurements taken on bulk glasses. Is this a realistic representation of the scattering losses in an optical fiber waveguide, where the actual core dimensions are about 50μm to 100μm in diameter? When probing a bulk glass by light scattering, in essence, one looks at a scattering volume that is a small cylinder of dimensions equivalent to

an optical waveguide fiber. Typically, if the optical system is worked at the diffraction limit, the experiment uses a scattering volume made up of a cylinder that has a diameter of about 27μm and a length of about 4.8 mm. Hence, the scattering volume is even somewhat smaller in diameter than a single mode optical fiber. To gain more insight into these aspects we performed several experiments where a bulk fluoride glass sample and an actual bare fluoride glass optical waveguide were examined by Rayleigh-Brillouin scattering methods to give the intrinsic Rayleigh scattering for each sample configuration. A hard focussed, single frequency singe mode laser beam was launched into one end of the freshly cleaved optical fiber. The scattering volume that was selected in this experiment had dimensions on the order of about 25 μm in diameter and 125μm in length, as selected by employing a spatial filter in the collecting optics that used very small pinholes. The scattered light that was emitted from the core section of the optical fiber was collected in a pure VV mode at a 90° scattering angle and then analyzed by our standard techniques. Comparing the measured Landau-Placzek ratios for fiber optic waveguide core material with bulk sample measurements we find the interesting but expected result that both sample configuratons give values of the Landau-Placzek ratio that agreed with each other within fluctuations of about ± 20%. The specific optical fiber that was used in the measurement came from British Telecommunication Inc. and had a core composition equivalent to our ZBLA glass.

Hence, we conclude from the experiment that considered both configurations of samples, bulk and optical fiber waveguide, that either measurements will give compatible results and investigating bulk samples is indeed a realistic method of determining the ultimate low intrinsic Rayleigh scattering level in a material that will be used for fiber optic waveguides.

The elastic and elastooptic properties of the fluoride glasses exhibit substantial differences from oxide glasses as is seen in Table IIb and IIc and Figure (4). The longitudinal and transverse velocities in the fluoride glasses are about two-thirds of their counterpart in SiO_2 glass. The Poisson's ratio of the fluoride glasses seems to be in the range of 0.25 to 0.31 whereas SiO_2 shows this ratio to be 0.166.

Basically, the higher Poisson's ratio may come about since most of the bonds are ionic as compared to SiO_2 which is predominantly covalent. Central force fields seem to be the predominant effect in the fluoride glasses when the Poisson's ratio is about 0.25.[14,15] Larger values of the Poisson's ratio may arise if in addition to network distortion, the ions in the network are also deformed.[14] This, of course, is possible if the system shows a high coordination number or if a system that is initially tetrahedrally coordinated is compressed to very high densities.[16,17] The fluoride glasses fall into the category of being highly coordinated solids. Thus, the fluoride glasses should also show a relatively low value of the transverse Brillouin shift (or transverse sound velocity) with respect to the tetrahedrally coordinated SiO_2, and this is exactly what is observed since the high coordination number of the fluoride glasses inhibit transverse vibrations in these glasses.

The Pockels' elastooptic coefficients of the fluoride glasses also showed differences from the oxide glasses. The transverse P_{44} coefficients were rather small in most cases and difficult to measure. On the basis of equation (7) or (8) the Brillouin scattering cross section is proportional to the transverse coefficient squared. If this coupling coefficient is small then the Brillouin cross section will be very small and difficult to resolve. The high coordination number of the fluoride glasses again influence the elastooptic properties.

CONCLUSION

We have successfully measured the intensity and spectral distribution of the various Heavy Metal Fluoride Glasses. Some of the Heavy Metal Fluoride Glasses exhibit less Rayleigh scattering than the best SiO_2 glass. The Rayleigh scattering depends to a great extent upon the melting rate and on the subsequent cooling rate during the sample preparation process. The relatively low value of the transverse Brillouin shifts for the fluoride glasses are due to the higher coordination number of this material compared to oxide glasses. The high coordination number inhibits transverse vibrations in fluorides that normally dominate the elastic and elastooptic behavior of tetrahedrally coordinated glasses. Mulitple scattering is the predominant extrinsic scattering mechanism. On the basis of λ^{-4} scaling, some heavy metal fluoride glasses with low Rayleigh scattering losses are prime optical wave guide material for the near infra-red regime.

REFERENCES

1. M.G. Drexhage et al. Advances in Ceramics, Vol. II: Physics of Fiber Optics. B. Bendow and S. Mitra, editors. Amer. Cer. Soc., Columbus, Ohio, 1981, P. 57-73.
2. B. Bendow et al. J. Appl. Phys. 52, 1460 (1981).
3. B. Bendow et al. Sol. State Comm. 37, 485 (1981).
4. J. Schroeder et al. J. Amer. Cer. Soc. 56, 510 (1973).
5. J. Schroeder, Treatise on Material Science and Technology, Vol. 12, Edit. by M. Tomozawa and R.H. Doremus. Academic Press, NY, 1977, pp. 157-222.
6. J. Schroeder, J. Non-Crystalline Solids 40, 549 (1980).
7. L. Brillouin, Ann. Phys. (Paris) 17, 88 (1922).
8. M.G. Drexhage, C.T. Moynihan and M. Saleh-Boulos, Mat Res. Bull. 15, 213 (1980).
9. J. Schroeder, R.K. Mohr, C.J. Montrose, P.B. Macedo J. Non-Cryst. Solids 13, 313 (1973-74).
10. W. Hayes, R. Loudon, "Scattering Light by Crystals", John Wiley and Sons, Inc. 1978, NY.
11. R.D. Maurer J. Chem. Phys. 25, 1206 (1956).
12. J. Schroeder et al., Electronic Letters, vol. 20, p. 860-862 (1984).
13. D.C. Tran, G.H. Sigel, K.H. Levin and R.J. Ginther, Electronic Letters, vol. 18, p. 1046-1048 (1982).
14. M.P. Brassington, Tu Hailing, A.J. Miller and G.A. Saunders Mat. Res. Bull. 16, 613 (1981).
15. R. Ota and N. Soga J. of Non-Cryst. Solids 56, 105 (1983).

16. J. Schroeder, K.J. Dunn, F.P. Bundy and L. J. Schowalter Phys. Rev. B. in Press.

17. J. Schroeder, K.J. Dunn and F.P. Bundy, Proc. of the 8th AIRAPT Conference Uppsala, Sweden, Edit. by C.M. Backman. T. Johannisson and L. Tegner, pp. 259-267 (1982).

18. H.C. Van de Hulst, "Light Scattering by Small Particles", Wiley, New York, (1957), "Multiple Light Scattering", vol. 1, vol. 2, Academic Press, New York (1980).

Table I summarizes the constituents of the seventeen fluoride glass samples used in this study and identifies each glass.

Table I. Selected Heavy-metal Fluoride Glass Compositions in Mole %

Glass #	ZrF_4	BaF_2	LaF_3	Alf_3	HfF_4	PrF_4	HoF_3	Euf_3	NaF
ZBL-SI-11	62	33	5	-	-	-	-	-	-
ZBLA-139	57	36	3	4	-	-	-	-	-
ZBLA-129	57	36	3	4	-	-	-	-	-
HBLA-153	-	36	3	4	57	-	-	-	-
HBLA-148	-	36	3	4	57	-	-	-	-
ZBLA-131	57	34	3	4	-	2	-	-	-
ZBLAH-144	57	34	3	4	-	-	2	-	-
ZBLAEu-147	57	34	3	4	-	-	-	2	-
HBLAP-286	-	34	3	4	57	2	-	-	-
HBLAH-287	-	34	3	4	57	-	2	-	-
HBLAEu-240	-	34	3	4	57	-	-	2	-
ZBLAN-428	55.7	14.4	5.8	4	-	-	-	-	20.1

Glass #	BaF_2	NaF	AlF_3	HoF_3	ZuF_2	LaF_3	ThF_4	YbF_3	MnF_2	DyF_3
BZLT-268	19	-	-	-	27	27	27	-	-	-
BZYbT-265	19	-	-	-	27	-	27	27	-	-
BMDNT-357	9.5	5	-	-	-	-	38	-	38	9.5
BMAYT-384	8.5	-	5	-	-	-	34	10	42.5	-
BMHT-335	10	-	-	8	-	-	40	-	42.0	-
BMYT-382	9	-	-	-	-	-	36	10	45.0	-

Table IIa Landau-Placzek Ratio and Scattering Attenuation Coefficients for Heavy Metal Fluoride Glasses at 488 nm and at 300°K

Glass #	Landau-Placzek Ratio	Scattering Loss (dB/km)
ZBLA-139	22.1	4.00
ZBLA-129	838.0	195
HBLA-153	26.7	10.94
HBLA-148	78.8	33.00
ZBLAP-131	201	-
ZBLAH-144	341	-
ZBLAEu-147	36.4	8.00
HBLAP-286	2112	-
HBLAH-287	2059	-
HBLAEu-240	543	-
ZBLAN-428	16.9	-
BZLT-268	549	87.6
BZYbT-265	1276	-
BMDNT-357	44.5	13.5
BMAYT-384	147	12.4
BMHT-335	11690	-
BMYT-382	1098	-
SiO_2	21.9	11.6

Table IIb Longitudinal Sound Velocity, Elastic Constant (C_{11}) and the Verdet Constants for Some Selected Heavy Metal Fluoride Glasses

Glass #	$V_{L,\infty}$ (m/s)	C_{11} (GPa)	Verdet Constant (min/cmG) (442 nm)	(632.8nm)
ZBLA-139	4026	74.7	0.0137	0.0073
ZBLA-129	4231	82.5	0.0161	0.0071
HBLA-153	3615	76.9	0.0145	0.0059
BHLA-148	3680	79.6	0.0134	0.0098
ZBLAEu-147	4218	82.0	0.0146	0.0061
BZLT-268	3707	88.6	0.0302	0.0114
BMDNT-357	4090	107.9	-0.0519	-0.0143
BMAYT-384	4175	112.4	0.0048	0.0121

Table IIc Sound Velocities (Longitudinal and Transverse) Elastic Constants (C_{11},C_{44}) and Poisson's Ratio (σ) of Some Selected Heavy Metal Fluoride Glasses and SiO_2

Glass #	V_L(m/s)	V_T(m/s)	C_{11} (GPa)	C_{44} (GPa)	σ
ZBLA-139	4026	2333	74.7	25.1	0.250
ZBLAEu-147	4218	2384	82.0	26.2	0.265
Fluorozirconate*	3980	-	76.1	23.2	0.279
SiO_2	5944.2	3748.7	79.0	30.97	0.166
ZBLAN-428	-	-	-	-	0.31
ZBL	-	-	-	-	0.30

Table III. Landau-Placzek ratio and scattering attenuation coefficients (some of this data is from reference (14)) for a particular class of Heavy metal fluoride glasses: the ZBLA series; at 488 nm and 300K°.

Sample #	Remarks	Landau-Placzek Ratio	Loss (Scattering) (dB/km)
ZBLA-SI-1	Slow melting in closed induction furnace.	34.5	6.15
" " 3		13.8	2.56
" " 4		13.0	2.42
" " 5		35.4	6.30
" " 7		30.4	5.44
ZBLA-SI-10	Rapid melting in closed induction furnace.	48.1	8.50
" " 11		16.7	3.06
" " 12		24.0	4.33
" " 13		25.9	4.66
" " 14		16.5	3.03
" " 15		32.7	5.84
ZBLA-550	Cullet - open pot melting	39.3	6.98
ZBLA-CH-4	Remelt of ZBLA-550	74.6	13.09
ZBLA-1019	Conventional melting technique used	5661	980.43

Note: All samples were rate cooled at ~ 144°C/min.

Figure 1. Schematic of Rayleigh-Brillouin Scattering Apparatus.

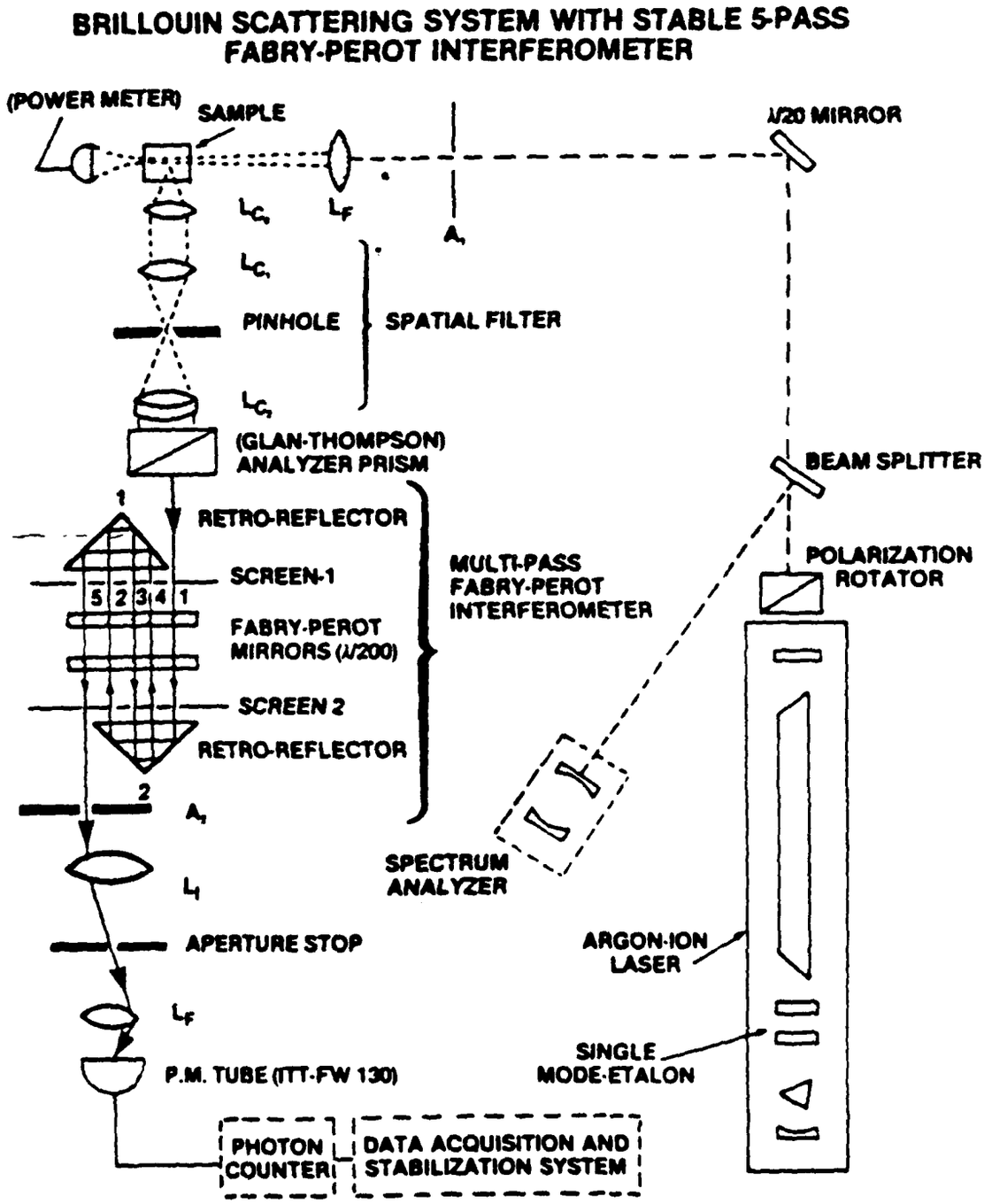

Figure 2. Landau-Placzek ratio of Heavy metal fluoride glasses versus dopant concentration with sample identification given as 57Mo[36-X] BaF_2 • $3LaF_3$ • $4AlF_3$ • X {PrF_3, HoF_3, EuF_3.}

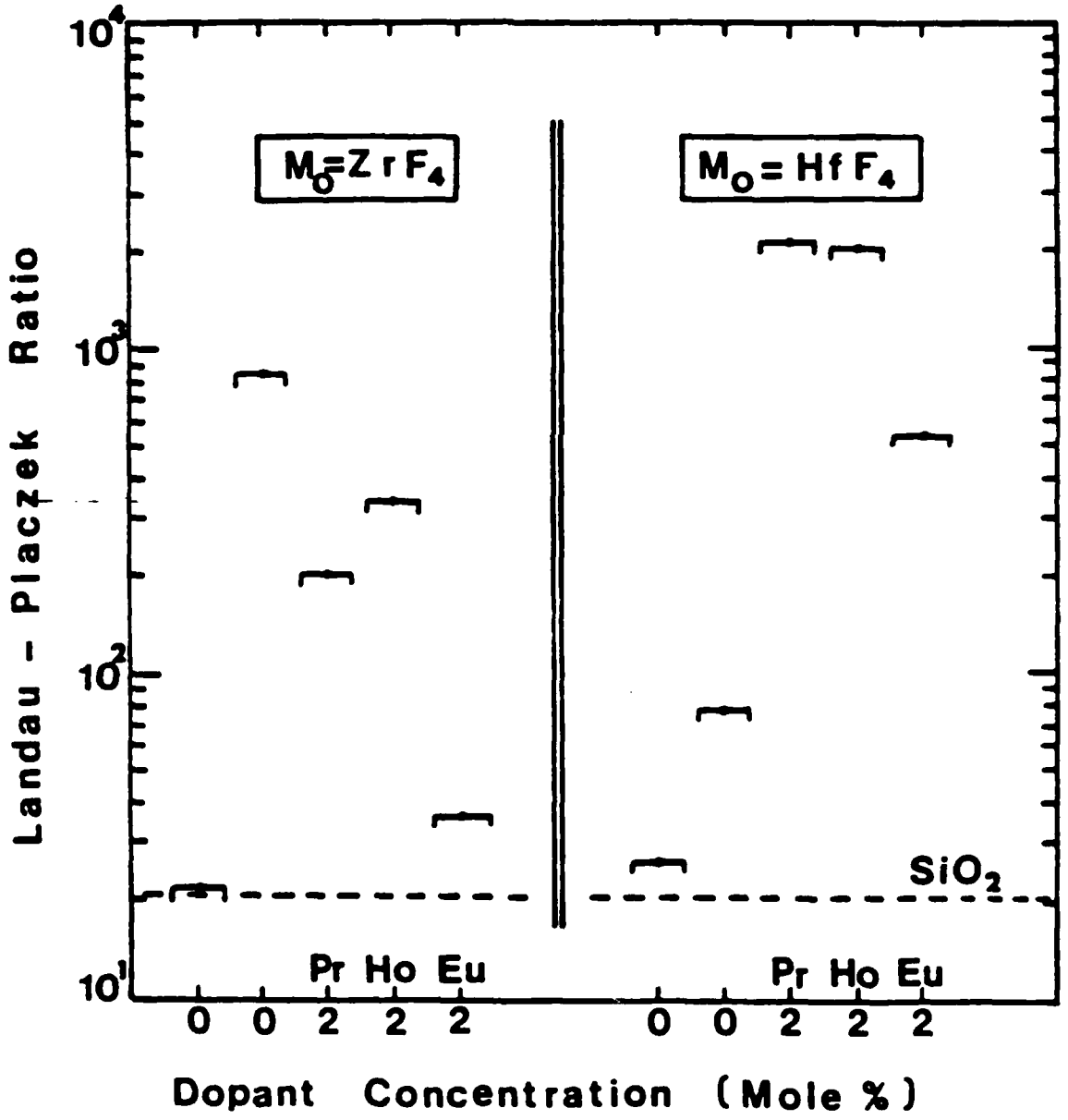

Figure 3. Landau-Placzek ratio of Thoriated Fluoride Glass versus Thorium fluoride concentration. The total formulation is given as $BaF_2 \cdot ThF4$ {ZnF_2, MnF_2} {LuF_3, YbF_3, DyF_3, HoF_3}.

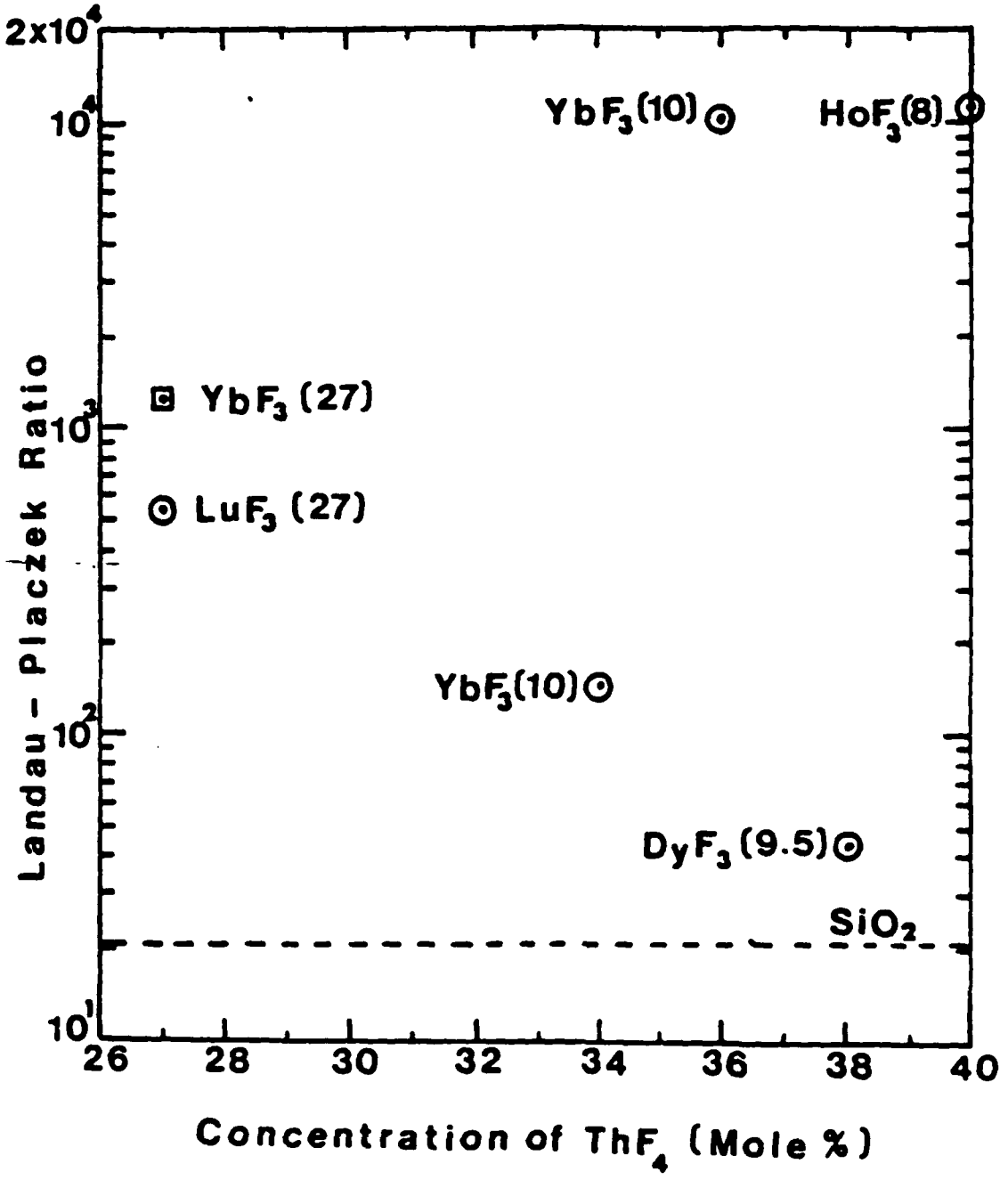

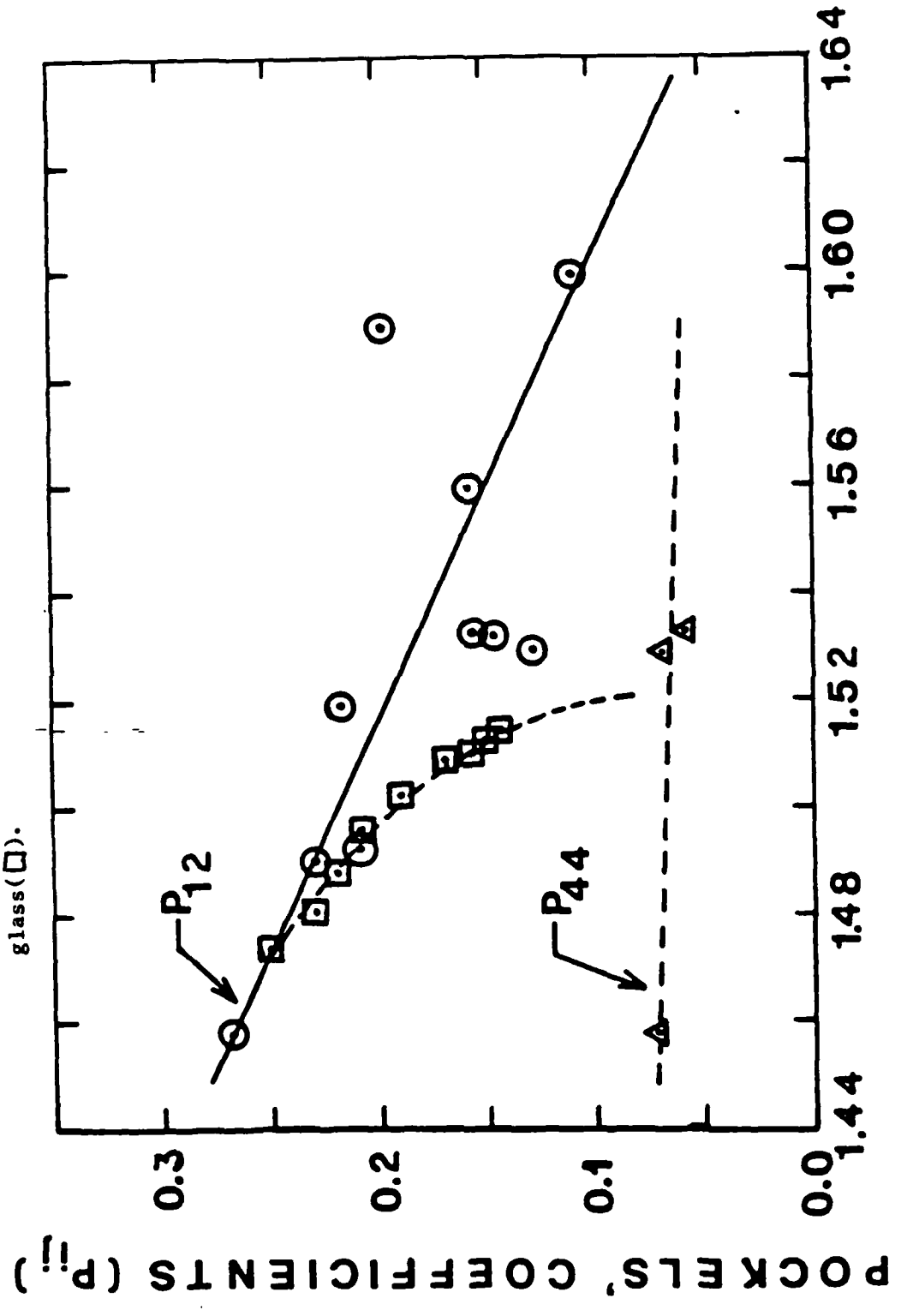

Figure 4. Pockels' elastooptic coefficients versus refractive index for heavy metal fluoride glasses (o , Δ) and a binary $Na_2O \cdot SiO_2$ glass(□).

HEAVY METAL FLUORIDE GLASSES WITH LOW INTRINSIC RAYLEIGH SCATTERING

John Schroeder, Veneta Tsoukala, Craig O. Staller, Marc A. Stiller, Physics Department, Rensselaer Polytechnic Institute, Troy, NY, 12181, USA

Allen Bruce, Cornelius T. Moynihan, Materials Engineering Department, Rensselaer Polytechnic Institute, Troy, NY 12181, USA

Joseph J. Hutta, Michael J. Suscavage and Martin Drexhage, Solid State Sciences Division, Rome Air Development Center, Hanscom AFB, Massachusetts, 01754, USA

ABSTRACT

The results of Rayleigh light scattering measurements in bulk multicomponent fluorozirconate glasses are described. We observe for the first time that such materials may be reproducibly prepared with uniformly low scattering levels throughout their volume. In 13 of the 15 specimens studied, the magnitude of the Rayleigh scattering loss was one-third to one-half that typically observed in fused silica glass.

Introduction: Heavy metal fluoride glasses (HMFG) are a family of potentially useful optical materials which exhibit a minimum in optical absorption in the 2-4 μm spectral region. Three major loss mechanisms govern the attentuation of HMFG in the mid-infrared regime: light scattering, multiphonon absorption, and losses due to extrinsic impurities such as transition metals, rare earths and hydroxyl species(1). Multiphonon absorption becomes improtant above 4 μm and impurity bands may be reduced through careful attention to raw materials and glass processing, thus leaving the intrinsic Rayleigh scattering as the limiting mechanism for light attentuation in the mid-IR. It has been demonstrated that the scattering loss in HMFG rods and fibers does indeed obey the λ^{-4} dependence demanded by the Rayleigh scattering law, thus allowing measurements made in the visible region to be projected into the infrared(2,3). Moreover, theory suggests that, on the basis of their material properties (e.g., low glass transition temperature T_g), the magnitude of the scattering losses in HMFG should be considerably lower than those observed in silica-based glasses(4,5). We report here the first experimental verification of the latter contention, and show that relatively large samples of fluoride glasses may be repeatedly synthesized with a high degree of homogeneity and optical isotropy such that intrinsic scattering losses may be held to very low levels.

Synthesis: Glasses of composition (in mole %) $57ZrF_4$-$36BaF_2$-$3LaF_3$-$4AlF_3$ ("ZBLA") were prepared from BaF_2 (EM Laboratories "Optipur"), LaF_3 (Alfa-Ventron, 99%), AlF_3 (Cerac, 99.5%) and ZrO_2 (Alfa-Ventron, 99%). The latter was converted to a fluoride via reaction with ammonium bifluoride and subsequently purified via sublimation; all materials handling was done in a glove box. Melting was carried out in vitreous carbon crucibles under CCl_4/Ar atmosphere in a hermetically sealed, RF induction-heated crystal growth

furnace[6]. These glasses, denoted by the suffix "SI" in Tables I-II, were allowed to solidify in situ within the furnace, and were later annealed. The resulting samples were 3.5 cm in diameter, with thicknesses of 1.0-2.0 cm before polishing. Three additional samples were prepared by melting powders or remelting glass cullet in a conventional resistance heated furnace (Table II).

Stability Against Crystallization: Differential scanning calorimetry (DSC) was used to examine the crystallization behavior of the glasses on reheating above their glass transition temperatures; typical traces for 3 samples are shown in Fig. 1. It is reassuring to observe the excellent reproducibility of the transition temperature (T_g = 589 ± 1°K), the onset of crystallization (Tx = 667 ± 1°K) and the enthalpy of crystallization (ΔH = -75 ± 4 J/g). Irreproducibility of these parameters for different ZBLA batches of the same nominal composition has been a recurring problem[7]. The reproducibility of the present results is significant to the reliable preparation of optical components and underscores the importance of raw materials and processing conditions on glass formation in HMFG system.

Measurement Techniques: The experimental apparatus used for Rayleigh scattering measurements has been described previously[8]. A single mode argon-ion laser at 0.488 μm acts as the exciting source and the scattered light was analyzed with a multi-pass Fabry-Perot interferometer and photon counting electronics. A spatial filter allowed the precise definition of the scattering volume in each data run. A polarization rotator and analyzer allowed separation of the scattered light into the various polarization components (i.e., VV, VH or HH). Both the quasi-elastic scattered Rayleigh line and the propagating inelastically scattered Brillouin lines were

detected. The main measured quantity was the Landau-Placzek ratio, a normalized Rayleigh intensity in the pure VV mode which reflects scattering information in the sample brought about by microscopic density and concentration fluctuations[9,10]. These fluctuations are modified respectively by $(\rho\frac{\partial\varepsilon}{\partial\rho})_{T,C}$ and $(\frac{\partial\varepsilon}{\partial C})_{\rho,T}$, the density and concentration gradients of the dielectric tensor[10]. The scattering loss in dB/Km is calculated from a combination of the measured Rayleigh and Brillouin data. The Brillouin scattering loss α_B in units of cm^{-1} is given by[9]:

$$\alpha_B = \frac{8\pi}{3}^3 \frac{kT}{\lambda^4} (n^4 P_{12})^2 \frac{1}{\rho V_L^2} \qquad (1)$$

and the Rayleigh scattering loss in dB/Km becomes.

$$\alpha_S = \alpha_B (R_{LP} + 1) (4.34 \times 10^5) \qquad (2)$$

where n, P_{12}, ρ, V_L, λ and T are the refractive index, Pockels' elastooptic coefficient, density, longitudinal velocity, laser wavelength and lattice temperature respectively. The depolarization ratio I(VH)/I(VV), which expresses the degree of anistropy of the glasses, was also determined for the samples.

Results and Discussion: The scattering volumes within each sample were selected visually via a low power microscope combination. Specimens prepared in the induction furnace were in general completely free of visible crystallites or inclusions throughout the volume of even the thickest samples, although some showed evidence of small, isolated gas bubbles. Tables I and II summarize the results of the light scattering measurements and the derived elastic parameters in the HMFG. Values in brackets indicate the average of 5 or more measurements carried out in different regions of a given specimen. It should be noted that the majority of the samples exhibit a scattering

attenuation at 0.488 μm consistently lower than that observed in the best fused silica. Only those glasses prepared by conventional melting and casting techniques show high values of the scattering loss. Based on the material properties of multicomponent fluorozirconate glasses, Poignant[4] and Shibata et al.[5] have suggested that scattering losses at 0.488μm should theoretically in the range of 2-7 dB/Km. From Table II it is evident that the present experimental results are in excellent agreement with these predictions. Projection of this data via a λ^{-4} scaling law would yield losses near 1×10^{-3} dB/Km in the 3-4μm region where the scattering curve intersects with the multiphonon edge. Moreover, low scattering levels are retained throughout the volume of these relatively large samples, suggesting a high degree of optical homogeneity. Measurements of the depolarization ratio, which reflects the "frozen in" orientation fluctuations (Table II) provide some insight into this question[11,12]. Typical values of depolarization ratios in HMFG (0.03-0.09) are seen to agree favorably with those observed in very isotropic and homogeneous fused silica (Homosil).

Conclusion: The present study has verified that the major intrinsic loss mechanism in carefully prepared bulk heavy metal fluoride glasses is Rayleigh light scattering. It has been shown for the first time that samples may be reproducibly prepared with very similar loss characteristics and a high degree of optical homogeneity. The results of Rayleigh scattering measurements (i.e. Landau-Placzek ratios) and the derived loss values approach or equal the theoretically predicted values at 0.488 μm, which in turn are lower than these observed in fused silica.

Acknowledgements: Work at RPI was supported by USAF, Rome Air Development Center, Hanscom AFB, Massachusetts under contract F19628-83-C-0016.

REFERENCES

1. Miyashita, T., and Manbe, T., "Infrared Optical Fibers", IEEE J. Quan. Elec. QE-18 (10) 1432-1450 (1982).

2. Tran, D.C., Levin K.H., Fisher, C.F., Burk, M.J., and Sigel, G.H., "Rayleigh Scattering in Fluoride Glass Optical Fibers", Electron. Lett. 19 (5) 165-166 (1983).

3. Tran, D.C., Siegel, G.H., Levin, K.H., and Ginther, R.J., "Rayleigh Scattering in ZrF_4-Based Glasses", Electron. Lett. 18 (24) 1046-48 (1982).

4. Poignant, H. "Dispersive and Scattering Properties of a ZrF_4-Based Glass", Electron. Lett. 17 973-974 (1981).

5. Shibata, S., Horiguchi, M., Junguji, K. Matachi, S., Kanomori, T., and Manabe, T., "Prediction of Loss Minima in Infrared Optical Fibers", Electron. Lett. 17 (21) 775-777 (1981).

6. Hutta, J.J., Suscavage, M.J., Drexhage, M.G., and El-Bayoumi, O.E., "Techniques for the Preparation of High Optical Quality Heavy Metal Fluoride Glasses", Proc. SPIE 484 (1984, in press).

7. Bruce, A.J., Moynihan, C.P., Loehr, S., Opalka, S., Perazzo, N., "Intrinsic Instabilities of Heavy Metal Fluoride Glasses", Proc. SPIE 484, (1984, in press).

8. Schroeder, J., Fox-Bilmont, M., Pazol, B.G., Tsoukala, V., Drexhage, M.G., and El-Bayoumi, O.E., "Rayleigh and Brillouin Scattering in Heavy Metal Fluoride Glasses", Proc. SPIE 484 (1984, in press).

9. Schroeder, J., Mohr, R.K., Macedo, P.B., and Montrose, C.J., "Rayleigh and Brillouin Scattering in K_2O-SiO_2 Glass", J. Am. Ceram. Soc. 56, 510-514 (1973).

10. Schroeder, J., Mohr. R.K. Montrose, C.J., and Macedo, P.B., "Light Scattering in a Number of Optical Grade Glasses", J. Non-Cryst. Solids 13 313-320 (1973/74).

11. Kielich, S. "Role of Molecular Interaction in Anisotropic Light Scattering by Liquids", J. Chem. Phys. 46 (10), 4090-4099 (1967).

12. Maurer, R.D., "Light Scattering by Glasses", J. Chem. Phys. 25, 1206-1209 (1956).

TABLE I.

Sound Velocities (longitudinal and transverse) Elastic constants and Pockels' Elasto-optic coefficients for a typical ZBLA-SI glass at 0.488μm and 300K.

	V_L(m/s)	V_T(m/s)	C_{11}(GPa)	C_{44}(GPa)	σ	P_{12}	$\lvert P_{44}\rvert$	$(\rho\frac{\partial\epsilon}{\partial\rho})$
ZBLA-SI	4026	2333	74.7	25.1	0.25	0.128	0.067	0.454
SiO_2	5944	3748	77.9	31.0	0.17	0.270	0.072	1.003

TABLE II. Results obtained from Light Scattering Measurements of various ZBLA-glasses at 488 nm and 300°K.

SAMPLE #	n(488 nm)	$R_{L.P.}$	Loss(dB/Km)	I(VH)/I(VV)
ZBLA-SI-1	1.538	<28.8>	<5.15>	0.077
" " -3	1.509	13.8	2.56	0.074
" " -4	1.542	13.0	2.42	0.054
" " -5	1.531	<37.3>	<6.62>	0.023
" " -7	1.544	30.4	5.44	0.088
" " -8	1.548	<21.9>	3.96	—
" " -10	1.528	48.1	8.50	0.026
" " -11	1.535	<29.1>	<5.20>	0.051
" " -12	1.540	24.0	4.33	0.057
" " -13	1.539	<33.6>	<5.99>	0.035
" " -14	1.531	16.5	3.03	0.050
" " -15	1.533	<23.7>	<4.28>	0.050
ZBLA-CH-4	1.527	74.6	13.09	0.022
" " -550	1.528	<34.1>	<6.08>	—
" " -1019	1.541	<5062>	<876.5>	0.331
SiO_2	1.461	21.9	11.6	0.050

NOTES: SI samples were melted and cooled in situ in RF-induction heated furnace. CH-4 = induction furnace re-melt of #550. #550 = prepared from glass cullet, melted in resistance heated furnace and cast. #1019 = prepared from fluoride powders in resistance heated furnace and cast.

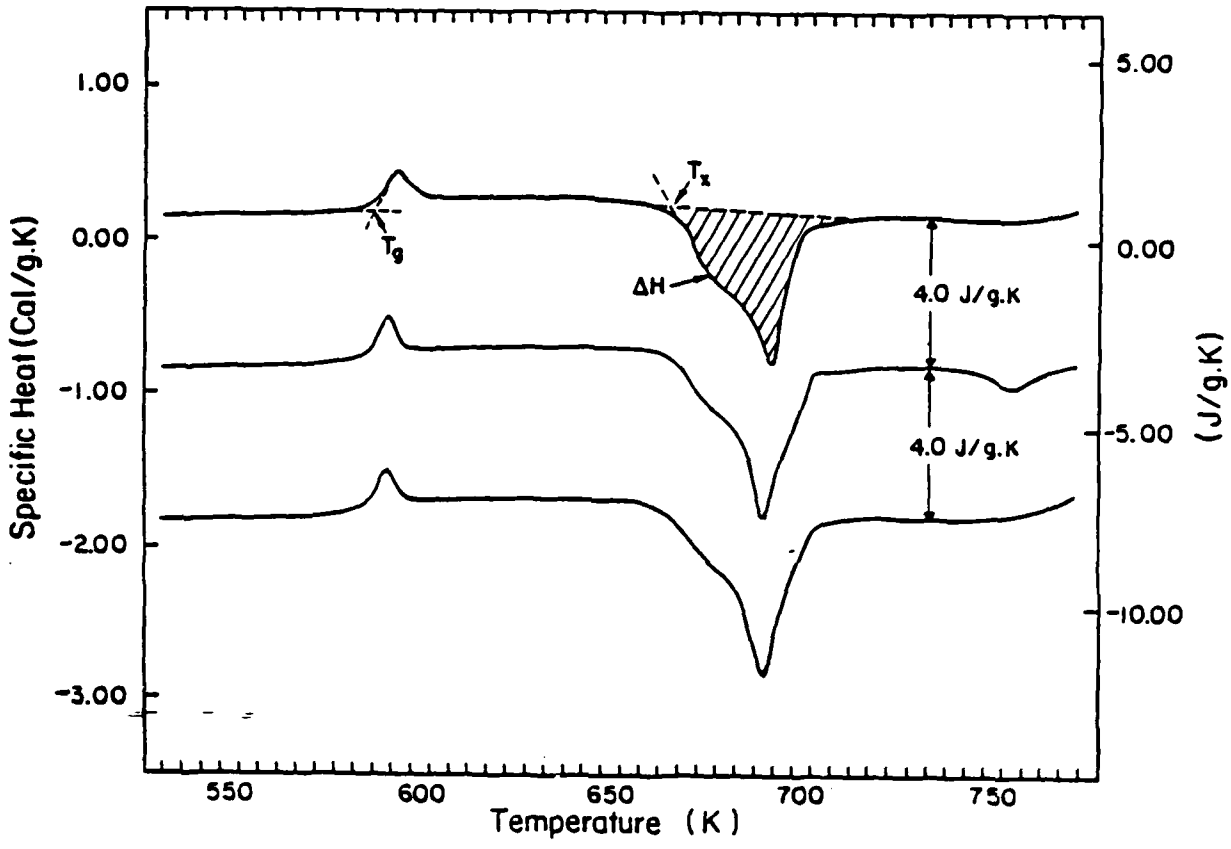

Figure 1: Differential scanning calorimeter traces for three different melts of ZBLA-SI glass.

Pockels' Elastooptic Coefficients and Brillouin Linewidths in Halide Glasses

J. Schroeder and G. A. Floudas
Physics Department
Rensselaer Polytechnic Institute
Troy, N. Y. 12181 U.S.A.

M. A. Stiller
Lockheed Corporation
Palo Alto, CA

M.G. Drexhage
Rome Air Development Center
Hanscom AFB, MA 01754

Brillouin scattering measurements on various multicomponent halide glass compositions were done as a function of annealing time and temperature. The results show that the magnitude of the Pockels' coefficients exhibit a time and temperature dependence. These findings indicate that the Pockels' coefficients are also affected by the metastable properties that characterize a glass. Hence, the configurational temperature that affects Rayleigh scattering so dramatically must also be invoked in a proper description of the elastooptic properties of a glass. The above findings in conjunction with Brillouin linewidth measurements may offer a new insight into a method of suppressing optical non-linear effects in halide glass optical waveguides.

The Brillouin scattering spectrum of glass exhibits five identifiable components, two frequency shifted doublets and a strong unshifted central component. Usually the central or Rayleigh component may be orders of magnitude greater in intensity than the shifted doublets. The linewidth of the Rayleigh

component is much narrower spectrally than any of the shifted doublets. Each doublet consists of Stokes and anti-Stokes components, shifted equally in frequency from the laser exciting frequency. Both shear and compressional restoring forces exist in an amorphous solid hence two pairs of doublets will exist.

The spectral measurements of the Brillouin lines allows the determining of the sound velocity and attenuation of the acoustic phonons in a solid, while the magnitude of the intensity of the Brillouin lines gives values for the Pockels' elastooptic coefficients.

In Brillouin scattering for a given incident and scattered light direction in an isotropic solid, four possible scattered light components exist; namely, VV, VH, HV and HH. Here V denotes polarization perpendicular to the scattering plane and H polarization parallel to the scattering plane. For the case of 90° scattering, which is what is used in this work, the following equations give the Brillouin scattering cross section for scattering in glasses[1]

$$\left(\frac{d\sigma}{d\Omega}\right)_{VV} = \epsilon_o^4 \left(\frac{\omega_s}{c}\right)^4 \frac{V k T}{32\pi^2} \frac{P_{12}^2}{C_{11}} \tag{1a}$$

$$\left(\frac{d\sigma}{d\Omega}\right)_{HH} = \epsilon_o^4 \left(\frac{\omega_s}{c}\right)^4 \frac{V k T}{32\pi^2} \frac{P_{44}^2}{C_{11}} \tag{1b}$$

$$\left(\frac{d\sigma}{d\Omega}\right)_{VH} = \epsilon_o^4 \left(\frac{\omega_s}{c}\right)^4 \frac{V k T}{32\pi^2} \frac{P_{44}^2}{2 C_{44}} \tag{1c}$$

$$\left(\frac{d\sigma}{d\Omega}\right)_{HV} = \epsilon_o^4 \left(\frac{\omega_s}{c}\right)^4 \frac{V k T}{32\pi^2} \frac{P_{44}^2}{2 C_{44}} \tag{1d}$$

Hence, the choice of polarization for the incident light and scattered light selects specific acoustic modes. The two sets of material constants, the elastic constants C_{ij} and the Pockels' elastooptic coefficients P_{ij} determine the Brillouin spectra. P_{ij}^2 determines the intensity of each line and C_{ij} the extent of the shift with respect to frequency from the incident light frequency.

From the Brillouin line shifts that are measured the sound velocity at hypersonic frequencies may be calculated and this is done with the Brillouin equation[2] in the form:

$$\frac{\Delta\nu}{\nu_o} = \pm 2\frac{n}{c} V(\omega_\mu, \hat{i}_\kappa) \sin\frac{\phi}{2} \qquad (2)$$

where V is the phase velocity, n and c the refractive index and speed of light, respectively and ϕ the scattering angle. For a glass the velocity is independent of the direction of propagation and only one longitudinal and one transverse acoustic branch exist. From equation (2) it is evident that measurement of the Brillouin shifts allows the calculation of the sound velocity provided that the refractive index of the material is known. By measuring the Brillouin intensities at the various polarization states the Pockels' elastooptic coefficients may also be determined. For a glass only P_{11}, P_{44} and P_{12} will be non-zero and $P_{11} = 2P_{44} + P_{12}$.

The methods employed to obtain the Brillouin spectra of heavy metal fluoride glasses are laser excitation (Argon-ion) operating at 488 nm coupled to stabilized multi-pass high contrast Fabry-Perot interferometer with a photon counting

detection system and associated data handling electronics. A comprehensive schematic of this equipment will be found in Figure 1.

The entire Fabry-Perot is contained in a thermally stabilized box and the whole system (laser, interferometer, detector and optics) is mounted on a vibration isolated optical table. The detector consists of an ITT-FW 130 photo-multiplier tube with a photo-cathode that is cooled to -20°C. The dark count of this photo-multiplier tube in the cooled state is persistently about 0.4 counts/sec and it has a quantum efficiency of 10% at 488 nm. The current generated by the photo-multiplier is shaped, amplified, discriminated and converted to counts/sec and the data of subsequent scans are stored in a 1024 channel multi-channel analyzer of the Burleigh DAS-1 system. This Burleigh DAS-1 system scans the Fabry-Perot and assures long-term stability of the interferometer by providing servo-control for the piezo-electric stacks of the Fabry-Perot. The scattering experiments reported here were done in a three-pass mode with mirrors of 93% reflectivity resulting in a finesse of about 80, a contrast of about 10^8 and overall measured transmission of about 0.40. The high contrast of about 10^8 was especially important in being able to measure the transverse Brillouin lines in some of the strong scattering heavy-metal fluoride glasses. The auxiliary parameters of refractive index and density were independently measured in our laboratory. The refractive index was measured by determining the angle of minimum deviation of a sample that had been immersed in some well

characterized index matching oil (i.e. parafin oil, cyclo-hexane etc.), and from the measured angle the refractive index of the sample is calculated. The density was determined by an Archimedean technique where cyclo-hexane was the working fluid.

Prior to measurement all samples were polished on three sides and then immersed in water-free parafin oil in a glass scattering cell to minimize any parasitic scattering and also to protect the delicate surfaces from water vapor attack.

The glass samples employed for these measurements were prepared at our laboratories utilizing techniques described elsewhere.[3] The primary quantities that are measured in this study are the Brillouin intensities, the shift of the Brillouin lines and the Brillouin linewidths (FWHM-full width at half maximum).

The Brillouin intensities at the various polarization selections and Brillouin shifts coupled with the auxiliary parameters of density and refractive index give the Pockels' elastooptic coefficients for glasses. The Pockels' coefficients are determined for heavy metal fluoride glasses with respect to the SiO_2 glass by the following equations:[1]

$$P_{12} = \left[I_B(VV)/I_B(VV)_o\right]^{1/2}\left[\Delta\nu_B^L/\Delta\nu_B^L(0)\right]\left[\frac{n(0)}{n}\right]^5\left[\rho/\rho(0)\right]^{1/2}P_{12}(0) \quad (3)$$

and

$$P_{44} = \pm P_{12}\left(V_T/V_L\right)\left[2\, I_B(VH)/I_B(VV)\right]^{1/2} \quad (4)$$

In the above equations $I_B(VV)_o$, $\Delta\nu_B^L(o)$, $n(o)$, $\rho(o)$, $P_{12}(o)$ refer to the Brillouin intensity, Brillouin shift, refractive index, density and Pockels' coefficient of SiO_2, while the same

quantities without the zero designator refer to the actual sample parameters. In equation (4) V_T, V_L are the transverse and longitudinal sound velocities, and (VH) and (VV) are the different polarization modes. The Pockels' elastooptic coefficients are summarized in Table 1.

In our experiment besides measuring the position and intensity of the Brillouin components in the spectrum of the scattered light we also measured the natural linewidth of the Brillouin components. The observed Brillouin component profile is a convolution of a Gaussian instrumental function and a Lorentzian shaped spectrum. This instrumental width results from a convolution of several contributions such as the finite frequency width of the laser, the finite acceptance angle of the light gathering optics and the Fabry-Perot interferometer. Hence, the observed Brillouin component, $B_1(w)$, is given by:

$$B_1(\omega) = \int_{-\infty}^{\infty} S(\omega) * G(\omega - \chi)\, d\chi \qquad (5)$$

where the instrumental function G(w-x) is given by

$$G(\omega) = G_0 e^{-\omega^2/\beta^2}$$

and the Lorentzian shaped spectrum has the form

$$S(\omega) = S_0 \left[1 + \left(\frac{\omega}{\Gamma}\right)^2 \right]^{-1}$$

Here G(w) has a half-width at half-height given by $\Delta G_{\frac{1}{2}} = \sqrt{\ln 2}\,\beta$, and S(w) has a half-width at half-height given by $\Delta S_{\frac{1}{2}} = \Gamma$. Hence, we measure $\Delta B_{2(\frac{1}{2})}$ and $\Delta G_{(\frac{1}{2})}$ and want to determine Γ. Fortunately several techniques exist that allow the deconvolution to obtain the natural Brillouin linewidth.[4,5,6,7] The results of the Brillouin linewidth measurements are given in

Table II.

Measurements of Pockels' coefficients of halide glasses as a function of annealing time and temperature have also been carried out. The results for ZBLAN and HBLA-148 glasses are given in Figures 2 and 3. Both figures show the time dependence of P_{12} the longitudinal Pockels coefficient quite clearly. From Figure 3 it is also evident that P_{44} is constant with time.

The onset of Stimulated Brillouin Scattering (SBS) has recently been observed and identified as an additional loss parameter in single mode optical waveguide fibers.[8] The non-linear process of stimulated Brillouin Scattering (SBS) can occur if the optical power launched into a single mode fiber exceed some critical threshold level. Cotter[8] has shown that this critical threshold energy is proportional to the Brillouin linewidth and inversely proportional to the square of the longitudinal Pockels' coefficient; namely, $E_{Th}^{B} \propto (\Delta\nu_B)/P_{12}^2$ and having measured both parameters we now can calculate a relative threshold energy for the occurrence of SBS. In Table II calculated values of E_{Th}^{B} normalized by the SBS threshold value for SiO_2 are given. The findings for halide glasses are in contrast with the estimates given by Cotter.[8] Cotter predicts that the SBS threshold power for fluoride glasses could be in the microwatt region. Our measurements and ensuing calculations at 488 nm show that some fluoride glasses have a higher energy threshold for SBS than SiO_2. This relationship should also hold at μ 3.0 since the dispersion relations of the responsible parameters should show no anomalous behavior.

The observations that P_{12} is time dependent allows for the tailoring of a desired value, preferable a minimum value, and thereby attain a maximum SBS threshold energy.

Measured losses in silica glass based and fluoride glass based optical fibers are approaching levels that correlate rather well with the theoretical limits imposed by Rayleigh scattering and multi-phonon absorption. This means that non-linear optical effects, primarily stimulated Brillouin scattering, has become a major systems limitation. We have shown here for the first time that fluoride based optical waveguide systems can be superior to silica based optical waveguides as non-linear optical effects such as stimulated Brillouin scattering become a limiting criteria.

Acknowledgement

This work supported by AF contract F19628-83-C-0016.

References

1. J. Schroeder, Treatise on Material Science and Technology, Vol. 12, Edit. by M. Tomozawa and R. H. Doremus. Academic Press, NY, 1977, pp. 157-222.

   J. Schroeder, J. Non-Crystalline Solids 40, 549 (1980).
2. L. Brillouin, Ann. Phys. (Paris) 17, 88 (1922).
3. M. G. Drexhage, C.T. Moynihan and M. Saleh-Boulos, Mat. Res. Bull. 15, 213 (1980).
4. D. Walton, J.J. Vanderwal and H.C. Teh, Solid State Comm. 42, 737 (1982).
5. H.W. Leidecker and J.T. LaMacchia, J. Acoustic Soc. Am. 43, 143 (1967)
6. A.S. Pine, Phys. Rev. 185, 1187 (1969).
7. G.E. Durand and A.S. Pine, IEEE J. Quantum Electr. 4, 523 (1968).
8. D. Cotter, J. of Optical Communications 4, 10 (1983).

Table I

Pockels' Elastooptic Coefficients, P_{12} and P_{44}, Longitudinal and Shear, Respectively for Halide Glasses at 488 nm and 300°K.

Sample	P_{12}	$\lvert P_{44} \rvert$	Remarks
BeF_2	0.398	0.082	
$95BeF_2 \cdot 5ThF_4$	0.380	0.085	
ZBL	0.255	-	
ZBLA-139	0.128	0.067	Same composition but different thermal history
ZBLA	0.251	-	
ZBLA-129	0.156	-	
ZBLAN	0.231	0.019	
ZBLAEu-147	0.149	0.064	
HBL	0.149	-	
HBLA-153	0.210	-	Same composition but different thermal history
HBLA	0.128	-	
HBLA-148	0.218	-	
HBLAPC	0.150	-	
BMAYT-384	0.109	-	
BMDNT-357	0.201	-	
BZLT-268	0.132	-	
SiO_2	0.270	0.072	

Table II

Brillouin Linewidth Measurements of Selected Heavy Metal Fluoride Glasses at $300^{0}K$ and 488 nm. Threshold Energies for the Onset of Stimulated Brillouin Emission in Halide Glasses Normalized to a Typical Threshold Energy for SiO_2

Sample	Brillouin Linewidth (MHz)			$\frac{\Delta\nu_B(VV)}{P_{12}^2}$	$\left(\frac{E_T^B}{E_S^B}\right)$
	$\Delta\nu_B(VV)$	$\Delta\nu_B(HH)$	$\Delta\nu_B(VH)$		
SiO_2	153.8	150.4	64.0	2.1×10^3	1.0
ZBL	213.6	-	-	3.4×10^3	1.63
ZBLA	153.9	-	-	9.4×10^3	4.5
ZBLAN	59.5	-	-	3.4×10^3	1.6

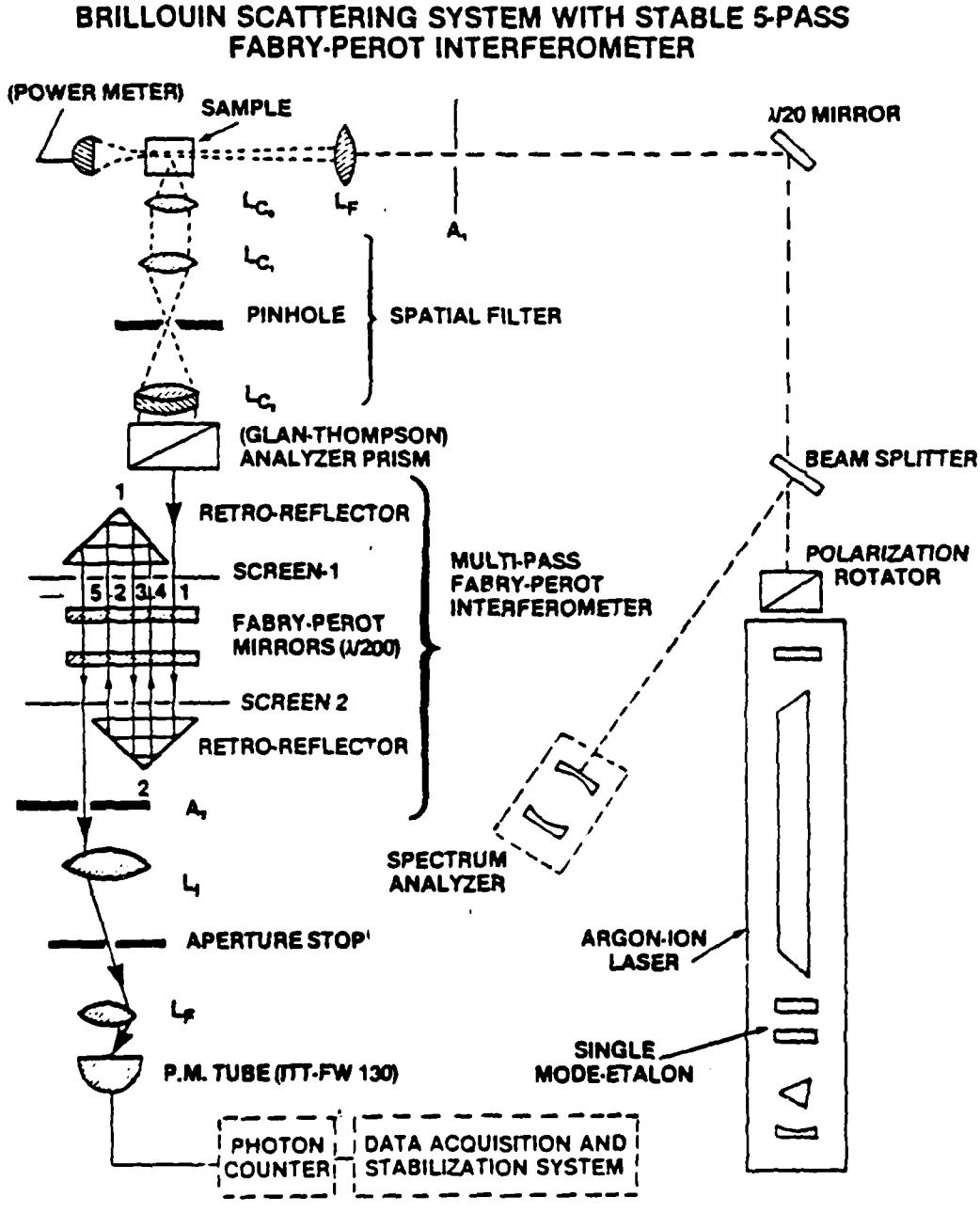

Figure 1. Schematic of Rayleigh-Brillouin Scattering Apparatus.

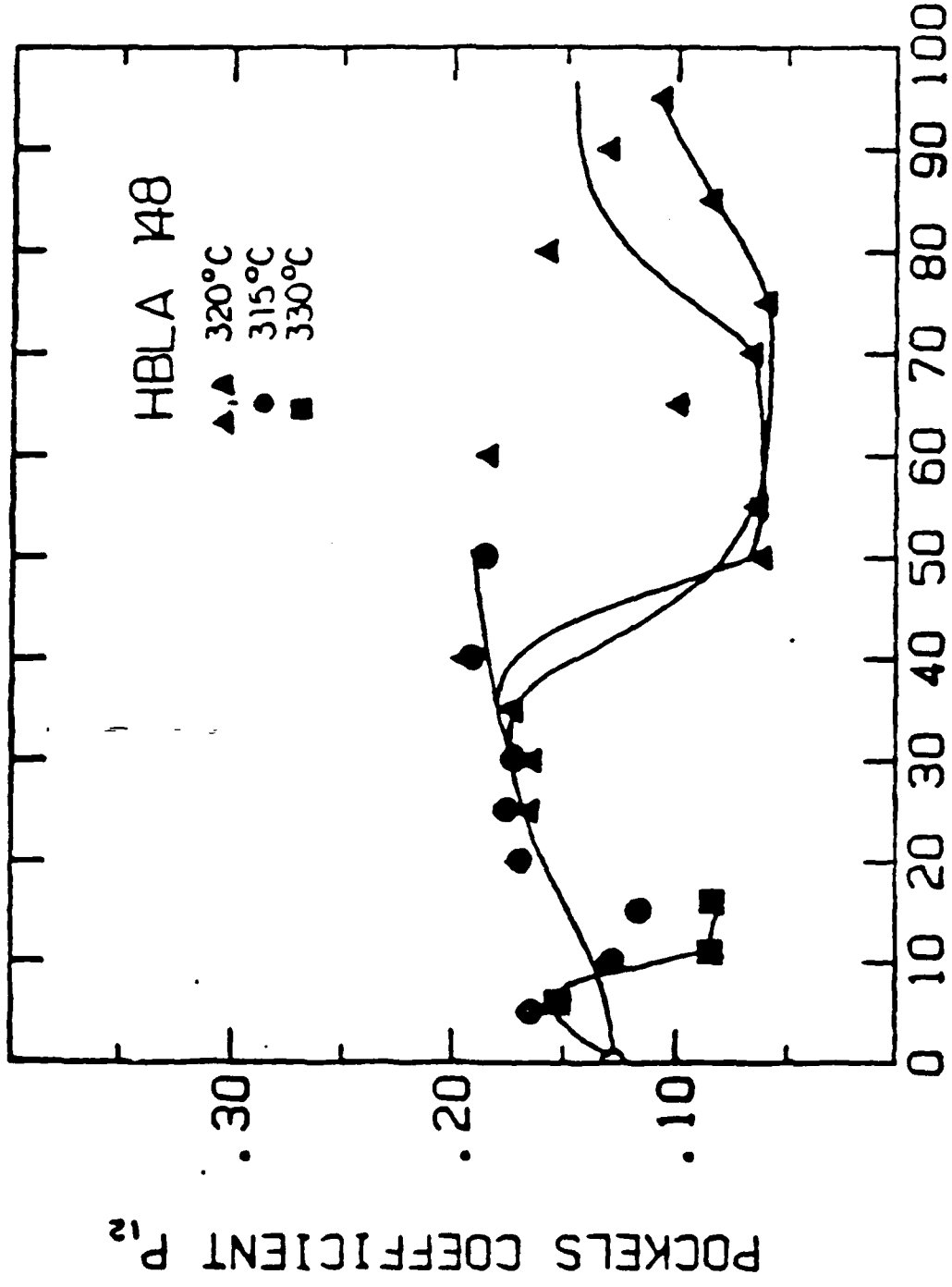

Figure 2. Pockels elastooptic coefficient P_{12} as a function of annealing time for HBLA. Annealing performed at three different temperatures, as indicated.

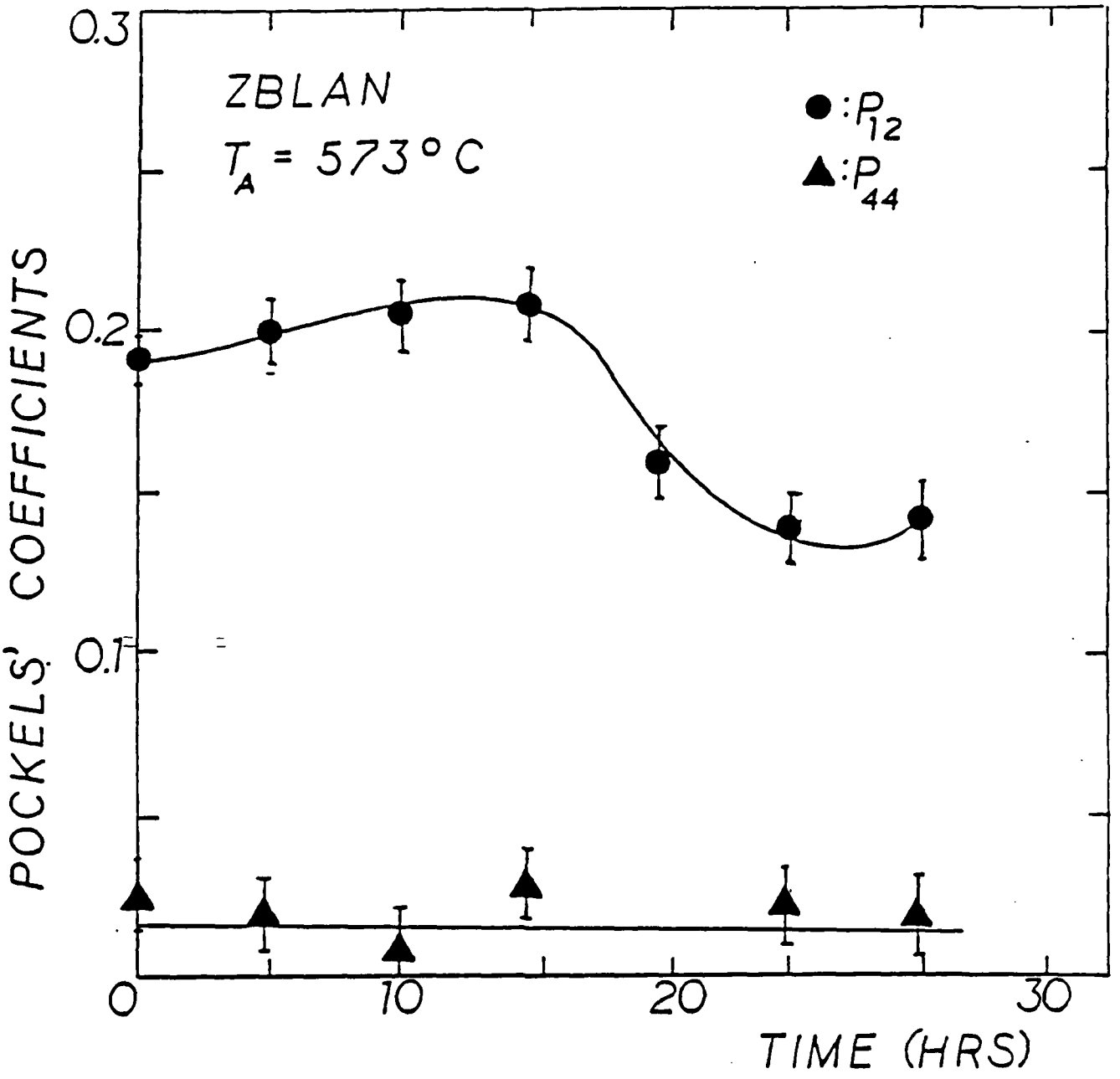

Figure 3. Pockels' elastooptic coefficients, P_{12}, P_{44}, as a function of annealing time for ZBLAN glass. Annealing performed at 573°K.

Composition and Structural Relaxation Effects on the Intrinsic Rayleigh Scattering of Halide Glasses: Annealing Studies

J. Schroeder, V. Tsoukala
Physics Department
Rensselaer Polytechnic Institute
Troy, N.Y. 12181

A. J. Bruce
AT and T Bell Labs
Murray Hill, N. J.

C. O. Staller
General Dynamics Corp.
Pomona, CA

J. J. Hutta, M. J. Suscavage, M. G. Drexhage
Solid State Sciences Division
Rome Air Development Center
Hanscom AFB, MA 01754

Light scattering characteristics for various multi-component halide glasses subjected to structural relaxation or physical aging during annealing at or slightly above the respective glass transition temperature of each sample were measured by Rayleigh-Brillouin spectroscopy. Both spectrum and intensity of the scattering light were determined and thereby it was possible to isolate some of the scattering mechanisms that contribute to the intrinsic Rayleigh scattering. The role of valence and reduced mass on the scattering characteristics will be discussed and the utility of these materials for near infra-red optical applications is addressed.

Attenuation of light in a glass is brought about by several mechanisms. Fortunately, the different mechanisms may be isolated, since they are not of equal magnitude at the same wave-

length of the exciting light. Rayleigh scattering seems to dominate below 2μm. At longer wavelengths, absorption features, for example those of the OH^- ion dominate and beyond 5μm, multi-phonon absorption is many orders of magnitude larger than the Rayleigh scattering or the OH^- absorption. Hence, it is most important to understand the basic Rayleigh scattering behavior of a glass if we wish to make predictions about its attenuation up to about 3μm and be able to reduce the scattering losses such that a fluoride glass could be employed as a suitable material for fiber-optic applications in the near infra-red regime.

Rayleigh scattering in dense disordered materials is brought about by microscopic fluctuations in the dielectric susceptibility about its equilibrium value. Consequently, the intensity of the scattered light is given by: $I(\theta) \propto \langle \delta\epsilon_K^2 \rangle$ where $\langle \delta\epsilon_K^2 \rangle$ is the K-th component of the mean square fluctuations of the dielectric constant. For a multi-component liquid we have[1]

$$\langle \delta\epsilon_K^2 \rangle = \left(\partial\epsilon/\partial\rho\right)^2_{T,\{c\}} \left(\partial\rho/\partial s\right)^2_{\rho,\{c\}} \langle \delta s^2_{red} \rangle + \left(\partial\epsilon/\partial\rho\right)^2_{T,\{c\}} \left(\partial\rho/\partial p\right)^2_{s,\{c\}} \langle \delta p^2 \rangle + \sum_{j=1}^{n-1} \sum_{k=1}^{n-1} \left(\partial\epsilon/\partial c_j\right)_{T,p,\{c'\}} \left(\partial\epsilon/\partial c_k\right)_{T,p,\{c'\}} \langle \delta c_j \delta c_k \rangle . \quad (1)$$

where $\langle \delta p^2 \rangle$ represents propagating pressure fluctuations which manifest themselves in sound waves and result in the Brillouin scattering lines. $\langle \delta s^2_{red} \rangle$ and $\langle \delta c_j \delta c_k \rangle$ are

entropy and concentration fluctuations, respectively. These are diffusive, consequently non-propagating modes and will be found as quasi-elastic scattering or the Rayleigh line. For a binary or pseudo-binary liquid the above equation reduces to the form:[1]

$$\langle \delta\epsilon_K^2 \rangle \propto \left(\partial\epsilon/\partial\rho\right)_{c,T}^2 \langle \delta\rho_K^2 \rangle + \left(\partial\epsilon/\partial c\right)_{\rho,T}^2 \langle \delta c_K^2 \rangle \qquad (2)$$

where we have contributions only from density and concentration fluctuations respectively. At this point several additional parameters should be introduced: configurational temperatures that reflect the thermodynamic state of the system where density and concentration fluctuations are in thermal equilibrium; compressibilities at very low and at very high frequencies are also required. Once these concepts are introduced in equation (2), a normalized intensity ratio, the Landau-Placzek ratio, may be defined as follows:[1]

$$R_\rho \equiv \frac{I_R(\rho)}{2I_B} = \frac{T_f}{T}\left[\frac{K_{T,o}(T_f)}{K_{S,\infty}(T)} - 1\right] \qquad (3)$$

which is valid for Rayleigh scattering by density fluctuations only; and

$$R_c \equiv \frac{I_R(c)}{2I_B} = \frac{T_f}{T}\frac{\left(\partial\epsilon/\partial c\right)_{\rho,T}^2}{\left(\rho\,\partial\epsilon/\partial\rho\right)_{T,c}^2}\left(\frac{V}{N}\right)\rho V_{L,\infty}^2\left(\frac{\partial\mu}{\partial c}\right)_{\rho,T}^{-1} \qquad (4)$$

which represents the concentration fluctuations in the Rayleigh line. Usually the total Landau-Placzek ratio is measured and the most important quantities that appear in equations (3) and (4) are: the configurational temperature for density

fluctuations, T_F; the configurational temperature for concentration fluctuations, T_F'; the isothermal compressibility at T_F, $K_{T,O}(T_F)$; and the derivative of the chemical potential with respect to the concentration, $(\partial\mu/\partial c)$.

The basic question that must be addressed is how does one minimize the four basic quantities as given in equation (2) where the entire scattering problem is described by four basic parameters; namely, the mean square fluctuation of density and concentration, and the gradients of the dielectric susceptibility with respect to density and also concentration.

Our samples were multicomponent heavy metal fluoride glasses, namely fluorozirconates and fluorohafnates, where the network formers are ZrF_4 and HfF_4, respectively, with modifiers being BaF_2 and fluorides of rare earths, group III elements and alkalis. Table I shows the composition of some of our glasses. More details about the preparation of the glasses can be found elsewhere.[2]

Some of the samples were heat treated near T_G for several hours. This annealing was achieved in a Perkin-Elmer DSC-4 Differential Scanning Calorimeter. This instrument besides its use for measuring and characterizing thermodynamic properties of glasses, it works also well as a precise temperature controlled oven.

The light scattering apparatus consists of a single-mode argon-ion laser at 0.488 μm as the exciting source and the scattered light is analyzed with a multi-pass Fabry-Perot interferometer and photon-counting electronics. A spatial

filter is used to precisely define the scattering volume in each sample.

Table 2 shows the measured Landau-Placzek ratio and scattering loss for various heavy metal fluorides. The latter is calculated as:[3]

$$\alpha_s = \alpha_B \left(R_{LP} + 1\right)\left(4.34 \times 10^5\right) \; dB/km \tag{5}$$

where

$$\alpha_B = \frac{8\pi^3}{3}\frac{kT}{\lambda^4}\left(n^4 P_{12}\right)^2 \left(\rho V_{L,\infty}^2\right)^{-1} \tag{6}$$

the Brillouin scattering loss. Here n, P_{12}, p, $V_{L,\infty}$, λ and T are the refractive index, Pockels' elasto-optic coefficient, density, longitudinal velocity, laser wavelength, and lattice temperature, respectively.

Table 3 shows the light scattering results of various ZBLA glasses at 0.488 μm and 300°K. Values in brackets indicate the average of five or more measurements carried out in different regions of a given specimen.

Finally Figure 1 summarizes the light scattering results of some heat treated samples.

As can be seen from Tables 2 and 3 the best candidates for a low-scattering fluoride glass will come from the families of ZBLA and ZBLAN glasses. As the results on Table 3 show, reproducible results can be achieved for carefully prepared fluorides. The majority of these samples exhibit a scattering attenuation at 0.488 μm consistently lower than that observed in the best fused silica, in excellent agreement with theoretical predictions.[4] Moreover, low scattering levels are retained throughout the volume of these relatively large samples, suggesting a

high degree of optical homogeneity.

The light scattering measurements from the heat treated samples show very interesting behavior. Here the open and half open circles refer to two different ZBL glasses, heat treated near the glass transition temperature, while the closed circles represent the light scattering results from BZnYbTN heat treated near the crystalization temperature. The scattering of the glass samples seems to increase with heat treatment time initially, while latter it levels off at a certain value. Such a time dependence of the scattering suggests that these systems might phase separate following a spinodal mechanism.

ACKNOWLEDGMENT

This work supported by AF contract F19628-83-C-0016.

REFERENCES

(1) J. Schroeder, Treatise on Material Science and Technology, Vol. 12, Edit. by M. Tomozawa and R. H. Doremus. Academic Press, N. Y., 1977, pp. 157-222.
(2) J. Schroeder et al., Electronic Letters, 11 October 1984, Vol. 20, No. 21, pp. 860-862.
(3) J. Schroeder et al., J. Non-Cryst. Solids 13, 313 (1973-1974).
(4) H. Poignant, "Dispersive and Scattering Properties of a ZrF_4 Based Glass", Electronic Letters 17, 973-974 (1981).

Table 1

Selected Heavy Metal Fluoride
Glass Compositions

Sample	Composition (mol %)
ZB	$65ZrF_4 \cdot 35BaF_2$
ZBL	$62ZrF_4 \cdot 33BaF_2 \cdot 5LaF_3$
ZBLA-129	$57ZrF_4 \cdot 36BaF_2 \cdot 3LaF_3 \cdot 4AlF_3$
ZBLA-139	$58ZrF_4 \cdot 33BaF_2 \cdot 5LaF_3 \cdot 4AlF_3$
ZBLAN	$55.8ZrF_4 \cdot 14.4BaF_2 \cdot 5.8LaF_3 \cdot 3.8AlF_3 \cdot 20.2NaF$
ZBLAP-131	$57ZrF_4 \cdot 34BaF_2 \cdot 3LaF_3 \cdot 4AlF_3 \cdot 2PrF_4$
ZBLAEu-147	$57ZrF_4 \cdot 34BaF_2 \cdot 3LaF_3 \cdot 4AlF_3 \cdot 2EuF_3$
HB	$65HfF_4 \cdot 35BaF_2$
HBL	$62HfF_4 \cdot 33BaF_2 \cdot 5LaF_3$
HBLA-148	$57HfF_4 \cdot 36BaF_2 \cdot 3LaF_3 \cdot 4AlF_3$
HBLAP-286	$57HfF_4 \cdot 34BaF_2 \cdot 3LaF_3 \cdot 4AlF_3 \cdot 2PrF_4$
HBLAH-287	$57HfF_4 \cdot 34BaF_2 \cdot 3LaF_3 \cdot 4AlF_3 \cdot 2HoF_3$

Table 2

Landau-Placzek Ratio of Various Heavy Metal Fluoride Glasses at 488 nm and 300°K

Sample	R_{LP}	Loss (dB/Km)
ZB	8843.0	-
ZBL	18.9	-
ZBLA-129	338.0	195.0
ZBLA-139	22.1	4.0
ZBLAP-131	201.0	-
ZBLAH-144	341.0	-
ZBLAEu-147	36.4	8.0
ZBLAN	48.3	-
HB	40.3	-
HBL	27.0	58.7
HBLA-148	117.5	237.5
HBLAPC	55.0	113.0

Table 3

Results Obtained From Light Scattering Measurements of Various ZBLA Glasses at 488 nm and 300°K

Sample	R_{LP}	Loss (dB/Km)
ZBLA-SI-1	28.8	5.15
ZBLA-SI-3	13.8	2.56
ZBLA-SI-4	13.0	2.42
ZBLA-SI-5	37.3	6.62
ZBLA-SI-7	30.4	5.44
ZBLA-SI-8	21.9	3.96
ZBLA-SI-10	48.1	8.50
ZBLA-SI-11	29.1	5.20
ZBLA-SI-12	24.0	4.33
ZBLA-SI-13	33.6	5.99
ZBLA-SI-14	16.5	3.03
ZBLA-SI-15	23.7	4.28
ZBLA-CH-4	74.6	13.09
ZBLA-CH-550	34.1	6.08
ZBLA-CH-1019	5062	876.5
SiO_2	21.9	11.6

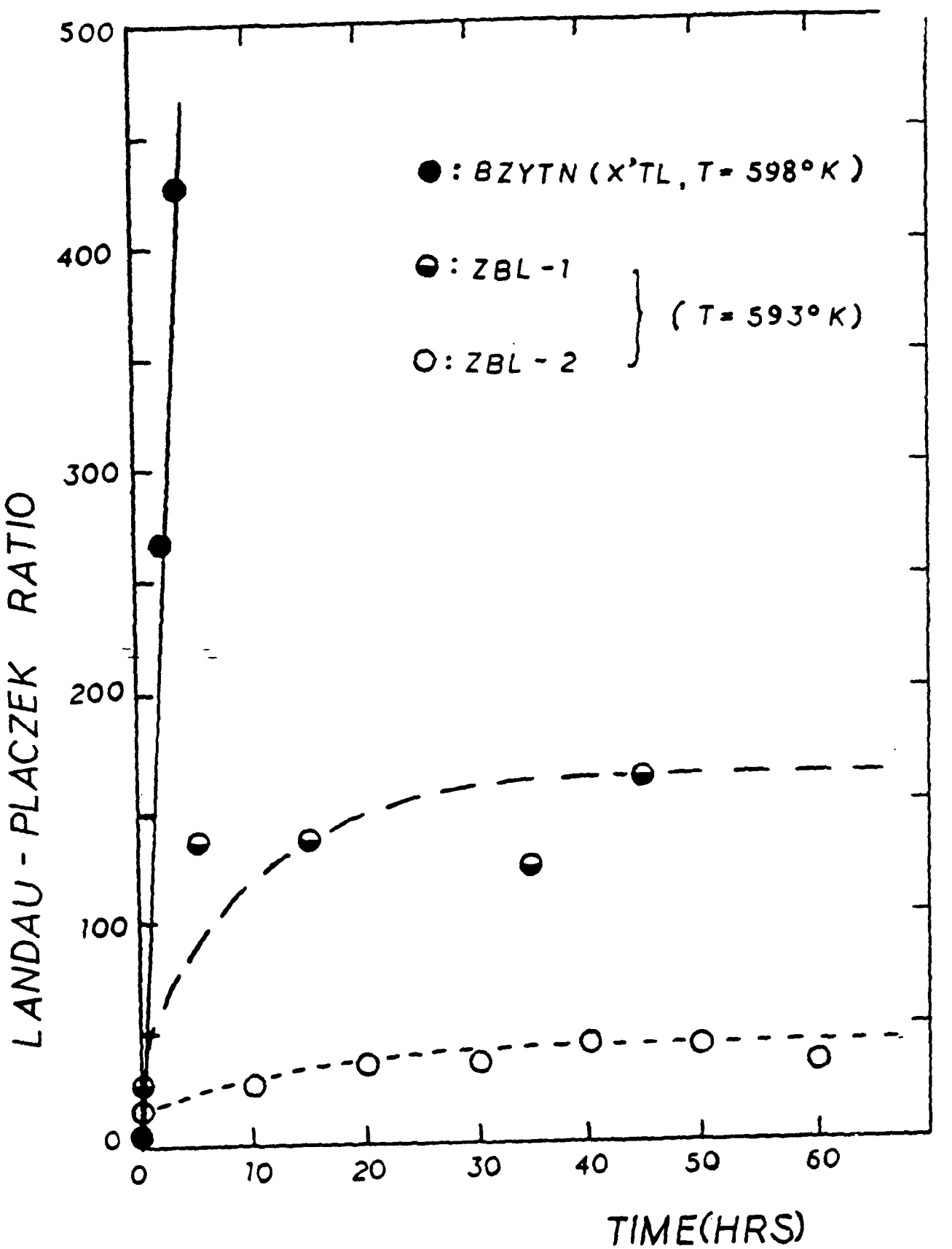

Figure 1. Landau-Placzek Ratio for Several Fluoride Glasses as a Function of Annealing Time.

IR SPECTROSCOPY STUDIES OF ATTACK OF LIQUID WATER ON ZrF_4-BASED GLASSES

S. R. Loehr, A. J. Bruce, R. Mossadegh, R. H. Doremus and C. T. Moynihan
Rensselaer Polytechnic Institute
Troy, New York 12180-3590, USA

INTRODUCTION

Although ZrF_4-based heavy metal fluoride glasses are quite durable in the presence of atmospheric water [1,2], they are rapidly attacked by liquid water. In the first careful study [2] of aqueous corrosion of these materials three effects were found: a) dissolution of the glass into the aqueous phase, b) development of a hydrated surface layer manifested by the appearance of a 3440 cm^{-1} (2.9 μm) -OH stretching band and a 1630 cm^{-1} (6.1 μm) H_2O bending band in the IR spectra, and c) precipitation of crystalline dissolution products on the surface. Subsequent studies [3,4] of the hydrated surface layer via IR spectroscopy and SIMS showed that its thickness increased with increasing time and temperature of exposure to liquid water, that the growth of the 2.9 μm -OH and 6.1 μm H_2O bands were correlated and that the kinetics of growth were complex. Since that time a number of additional papers [5-10] concerning surface layers produced on ZrF_4-based glass in liquid water have appeared. The present study is concerned with the dependence of the kinetics of the hydrated surface layer development on glass composition and its correlation with the dissolution rate of the glass.

EXPERIMENTAL SECTION

Four ZrF_4-based glasses, whose batch compositions to the nearest mol % and glass transition temperatures T_g are given in Table I, were studied. These were melted in vitreous carbon crucibles under either CCl_4 or 3.5% Cl_2 reactive atmospheres, cast into thin plates a few mm in thickness and anneal-

ed near T_g. The plates were polished prior to the start of any of the hydration/dissolution experiments; the final polishing step was done with 0.3 μm Al_2O_3 in H_2O.

TABLE I. Glass compositions and glass transition temperatures.

Glass	Composition (mol %)	T_g(°C)
ZBL	$62ZrF_4$-$33BaF_2$-$5LaF_3$	300
ZBLA	$58ZrF_4$-$33BaF_2$-$5LaF_3$-$4AlF_3$	310
ZBLAN	$56ZrF_4$-$14BaF_2$-$6LaF_3$-$4AlF_3$-20NaF	263
ZBLALi	$51ZrF_4$-$21BaF_2$-$5LaF_3$-$3AlF_3$-20LiF	250

Kinetic studies of the development of the hydrated surface layers were done in the following fashion. The glass sample was cleaned ultrasonically in acetone and then hexane, after which it was mounted in an IR spectrometer specimen holder. The sample was then immersed in a large beaker of deionized water for a measured time, removed from the water, rinsed in acetone and then in hexane to remove adhering liquid water, and its IR spectrum recorded on a Perkin-Elmer Model 983G spectrometer. It was then reimmersed in the water for an additional time and the above procedure continued. Experiments were done at two temperatures, 25±2°C and 60±2°C. The deionized water beakers were large (2L at 25°C and 0.4L at 60°C) and the water was changed frequently to keep the pH, which affects the dissolution rate and changes as the glass dissolves [2,6,9], in the range 4.6-6.0.

On three of the compositions an experiment was carried out to determine the thickness of the hydrated surface layer. The sample was weighed, immersed in 2L of deionized water for 2 or 3h, rinsed with acetone and then hexane to remove adhering liquid water, reweighed to determine the mass loss due to dissolution and its IR spectrum recorded. After this the sample was hand polished with 0.3 μm Al_2O_3 in water for short and equal times on both faces, rerinsed with acetone and hexane, reweighed and the IR spectrum rerecorded. This was continued until the intensities of the 3440 cm^{-1} and 1630 cm^{-1} water bands dropped to the initial values for the unhydrated glass, indicating that the hydrated layers had been removed completely by polishing.

Several additional measurements of the mass loss due to dissolution at 25±2°C over times ranging from 2 to 5h were also carried out. Finally, the surface layers formed during exposure to water were examined using both optical and scanning electron microscopy.

RESULTS

The appearances of the surfaces of our ZrF_4-based glasses after reaction with water were very similar to those displayed in a number of other papers [2,7-10]. Briefly, clumps of bladelike crystals covered the surface to varying degrees, under which could be discerned a somewhat cloudy but still translucent surface layer. A recent study by Doremus et al. [7] has indicated that the bladelike crystals are ZrF_4 reprecipitated from solution.

In Figure 1 are shown IR spectra of a ZBLAN glass after immersion in water at 27°C for several different total (or cumulative) times t. Both the 3440 cm^{-1} -OH stretching band and the 1630 cm^{-1} H_2O bending vibrational band grow with increasing time. Interestingly, the flat background loss in frequency regions outside of the absorption peaks or the IR edge initially decreases, but later increases substantially at longer times. The long time increase in the background loss is due to scattering from surface crystals and the cloudy hydrated surface layer. The initial decrease in background loss is presently unexplained, although it is probably connected at least in part with a change in the refractive index and reflectivity of the surface due to hydration. The hydrated layers are moderately stable in air at room temperature. The intensities of the 3440 and 1630 cm^{-1} absorption bands did not change when a hydrated sample was allowed to sit for a few hours in the ambient laboratory atmosphere. However, after six days in the laboratory atmosphere a moderate drop (10-20%) in the absorption band intensities occurred, presumably due to evaporation of some of the water.

The total mass of absorbing species per unit area measured spectroscopically is proportional to the absorbance $A (= \ln(T_0/T) = 2.3 \log (T_0/T))$ of the sample, where T is the transmission at the peak of the absorption band and T_0 the transmission in adjacent frequency regions of negligible absorption. The dependence of the absorbance at 3440 cm^{-1} and 1630 cm^{-1} in the hydrated surface layer on total time t of immersion in water is shown in Fig. 2 for ZBLAN glass at 27°C. Different symbols (⊙ and X at 3440 cm^{-1} and ◇ and + at 1630 cm^{-1}) are results of duplicate experiments, i.e., the absorbance vs. time behavior is quite reproducible. The plots of Fig. 2 are typical of all four glass compositions at both temperatures. The ratio of the absorbance at 3440 cm^{-1} to that at 1630 cm^{-1} is constant (i.e., independent of temperature, hydration time and composition) and equal to 2.9 ± 0.2. The plots of A vs. t are not linear and curve downward at long times. Plots of A vs. $t^{1/2}$ are linear at long times, but appear to exhibit an initial induction period, so that the long time A vs. $t^{1/2}$ plots do not extrapolate linearly to the origin.

In Fig. 3 the time dependences at 25 ± 2°C of the absorbance at 3440 cm^{-1} are compared for the four glass compositions. Filled and unfilled symbols (e.g., ⊙ and ●) correspond to duplicate experiments. As a rough measure of the rate of development of water absorbance in the hydrated surface layer, we have taken the initial slopes $d\ln(T_o/T)/dt|_{in}$ of the absorbance vs. time plots at the shorter times where the plots have not deviated greatly from linearity. These are listed in Table II for the four compositions, the two water absorption peaks and the two temperatures. $d\ln(T_o/T)/dt|_{in}$ at a given temperature and frequency consistently increases in the order ZBLA<ZBL<ZBLALi< ZBLAN. Note also that the rate of development of absorbance in the hydrated surface layer is highly temperature dependent.

TABLE II. Initial slopes $d\ln(T_o/T)/dt|_{in}$ (h^{-1}) of absorbance vs. time of immersion in water at the two water absorption band frequencies and two temperatures.

	3440 cm^{-1}		1630 cm^{-1}	
Glass	25±2°C	60±2°C	25±2°C	60±2°C
ZBL	0.91	8.5	0.31	2.4
ZBLA	0.38	3.4	0.09	1.2
ZBLAN	2.2	53	0.68	22
ZBLALi	1.1	12	0.46	3.3

In Fig. 4 the decrease in absorbance at 3440 cm^{-1} is shown as a function of thickness X polished off each of two opposite hydrated surfaces for three glass specimens. The specimens were initially immersed in water at 25 ± 2°C for times shown in the figure. The surface layer thickness removed from each face was calculated from the expression

$$X = \Delta_m/2S\rho$$

where Δ_m is the mass removed by polishing, ρ is the bulk glass density (assumed to be fairly close to the hydrated layer density), S is the area of one face of the specimen and the factor of two takes into account that two opposite faces, each of area S, were polished. The thicknesses X' of the hydrated surface layers developed in time t, taken as the value of X where the absorbance drops to that of the initial glass, are given in Table III, along with the corresponding mass removed per unit area by polishing, $\Delta_m(X')/2S$. The value of X' for ZBLA glass is in reasonable accord with the value of about 1.5 μm measured by SIMS [3] for penetration of hydrogen and oxygen into the surface of a ZBLA glass immersed for 20 min in water at a temperature (30°C)

close to that of the present study. In fact, the ratio of these two X' values (3.7 μm/1.5 μm = 2.5) scales closely with the square root of the ratio of the times ((180 min/20 min)$^{1/2}$ = 3.0). On the other hand, the hydrated layer thickness measured here for ZBL glass appears to be much larger than the surface hydrogen profile thickness (about 0.5 μm for 1h in water at 23°C) measured by Doremus and coworkers [8,10] by the nuclear resonant reaction technique, even allowing for the differences in experimental times.

The surface of the hydrated ZBLA glass was inspected microscopically at each stage of the polishing. On removal from the water bath isolated clumps of bladelike crystals covered a minor fraction of the surface. These were removed completely in the first polishing step (X = 0.4 μm in Fig. 4). This indicates that the crystalline material reprecipitated on the surface does not contribute to the 3440 cm^{-1} and 1630 cm^{-1} absorption bands and that these bands are due solely to water in the hydrated glass on the surface.

TABLE III. Thickness of hydrated layer X', mass of hydrated layer per unit area $\Delta_m(X')/2S$ and mass loss due to dissolution per unit area $\Delta_{m_{diss}}/S_{tot}$ for glasses immersed in water for time t at 25 ± 2°C.

Glass	t(h)	X'(μm)	$\Delta_m(X')/2S$ (mg/cm^2)	$\Delta_{m_{diss}}/S_{tot}$ (mg/cm^2)
ZBL	2	4.6	2.0	1.4
ZBLA	3	3.7	1.7	1.1
ZBLAN	2	8.5	3.7	1.7

In Table IV are listed the dissolution rates at 25 ± 2°C for three of the glasses calculated from the expression $\Delta_{m_{diss}}/S_{tot}t$, where $\Delta_{m_{diss}}$ is the mass loss of a sample of total surface area S_{tot} immersed in water for time t. These are averages of from three to seven determinations with immersion times varying from 2 to 5h. Although previous studies [2,6,9,10] have shown that dissolution rates or rates of appearance of dissolution products in solution generally decrease with time for ZrF_4-based glasses, the range of immersion times for the dissolution rates of Table IV was small and no time dependence of dissolution rate was detectable. It is interesting to note (see Table III) that the mass of hydrated layer formed per unit area, $\Delta_m(X')/2S$, is comparable to the amount of glass dissolved in the water, m_{diss}/S_{tot} - both typically a few mg/cm^2 in 2 or 3h at 25°C.

TABLE IV. Dissolution rates, ratio of hydrated layer thickness to water immersion time and initial rate of development of hydrated layer absorbance at 3440 cm^{-1}. All data for 25 ± 2°C.

Glass	dissolution rate (mg/cm^2h)	X'/t (μm/h)	$d\ln(T_o/T)/dt_{in}$ @ 3440 cm^{-1}
ZBL	0.53 ± 0.08	2.3	0.91
ZBLA	0.38 ± 0.01	1.2	0.38
ZBLAN	0.88 ± 0.02	4.3	2.2

DISCUSSION

On immersing ZrF_4-based glasses in water a hydrated surface layer forms and increases in thickness with time, as shown by the absorbance vs. time plots of Figs. 2 and 3 and the surface H_2O profiles determined by IR spectroscopy (Fig. 4) and SIMS [3]. Since the layer forms in the face of constant dissolution of the glass, it follows that the hydrated layer formation is a necessary precursor step to the dissolution process. Given this, it might be expected that glasses in which the hydrated layer is produced most easily or rapidly would also be the ones which dissolve most quickly. The data in Table IV bear this out. There is a definite— although not 1:1— correlation between the rate of growth of the hydrated surface layer, as measured by the ratio of the layer thickness to immersion time X'/t or the initial slope of the absorbance vs. time curve $d\ln(T_o/T)/dt_{in}$, and the dissolution rate. In both cases these quantities increase in the order ZBLA<ZBL<ZBLAN. Although we did not measure the dissolution rate for the ZBLALi glass, its $d\ln(T_o/T)/dt_{in}$ values in Table II suggest that its dissolution rate should lie between those for the ZBL and ZBLAN glasses. Our observation (Table IV) that addition of small amounts of AlF_3 to the base ZBL glass decreases the dissolution rate, while large NaF additions increase the dissolution rate, has also been made by Frischat and Overbeck [9] and Simmons and coworkers [11]. On the other hand, Mitachi [6] reported that AlF_3, NaF and LiF additions all increased the F^- ion leach rate of ZrF_4-BaF_2-GdF_3 glasses.

The linearity of the absorbance vs. $t^{1/2}$ plots at long times (see Fig. 2) initially suggested to us that the hydrated layer was formed by diffusion of water into the glass [4]. The non-zero intercept on the $t^{1/2}$ axis, i.e., the apparent induction period for the hydrated layer formation, was attributed to the presence of a surface layer left on the initial glass after polishing which had to be dissolved away before water attack on the glass could commence.

More recently, Doremus et al. [10] have pointed out that a diffusional process coupled with a reaction which continually increases the concentration of the diffusing substance (H_2O) right at the surface of the medium (the glass) would also lead to plots vs. $t^{\frac{1}{2}}$ of the total amount of substance diffused into the medium similar in shape to the absorbance vs. $t^{\frac{1}{2}}$ plots of Fig. 2. Interestingly, Doremus et al. [10] have also found that plots vs. $t^{\frac{1}{2}}$ of the amounts of Zr, Ba and F produced by dissolution of the glass are also linear at long times, but with non-zero intercepts on the $t^{\frac{1}{2}}$ axis, for leaching in a small volume (50 mL) of unbuffered, static water solution. On the other hand, plots vs. $t^{\frac{1}{2}}$ of the amount of F leached into a stirred solution buffered at pH 5.1 were linear and extrapolated to the origin. Even though the water volumes used in our experiments were large, the water was changed periodically, and the overall change in pH during immersion of the glass samples was small, it remains a possibility that the induction period for hydrated layer formation apparent in the plot of absorbance vs. $t^{\frac{1}{2}}$ in Fig. 2 may be due to a rapid, local, initial drop in the solution pH right at the sample surface when it is first immersed in the solution.

The appearance of both the 3440 cm^{-1} -OH stretching band and the 1630 cm^{-1} H_2O bending band in the IR spectra shows that the hydrated layer contains molecular H_2O rather than only -OH bonded to a metal cation. The identity of the mobile diffusing species that produces the H_2O in the hydrated layer remains a question, however.

H_3O^+ has been suggested as the mobile diffusing species [9]. This appears unlikely, however, since H_3O^+ would have to interdiffuse with a mobile cationic species, and it has been shown [12] that ZrF_4-based glasses— at least those containing no alkali fluorides— are anionic fluoride ion conductors.

Because the pH of the water solution decreases as the glass dissolves, some workers [2,9] have suggested a simple anion exchange between the F^- ions at the glass surface and OH^- from the water solution:

$$H_2O(l) + F^-(glass) \rightarrow OH^-(glass) + H^+(aq) + F^-(aq) \qquad (1)$$

OH^- could be transported into the interior of the bulk glass by interdiffusion with the mobile F^- ions. Finally, a local equilibration could take place to produce molecular H_2O:

$$2OH^-(glass) \rightleftharpoons H_2O(glass) + O^{-2}(glass) \qquad (2)$$

H_2O, OH^- and O^{-2} will all be bonded to metal cations in the glass. The metal-oxygen bond will give rise to an IR absorption band around 1400 cm^{-1}, which gener-

ally appears as a shoulder on the multiphonon edge [13]. That 1400 cm^{-1} shoulder does indeed appear to be present in the hydrated glass spectra of Fig. 1. Doremus et al. [10] have commented, however, that Eq. (1) is not required to explain the drop in pH that occurs on glass dissolution; this may be accounted for by ionization of the Zr^{+4} aquocomplexes arising from the glass dissolution.

A final possibility is that the mobile diffusing species producing the hydrated glass layer is simply molecular H_2O.

A final question is that of the actual water concentration in the hydrated surface layers. The absorbance vs. X plots of Fig. 4 are not linear and are concave upwards, indicating that the concentration of water $C_{H_2O}(x)$ in the hydrated layer is not uniform and is largest at the surface. If, as a first approximation, we assume that $C_{H_2O}(x)$ is linear in distance x from the surface and drops to zero at x = X', then it is easily shown that the concentration of H_2O right at the front surface of the hydrated layer is given by

$$C_{H_2O}(0) = 2A(0)/\varepsilon_{H_2O}X' \qquad (3)$$

where A(0) is the absorbance of the hydrated layer and $_{H_2O}$ the molar extinction coefficient of the water. Maximum hydrated layer water concentrations estimated from Eq. (4) for three glasses are listed in Table V. For A(0) we used $0.5\ \ln(T_0/T)$ at X = 0 from Fig. 4, the factor of 0.5 being introduced because $\ln(T_0/T)$ in Fig. 4 is the absorbance of two hydrated layers, one on each specimen face. X' was taken from Table III. For $_{H_2O}$ we used two values—1.8×10^5 cm^2/mol H_2O obtained from the extinction coefficient of ^-OH reported by Tregoat et al. [14] for a BaF_2-ZnF_2-YbF_3-ThF_4 glass and 4.2×10^5 cm^2/mol H_2O reported by Shelby et al. [15] for water in vitreous SiO_2— giving rise to a range in our estimates of $C_{H_2O}(0)$. For comparison, the fluoride and zirconium ion concentrations, C_F and C_{Zr}, calculated from the bulk glass compositions and densities are also listed. It appears that the water concentrations in the hydrated layers are substantial, but not excessively large, i.e., roughly one H_2O per Zr^{+4}. Interestingly, the hydrated layer H_2O concentrations are comparable to the maximum ^-OH surface layer concentration (0.013 mol OH/cm^3) produced by reaction of a BaF_2-ZnF_2-YbF_3-ThF_4 glass with gaseous water at a high temperature near T_g [14].

TABLE V. Maximum hydrated surface layer water concentrations and bulk glass F and Zr concentrations.

Glass	$C_{H_2O}(0)$ (mol H_2O/cm^3)	C_F (mol F/cm^3)	C_{Zr} (mol Zr/cm^3)
ZBL	0.013-0.031	0.083	0.016
ZBLA	0.005-0.013	0.089	0.016
ZBLAN	0.011-0.025	0.093	0.017

CONCLUSIONS

There clearly remain many unresolved questions regarding the reaction of ZrF_4-based glasses with liquid H_2O. There are contradictions in the results reported in the current literature relative to, e.g., whether or not the glasses dissolve congruently [2,9,10,16] and the identity of the surface crystals [7,9]. Particularly interesting are reports [8,16] of orders of magnitude differences in dissolution or leach rates of glasses of the same bulk composition which differ only in surface preparation or melt history. An explanation given in one report [16] attributing the differences in leach rates to the presence or absence of ammonium bifluoride in the glass should likely be discounted. IR spectra of ZrF_4-based glasses [17] show in extreme cases ammonium ion contents which, assuming an NH_4^+ extinction coefficient of the order of 10^5 cm^2/mol, must be no larger than about 1 ppm. This is far too small to have any appreciable effect on the bulk glass properties or to perturb the local pH of a leaching solution, given the major effects on pH caused by the presence of dissolution products of the major glass components, e.g., Zr^{+4} aquocomplexes. Taking the reported differences in leach rates [8,16] as experimental fact, however, raises some intriguing questions and prospects for future research.

REFERENCES

1. E. O. Gbogi, K.-H. Chung, C. T. Moynihan and M. G. Drexhage, J. Am. Ceram. Soc., 64, C-51 (1981).

2. C. J. Simmons, H. Sutter, J. H. Simmons and D. C. Tran, Mat. Res. Bull., 17, 1203 (1982).

3. C. A. Houser and C. A. Pantano, Paper No. 15, Extended Abstracts, 2nd Int. Sym. on Halide Glasses, Troy, NY, 1983.

4. A. J. Bruce, S. R. Loehr, N. P. Bansal, D. M. Murphy, C. T. Moynihan and R. H. Doremus, Paper No. P5, Extended Abstracts, 2nd Int. Sym. on Halide Glasses, Troy, NY, 1983.

5. M. Robinson and M. G. Drexhage, Mat. Res. Bull., 18, 1101 (1983).

6. S. Mitachi, Phys. Chem. Glasses, 24, 146 (1983).

7. R. H. Doremus, N. P. Bansal, T. Bradner and D. Murphy, J. Mater. Sci. Lett., 3, 484 (1984).

8. C. Burman, W. A. Lanford, R. H. Doremus and D. Murphy, Appl. Phys. Lett., 44, 845 (1984).

9. G. H. Frischat and I. Overbeck, J. Am. Ceram. Soc., 67, C-238 (1984).

10. R. H. Doremus, D. Murphy, N. P. Bansal, W. A. Lanford and C. Burman, J. Mater. Sci., in press.

11. C. J. Simmons, private communication.

12. D. Ravaine and D. Leroy, J. Non-Cryst. Solids, 38 & 39, 575 (1980).

13. M. G. Drexhage, C. T. Moynihan, B. Bendow, E. Gbogi, K.-H. Chung and M. Boulos, Mat. Res. Bull., 16, 943 (1981).

14. D. Tregoat, G. Fonteneau, C. T. Moynihan and J. Lucas, J. Am. Ceram. Soc., 68, C-171 (1985).

15. J. E. Shelby, J. Vitko, Jr. and R. E. Benner, J. Am. Ceram. Soc., 65, C-59 (1982).

16. A. Barkatt and L. Boehm, Mater. Lett., 3, 43 (1984).

17. P. W. France, S. F. Carter and J. R. Williams, J. Am. Ceram. Soc., 67, C-243 (1984).

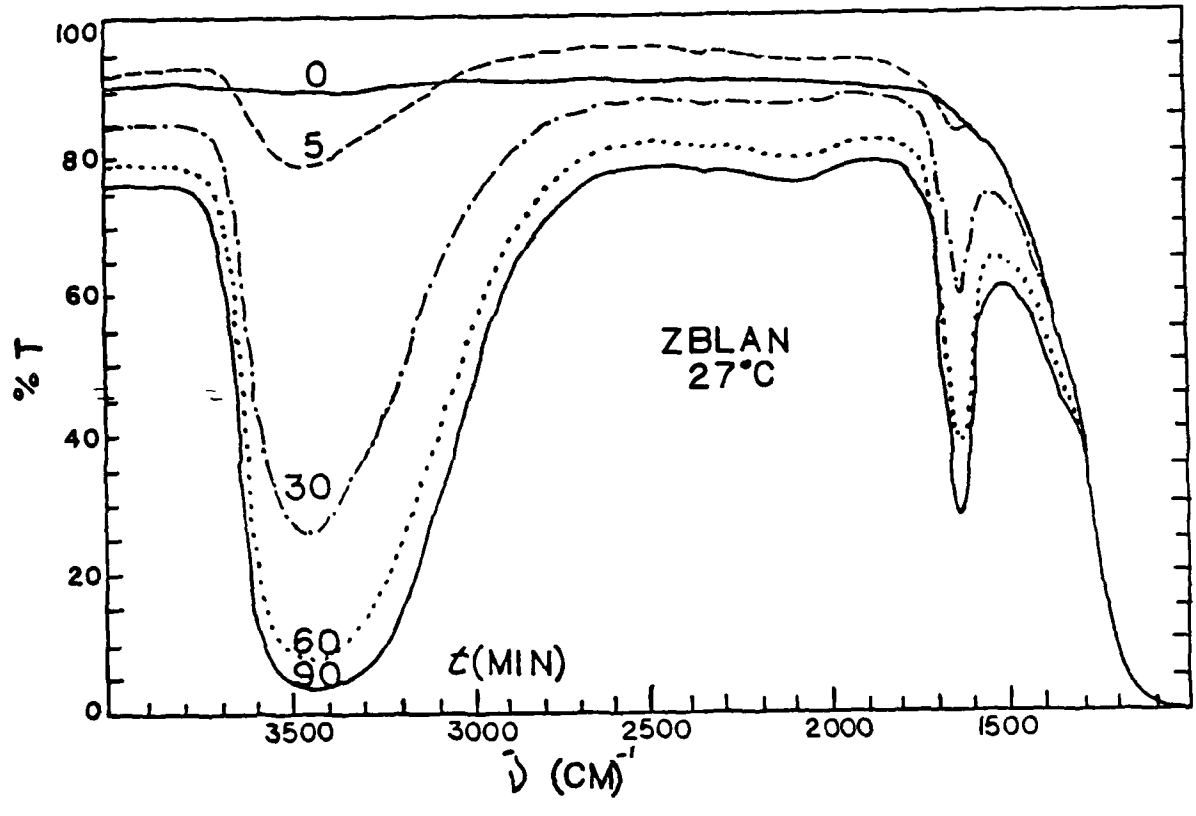

Figure 1. IR spectra of ZBLAN glass as a function of total immersion time t in water at 27°C.

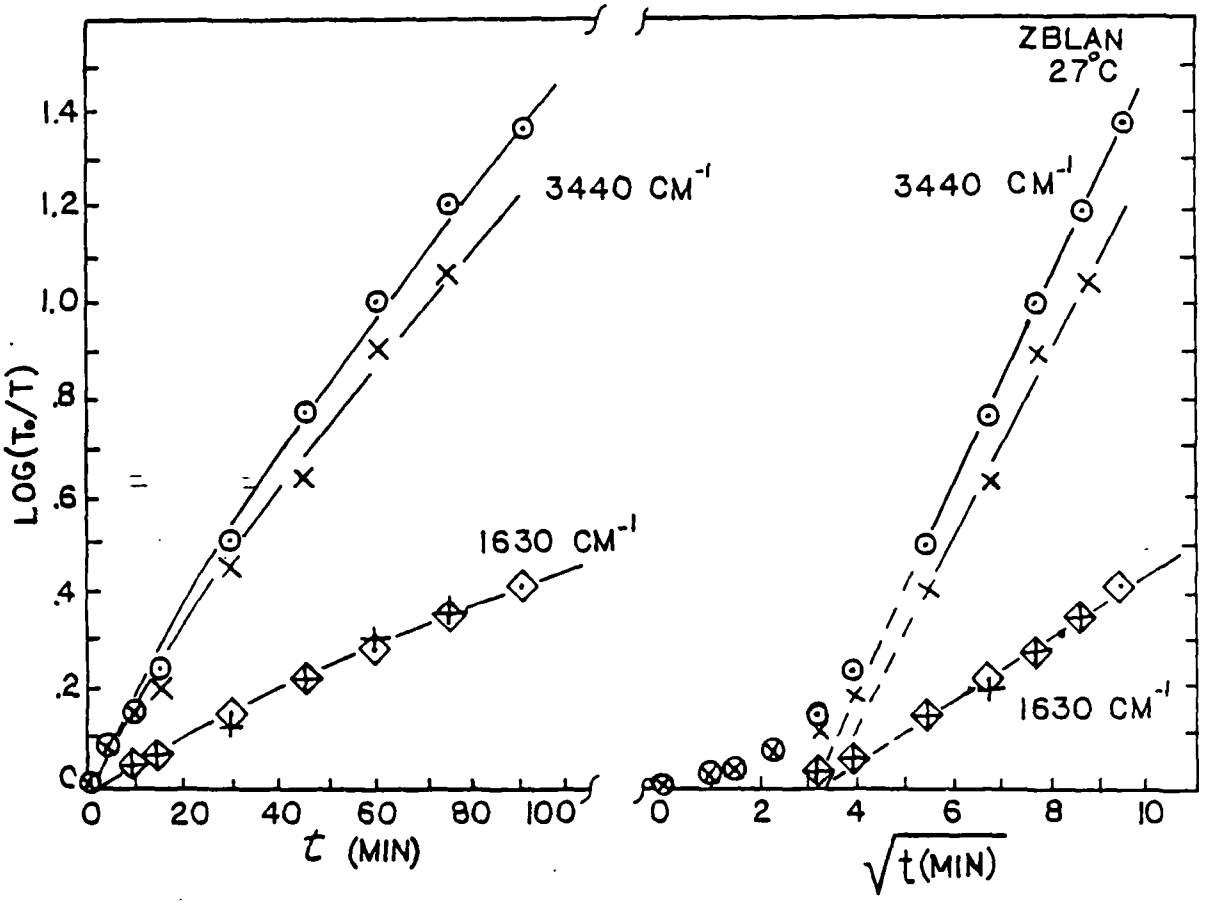

Figure 2. Development of 3440 and 1630 cm^{-1} bands with time during immersion of ZBLAN glass in H_2O at 27°C.

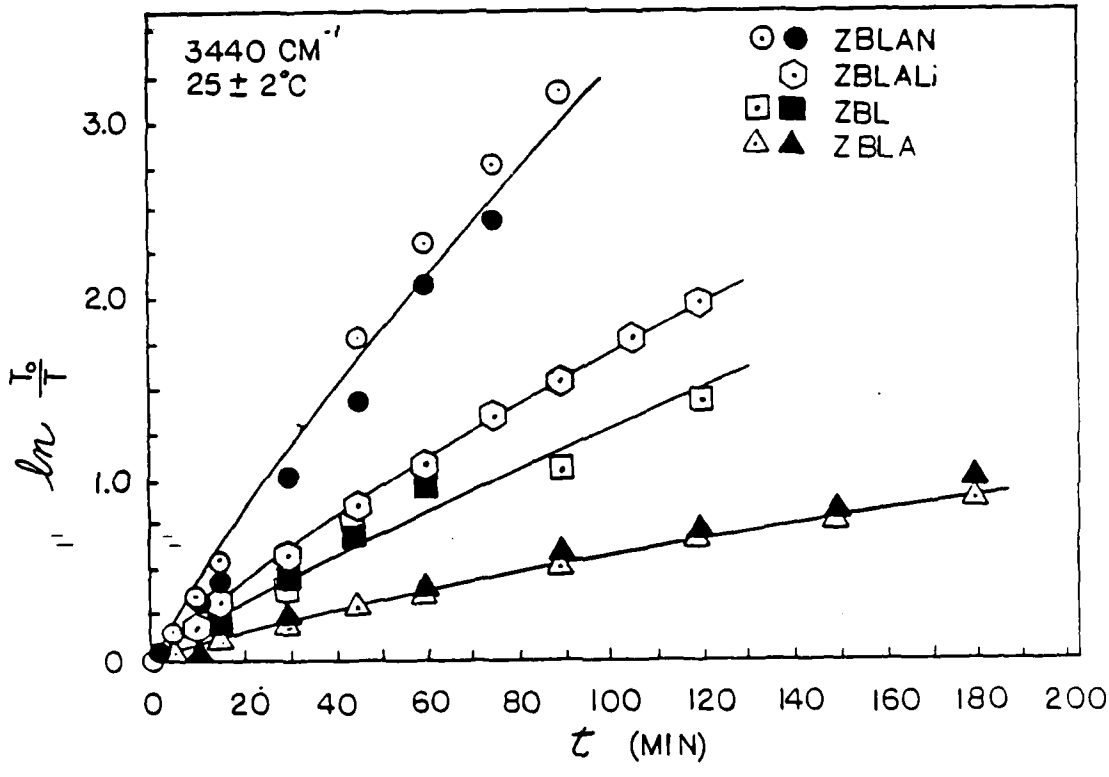

Figure 3. Development of 3440 cm^{-1} H_2O band with time during immersion of ZrF_4-based glasses in H_2O at 25 ± 2°C.

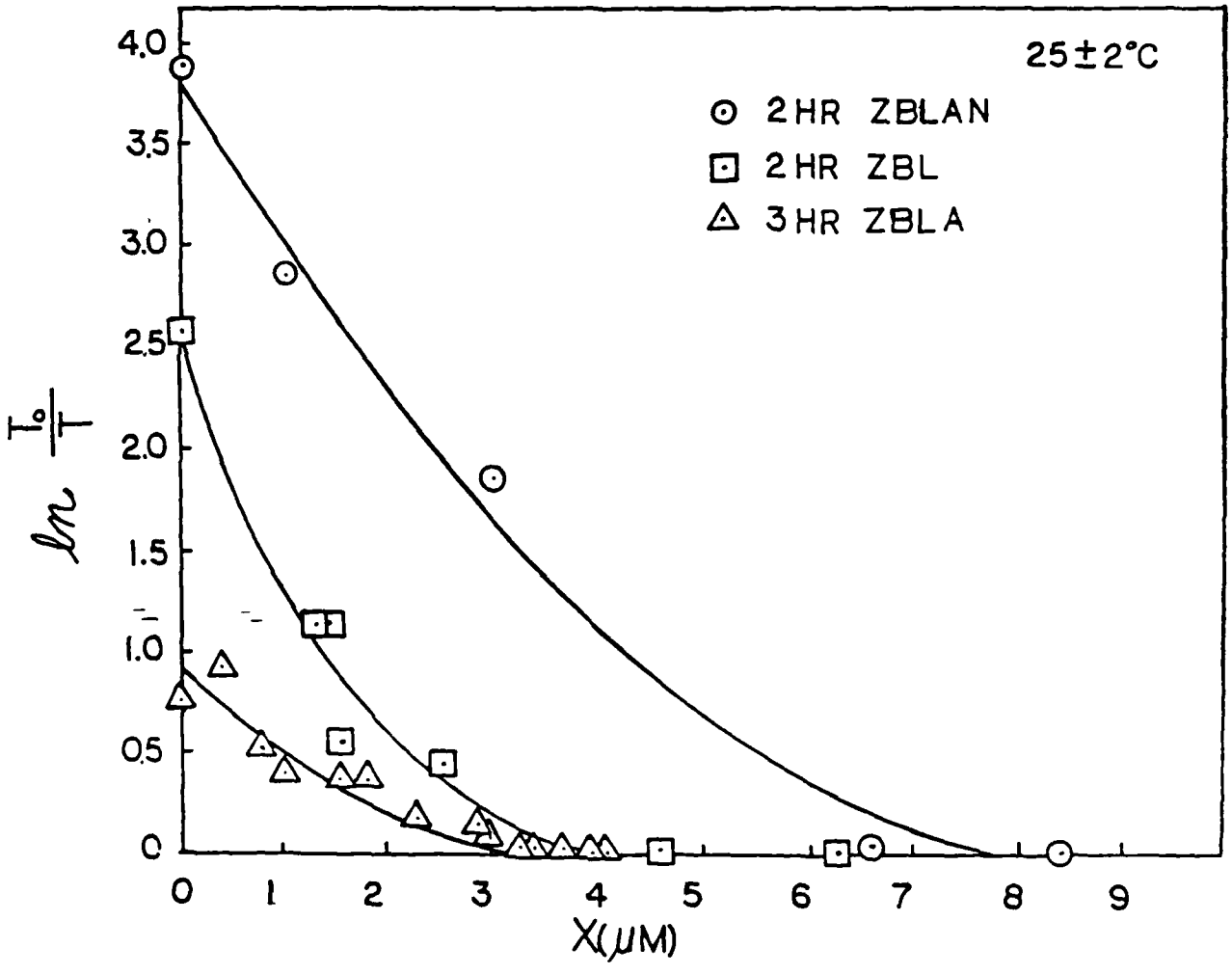

Figure 4. Decrease in intensity of 3440 cm^{-1} H_2O band as a function of thickness X polished off each hydrated glass surface.

MIXED ALKALI EFFECT AND EFFECT OF SUBSTITUTION OF HfF_4 FOR ZrF_4 ON HEAVY METAL FLUORIDE GLASS ELECTRICAL CONDUCTIVITIES

N. L. Perazzo, R. Mossadegh and C. T. Moynihan
Rensselaer Polytechnic Institute
Troy, NY 12180-3590, USA

INTRODUCTION

A number of previous studies of electrical conduction in ZrF_4-based heavy metal fluoride glasses have been carried out [1-5]. Concentration cell emf and transport number measurements [1,2] showed that alkali-free glasses were anionic fluoride ion conductors. Additions of NaF to ZrF_4-based compositions were found usually to lower the electrical conductivity [1-3], leading to the tentative conclusion that the alkali-containing glasses were still strictly F^- ion conductors. In the present paper electrical conductivity and relaxation measurements have been carried out to compare the properties of a ZrF_4-based glass with an HfF_4-based analog and to assess the mixed alkali (MA) effect of replacing NaF with LiF in a ZrF_4-based glass.

EXPERIMENTAL

Seven glasses, whose batch compositions are given to the nearest mol % in Table I, were melted in vitreous carbon crucibles under 3.5% Cl_2 in N_2 reactive atmosphere, cast into thin plates, given a preliminary anneal near T_g and cooled to room temperature. Glass transition temperatures, T_g, were determined at a heating rate of 10K/min on a Perkin-Elmer DSC and are also listed in Table I. Specimens for electrical measurements were cut and polished into plates (2-3 mm thick, ~10 mm on a side) and had sputtered gold electrodes applied to opposite faces. The real part of the electrical conductivity σ' and the dielectric constant ε' were measured over the frequency range 10^{-1} to 10^5 Hz using an updated version of the operational amplifier admittance bridge

originally designed by Berberian and Cole [6] and a dielectric cell designed by Syed and Moynihan [7].

TABLE I. Glass compositions, glass transition temperatures T_g and fictive temperatures T_f. ZBL-in is a glass with its initial, "as prepared" thermal history, while ZBL is the same specimen subsequently given a thermal history (annealed at 307°C, then quenched) identical to that of glass HBL.

Glass	Composition (mol %)	T_g(°C)	T_f(°C)
ZBL-in	$62ZrF_4$-$33BaF_2$-$5LaF_3$	295	292
ZBL	$62ZrF_4$-$33BaF_2$-$5LaF_3$	296	288
HBL	$62HfF_4$-$33BaF_2$-$5LaF_3$	315	299
ZBLAN	$56ZrF_4$-$14BaF_2$-$6LaF_3$-$4AlF_3$-20NaF	266	256
ZBLANLi(15/5)	$56ZrF_4$-$14BaF_2$-$6LaF_3$-$4AlF_3$-15NaF-5LiF	263	---
ZBLANLi(10/10)	$56ZrF_4$-$14BaF_2$-$6LaF_3$-$4AlF_3$-10NaF-10LiF	255	---
ZBLANLi(5/15)	$56ZrF_4$-$14BaF_2$-$6LaF_3$-$4AlF_3$-5NaF-15LiF	256	---
ZBLALi	$56ZrF_4$-$14BaF_2$-$6LaF_3$-$4AlF_3$-20LiF	254	---

Electrical conductivities of glasses depend markedly on their thermal histories in the glass transition region [3,8]. Consequently electrical measurements were carried out on only one specimen— designated ZBL-in in Tables I and II— with its initial, "as prepared" thermal history. In all other cases we attempted to make the thermal histories of glass specimens which were to be compared with one another uniform before measuring their electrical properties. Glass ZBL (which is the same specimen as ZBL-in, but with a different thermal history) and glass HBL were each annealed in a muffle furnace in a dry box for one hour at a temperature (307°C) in their glass transition regions, cooled quickly to below T_g by opening the furnace and removing the glass briefly, replaced in the furnace (which had been turned off and whose temperature had dropped to 275°C— well below T_g) and allowed to cool slowly to room temperature. A similar type of uniform thermal history was given to the alkali fluoride-containing glasses (ZBLAN through ZBLALi in Table I)— annealing for one hour at 250°C, quenching by removal from the furnace, followed by slow cooling in the furnace from 230°C to room temperature.

DSC measurements of specific heat while heating through the transition region at 10K/min were carried out on small specimens of four of the glasses.

RESULTS

DSC specific heat results are compared in Fig. 1 for ZBL and ZBL-in glasses. The differences in the specific heat overshoot of these two specimens in the transition region reflect the different amounts of relaxational enthalpy frozen in during their different thermal histories. The fictive temperatures of these two specimens, which can be thought of as a one parameter characterization of the frozen-in state of the glass, were calculated from the specific heat plots as explained in Ref. 9 and are listed in Table I, along with the corresponding T_f values for HBL and ZBLAN glasses. We had originally hoped to give the ZBL and HBL glasses the same fictive temperature by giving them a uniform thermal history. Evidently we picked our annealing temperature (307°C) a bit too high, so that both glasses relaxed somewhat during the rapid cool on removing them from the furnace. Nonetheless, we reduced the difference in fictive temperatures between ZBL and HBL to 11°C. If both these glasses had been cooled at the same rate from far above T_g their T_f's would have differed by 19°C— the difference in their T_g's. It is likely that we were more successful in imparting the same T_f's to the series of five alkali fluoride-containing glasses, since the value of T_f for ZBLAN, 256°C, is fairly close to the annealing temperature of 250°C.

Typical results for the frequency dependence of ε' and σ' are shown at three temperatures for ZBLAN glass in Figs. 2 and 3. These plots are similar in appearance to those observed for other ionically conducting glasses [8,10]. The high frequency dispersion in the ε' vs. f plots of Fig. 2 is due to bulk glass electrical (or dielectric) relaxation, while the low frequency dispersion (shown most clearly in the 146.5°C isotherm) is due to surface layer polarization. The low frequency plateau in the σ' vs. f plots of Fig. 3 corresponds to the bulk glass d.c. conductivity σ, while the high frequency dispersion is again due to bulk glass electrical relaxation.

Our data were also analyzed using the formalisms of complex resistivity ρ^* [1,2,10,11] and electric modulus M^* [7,12]:

$$\rho^* = \rho' - i\rho'' = 1/i\omega\varepsilon_0 [\varepsilon' - i(\sigma'/\omega\varepsilon_0)]$$

$$M^* = M' + iM'' = 1/[\varepsilon' - i(\sigma'/\omega\varepsilon_0)]$$

where ω is angular frequency and ε_0 the permittivity of free space. Typical complex plane plots of ρ^* and M^* are shown in Figs. 4 and 5 for ZBLAN glass.

Extrapolation of the low temperature M* plots to intersect the M' axis yields the reciprocal of the high frequency bulk dielectric constant ε_∞, as shown in Fig. 5. Values of ε_∞ are listed in Table II and seem to be nearly identical within experimental error for all eight glasses.

Neither the M* nor the ρ^* plots of Figs. 4 and 5 are arcs of a circle with its center on the real axis, indicating that the relaxation of the electric field due to ion migration in the bulk glass must be described by a spectrum of relaxation times or a non-exponential relaxation function [11,12]. In addition, the ρ^* arc is not exactly symmetric and does not have the shape of a circle with its center below the real axis, as has also been found with alkali silicate glasses [13]. The main part of the ρ^* arc of Fig. 4 (frequencies $\geq$ 10 Hz) is due to the electrical response of the bulk glass, while the small low frequency "tail", perceptible only in the enlargement of the low frequency region shown in the inset, is due to polarization of hydrated layers on the glass surface [5,10].

The bulk glass d.c. conductivity σ was obtained from the reciprocal of the low frequency intercept of the bulk glass part of the ρ^* arc with the real axis [1,10,11,13], as illustrated in Fig. 4. Note from the inset to Fig. 4 that the bulk glass ρ^* arc extrapolates to the ρ' axis at low frequencies at a 90° angle, in agreement with the conclusions of Ref. 13. The temperature dependence of the conductivities below the glass transition region followed the Arrhenius equation:

$$\sigma = \sigma_0 \exp(-\Delta H^*/RT)$$

TABLE II. Arrhenius equation parameters for electrical conductivity, conductivities at 100°C and high frequency dielectric constants.

Glass	T range (°C)	σ_0 ($ohm^{-1}cm^{-1}$)	ΔH^* (kJ/mol)	Std. Dev. $ln\sigma$	σ @ 100°C ($ohm^{-1}cm^{-1}$)	ε_∞
ZBL-in	3-206	278	72.46	0.027	2.00×10^{-8}	11.8
ZBL	25-197	359	73.44	0.024	1.89×10^{-8}	11.5
HBL	48-195	355	77.58	0.015	4.9×10^{-9}	11.3
ZBLAN	50-187	611	84.42	0.038	9.3×10^{-10}	11.2
ZBLANLi(15/5)	50-189	1740	90.86	0.019	3.32×10^{-10}	11.3
ZBLANLi(10/10)	68-190	2410	91.33	0.026	3.94×10^{-10}	11.2
ZBLANLi(5/15)	101-196	2230	92.33	0.009	2.65×10^{-10}	11.6
ZBLALi	74-195	1240	86.34	0.012	1.01×10^{-9}	11.3

where σ_0 is a pre-exponential constant, ΔH^* the activation enthalpy and R the ideal gas constant. Arrhenius plots of log σ vs. $10^3/T$ are shown in Fig. 6 for all eight glasses. Least squares Arrhenius equation parameters are listed in Table II, along with the conductivity values at 100°C. The values of Std. Dev. lnσ, the standard deviation of lnσ from the least squares fits, given in Table II indicate in all cases that the experimental conductivities scatter by no more than a few percent from the least squares Arrhenius equation lines.

DISCUSSION

Our conductivity results, both activation energies and magnitudes, are in quite good agreement with results reported previously [1-4] for similar ZrF_4-based compositions. In particular, Ravaine and coworkers [1,2] have reported values of $\sigma = 3.2 \times 10^{-6}$ ohm^{-1}cm^{-1} at 200°C and $\Delta H^* = 76$ kJ/mol for a $62ZrF_4$-$30BaF_2$-$8LaF_3$ glass, which are very close to the values ($\sigma = 2.8 \times 10^{-6}$ ohm^{-1}cm^{-1} at 200°C in both cases, $\Delta H^* = 72.5$ and 73.4 kJ/mol) for our glasses ZBL-in and ZBL which have nearly the same composition as Ravaine's glass. Ravaine et al. [1], on the other hand, report quite a spread ($\varepsilon_\infty = 6.8$ to 11.9) of values for the high frequency dielectric constants of ZrF_4-based glasses of very similar composition. These were measured with a Q-meter at 20 MHz at ambient temperature. Given the problems inherent in very high frequency permittivity measurements, we believe our ε_∞ values in Table II, which are much more self-consistent, are more accurate than Ravaine's ε_∞ values.

As expected in general from results on silicate glasses [8], the ZBL-in glass, which has a higher fictive temperature than the ZBL glass, also has a higher conductivity and lower activation enthalpy than ZBL. Similar results were found by Chandrashekar and Shafer [3], who saw roughly a factor of two difference in conductivity between a ZrF_4-based glass rapidly cooled from above T_g (high T_f) and the same glass slowly cooled from above T_g (low T_f). The difference in fictive temperatures between Chandrashekar and Shafer's glasses appears to be about 20K, much larger than the T_f difference between ZBL-in and ZBL, accounting for the much larger effect of thermal history on σ observed by them compared to that observed by us. There is, of course, not a 1:1 correspondence between T_f and σ for a glass [8]. The effect of thermal history on conductivities of heavy metal fluoride glasses needs further investigation. For the moment, however, we are probably safe in concluding that differences in conductivities within a series of glasses are more likely to be due to composition differences than to thermal history differences, as long as the T_g's of all the glasses are fairly close and as long as all

of the glasses have been given some sort of anneal in the glass transition region.

Given the above caveat, it is reasonable to attribute differences in the conductivity of the HBL glass and those of the ZBL-in or ZBL glasses to differences in compositions, since T_f for HBL is only roughly 10K higher than the T_f's of the latter glasses. The conductivity of the HBL glass is roughly a factor of 5 lower than that of the ZBL glasses at 50°C and a factor of 3 lower at 200°C (see Fig. 6). Moreover, since the HBL glass has the highest T_f, these factors would actually be slightly larger if the ZBL and HBL glasses all had the same T_f. The decrease in the ratio of ZBL to HBL conductivity with increasing temperature, of course, simply reflects the fact that the activation enthalpy of HBL is 4-5 kJ/mol higher than those for the ZBL glasses. Nonetheless, given the fact that electrical conductivity is a transport property and can be changed by orders of magnitude in some cases by relatively small changes in glass compositions, the proper conclusion here is that the conductivities of the ZrF_4-based and HfF_4-based glass analogs are remarkably similar. This similarity is, of course, anticipated because Zr and Hf both lie in the same group in the periodic table and have nearly identical ionic radii. ZrF_4-based and HfF_4-based analog glasses are expected to be almost isostructural and, provided proper allowance is made for the factor of two difference in masses of Zr and Hf, their physical properties should be nearly the same. Other similarities between the two types of glasses are in their glass transition temperatures [14-16], structural relaxation and viscous flow activation energies [16], heat capacities [15], molar volumes (calculated from densities [14]), fundamental IR and Raman spectra [17], multiphonon IR spectra [18] and dielectric constant (Table II).

The conductivities at 100°C (Table II) of the alkali fluoride-containing glasses ZBLAN and ZBLALi are about a factor of 20 lower than those of the non-alkali fluoride-containing ZBL glasses. The fictive temperature differences between the two types of glass (e.g., 32K between ZBL and ZBLAN) is sufficiently large, however, that it must be taken into account when comparing the conductivities. Let us carry out an estimate of the conductivity of the ZBL glass at 100°C if it had a fictive temperature not of 288°C but of 256°C, equal to that of the ZBLAN glass. Note from the data of Table II for ZBL-in and ZBL that a change in T_f affects both the pre-exponential constant σ_0 and the activation enthalpy, such that $d\ln\sigma_0/dT_f = -0.064\ \text{ohm}^{-1}\text{cm}^{-1}\text{K}^{-1}$ and $d\Delta H^*/dT_f = -0.25$ kJ/mol K. Using these figures we estimate that ZBL glass with a 256°C fictive temperature would have a pre-exponential constant $\sigma_0 = 2780\ \text{ohm}^{-1}\text{cm}^{-1}$,

an activation enthalpy $\Delta H^* = 81.4$ kJ/mol, and hence a conductivity at 100°C of 1.1×10^{-8} ohm^{-1}cm^{-1}. This is still a factor of 12 larger than σ at 100°C of the ZBLAN glass, so that we must tentatively conclude that the decrease in conductivity that occurs on adding alkali fluorides to ZrF_4-based glasses is due to a change in the inherent properties of the glass and not merely an artifact of the decrease in T_f (or T_g) that accompanies the alkali fluoride addition.

In the series of five alkali fluoride-containing glasses studied here NaF has been systematically replaced with LiF while keeping the total alkali fluoride content constant. In Fig. 7 conductivity isotherms are plotted versus cation fraction of Na for these glasses. Although there is some scatter in the data, the conductivity definitely passes through a minimum at intermediate compositions, such that at 75 or 100°C (Fig. 7 and Table II) the conductivity of the mixed alkali ZrF_4-based glasses is depressed by roughly a factor of 3 to 4 relative to that of the end member ZBLAN and ZBLALi glasses. Since the glasses in this series are all fairly close in T_g and were given a uniform thermal history, this minimum in the conductivity isotherms cannot be attributed to differences in fictive temperatures among the glasses.

The conductivity minima in Fig. 7 are analogous to those observed in mixed alkali network oxide glasses, except that in the latter cases the depths of the minima generally correspond to several orders of magnitude in σ [19-23]. The conductivity data for the ZrF_4-based MA glasses further mimic those for MA network oxide glasses [19,23] in that both the pre-exponential constants σ_0 and the activation enthalpies ΔH^* (Table II) pass through maxima at intermediate compositions.

It is now clear that the term "mixed alkali effect in glass" is something of a misnomer. The same sort of highly non-linear variations in conductivity with composition have also been observed in other mixed monovalent cation glasses such as Ag_2O/Tl_2O-B_2O_3 [24], in mixed monovalent cation crystals [25] and in mixed halide anionically conducting glasses [26]. Probably a better term for the phenomenon is "mixed mobile ion effect". Indeed, Almeida and Mackenzie [4] have suggested that a mixed mobile anion effect was responsible for a large drop in conductivity when BaF_2 in binary ZrF_4-BaF_2 glasses was partly replaced with $BaCl_2$. All the current data and recent thinking [22,23,25] on this subject suggest that mixed mobile ion effects are observed only when the bulk proportions of the mobile ionic species in the system are changed. Thus the occurrence of a mixed alkali effect in our alkali fluoride-containing ZrF_4- based glasses indicates that they are not

exclusively fluoride ion conductors. We might assume that these glasses are like the mixed alkali network oxide glasses in that alkali mobility is suppressed by several orders of magnitude at intermediate compositions. If so, the observed suppression of conductivity by a factor of 3 to 4 at intermediate compositions at 75 or 100°C would imply that the single alkali ZBLAN and ZBLALi glasses are mainly alkali ion conductors in which the Na^+ or Li^+ ions carry 2/3 to 3/4 of the electric current.

The mixed alkali ZrF_4-based glass data presented here and the conclusions drawn therefrom must be considered preliminary. Further investigations are needed to confirm substantial alkali ion mobility in these glasses. One obvious experiment is measurement of the Na^+ self-diffusion coefficient D_{Na} in the ZBLAN and the mixed ZBLANLi glasses. This could then be combined with the electrical conductivity via the Nernst-Einstein equation to yield an estimate of the Na^+ transport number t_{Na}:

$$t_{Na} = C_{Na}e^2D_{Na}/f_{Na}kT\sigma$$

where C_{Na} is the Na^+ concentration, k the Boltzmann constant, e the electronic charge and f_{Na} the Haven ratio (usually between 0.4 to 0.8 [23]). Another obvious experiment is to look for a mixed alkali effect in the internal friction or mechanical relaxation [20] of the ZBLANLi glasses.

If the ZBLAN and ZBLALi glasses are indeed alkali ion conductors, there would be a number of practical implications of this fact. Perhaps the most useful of these is the possibility that, although the mechanism of corrosion in water seems to be substantially different in ZrF_4-based glasses and alkali silicate glasses [27], mixed alkali ZrF_4-based glasses might exhibit the same improvement in chemical durability relative to single alkali systems that is observed in mixed alkali silicate glasses.

ACKNOWLEDGEMENT

This research was supported by Contract No. F19628-83-C-0016 from Rome Air Development Center, U.S. Air Force.

REFERENCES

1. D. Leroy, J. Lucas, M. Poulain and D. Ravaine, Mat. Res. Bull., 13, 1125 (1978).

2. D. Ravaine and D. Leroy, J. Non-Cryst. Solids, 38 & 39, 575 (1980).

3. G. V. Chandrashekar and M. W. Shafer, Mat. Res. Bull., 15, 221 (1980).

4. R. M. Almeida and J. D. Mackenzie, J. Mater. Sci., 17, 2533 (1982).

5. N. L. Perazzo, D. L. Gavin, A. J. Bruce, S. R. Loehr and C. T. Moynihan, Paper No. P6, Extended Abstracts, 2nd Int. Sym. on Halide Glasses, Troy, NY, 1983.

6. J. G. Berberian and R. H. Cole, Rev. Sci. Instrum., 40, 811 (1969).

7. R. Syed, Ph.D. thesis, Catholic University of America, 1983.

8. L. P. Boesch and C. T. Moynihan, J. Non-Cryst. Solids, 17, 144 (1975).

9. C. T. Moynihan, A. J. Bruce, D. L. Gavin, S. R. Loehr and S. M. Opalka, Polym. Eng. and Sci., 24, 1117 (1984).

10. E. N. Boulos, A. V. Lesikar and C. T. Moynihan, J. Non-Cryst. Solids, 45, 419 (1981).

11. D. Ravaine and J.-L. Souquet, J. Chim. Phys., 71, 793 (1971).

12. P. B. Macedo, C. T. Moynihan and R. Bose, Phys. Chem. Glasses, 13, 171 (1972).

13. R. Syed, D. L. Gavin, C. T. Moynihan and A. V. Lesikar, J. Am. Ceram. Soc., 64, C-118 (1981).

14. M. G. Drexhage, C. T. Moynihan and M. Saleh, Mat. Res. Bull., 15, 213 (1980).

15. D. L. Gavin, K.-H. Chung, A. J. Bruce, C. T. Moynihan, M. G. Drexhage and O. H. El Bayoumi, J. Am. Ceram. Soc., 65, C-182 (1982).

16. C. T. Moynihan, D. L. Gavin, K.-H. Chung, A. J. Bruce, M. G. Drexhage and O. H. El Bayoumi, Glastechn. Ber., 56K, 862 (1983).

17. B. Bendow, P. K. Banerjee, M. G. Drexhage, J. Goltman, S. S. Mitra and C. T. Moynihan, J. Am. Ceram. Soc., 65, C-8 (1982).

18. M. G. Drexhage, O. H. El Bayoumi, C. T. Moynihan, A. J. Bruce, K.-H. Chung, D. L. Gavin and T. J. Loretz, J. Am. Ceram. Soc., 65, C-168 (1982).

19. J. O. Isard, J. Non-Cryst. Solids, 1, 235 (1969).

20. D. E. Day, J. Non-Cryst. Solids, 21, 343 (1976).

21. C. T. Moynihan, N. S. Saad, D. C. Tran and A. V. Lesikar, J. Am. Ceram. Soc., 63, 458 (1980).

22. C. T. Moynihan and A. V. Lesikar, J. Am. Ceram. Soc., 64, 40 (1981).

23. H. Jain, N. L. Peterson and H. L. Downing, J. Non-Cryst. Solids, 55, 283 (1983).

24. S. Sakka, K. Matusita and K. Kamiya, Phys. Chem. Glasses, 20, 25 (1979).

25. J. A. Bruce and M. D. Ingram, Solid State Ionics, 9 & 10, 717 (1983).

26. A. A. Pronkin and K. K. Evstrop'ev, Soviet J. Glass Phys. Chem., 4, 209 (1978).

27. See paper by S. R. Loehr et al. in this volume and references cited therein.

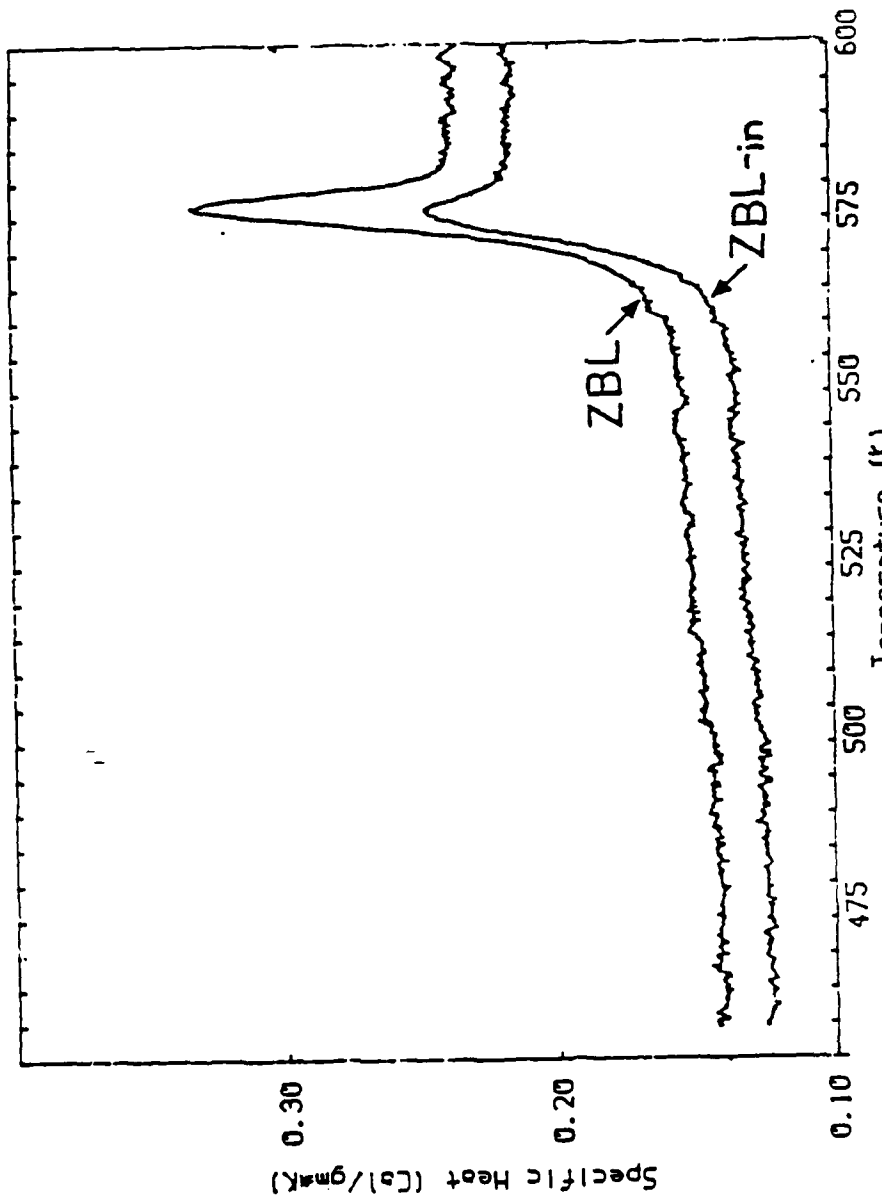

Figure 1. Specific heat measured by DSC at 10K/min heating rate for two ZBL glass specimens with different thermal histories. Cp scale is correct for ZBL; Cp plot for ZBL-in has been displaced downward by 0.02 cal/gK for clarity.

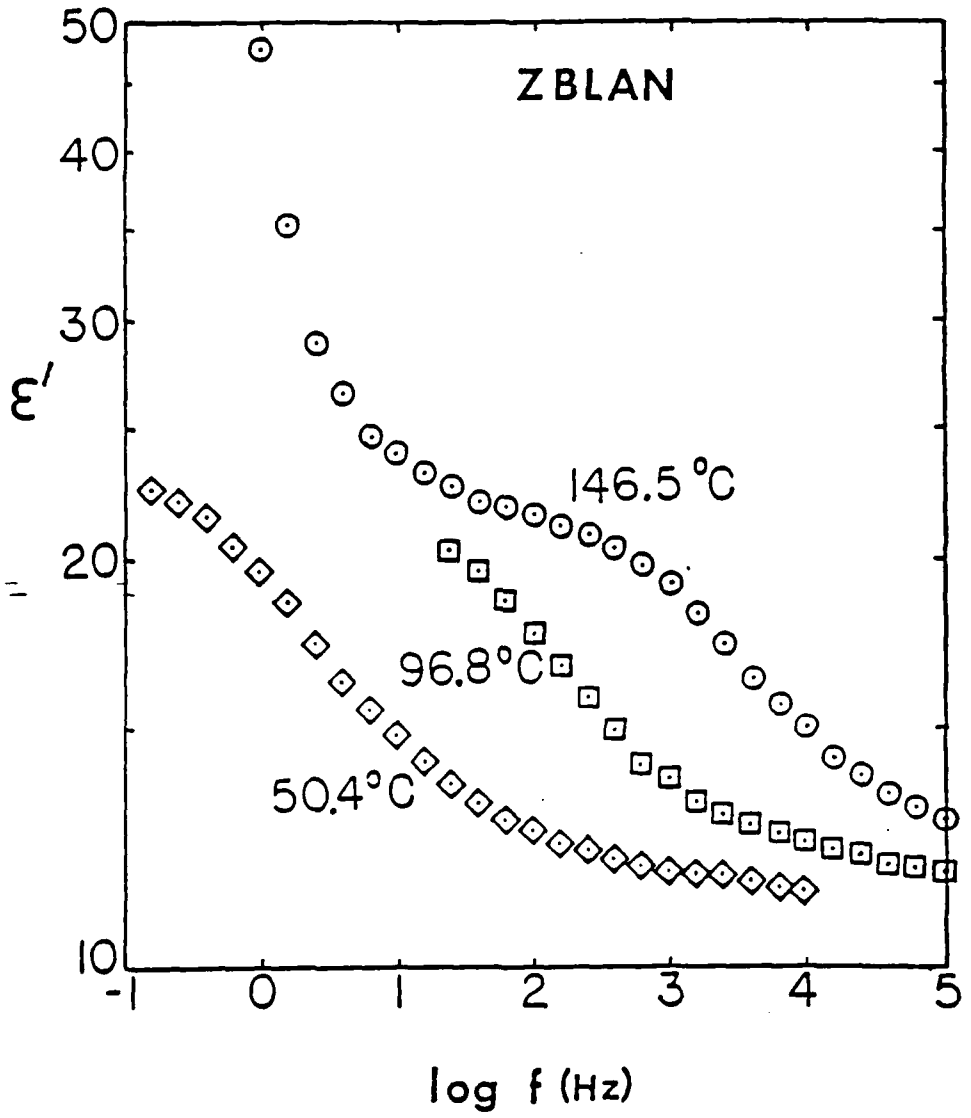

Figure 2. Frequency dependence of dielectric constant at three temperatures for ZBLAN glass.

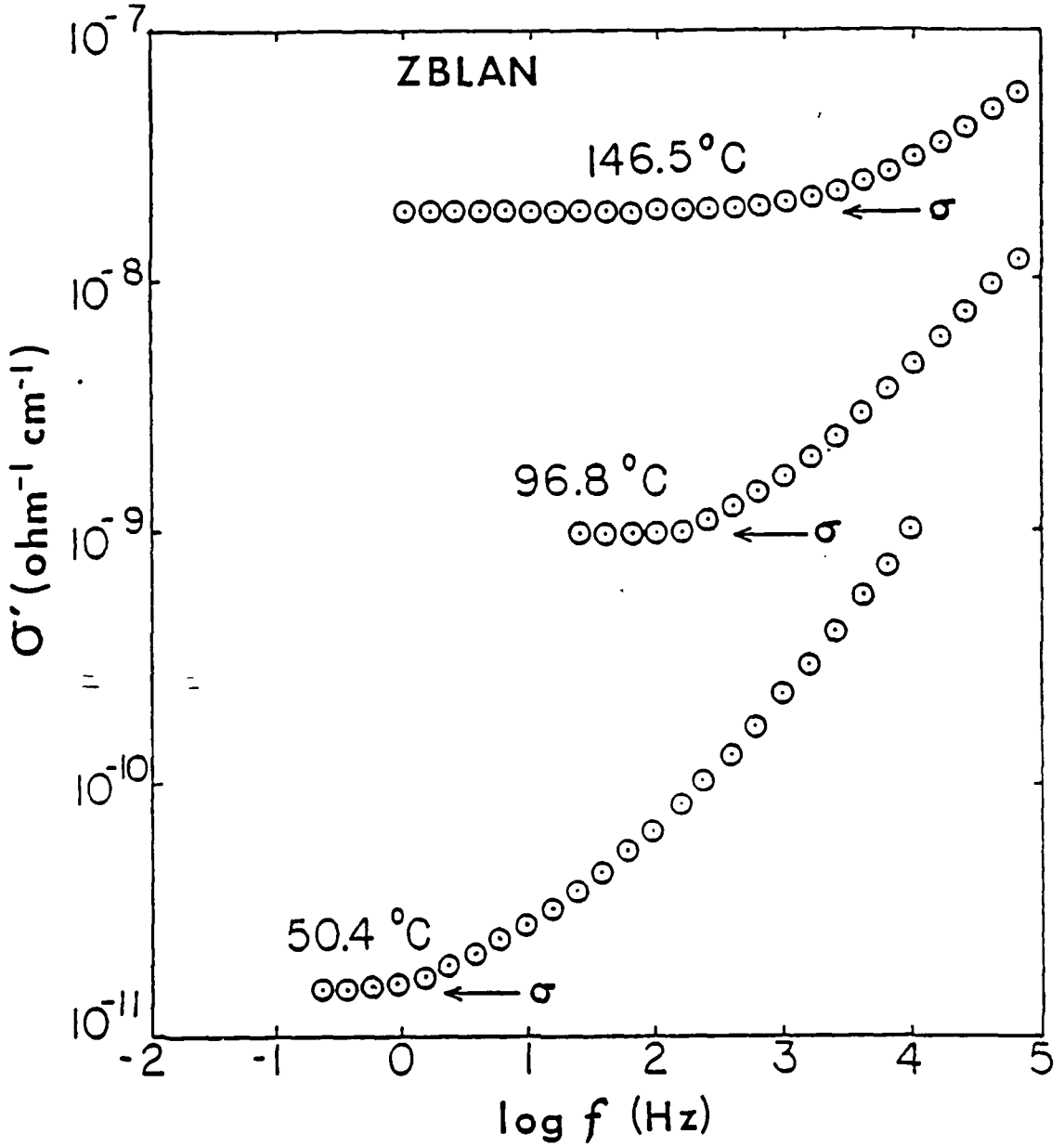

Figure 3. Frequency dependence of electrical conductivity at three temperatures for ZBLAN glass.

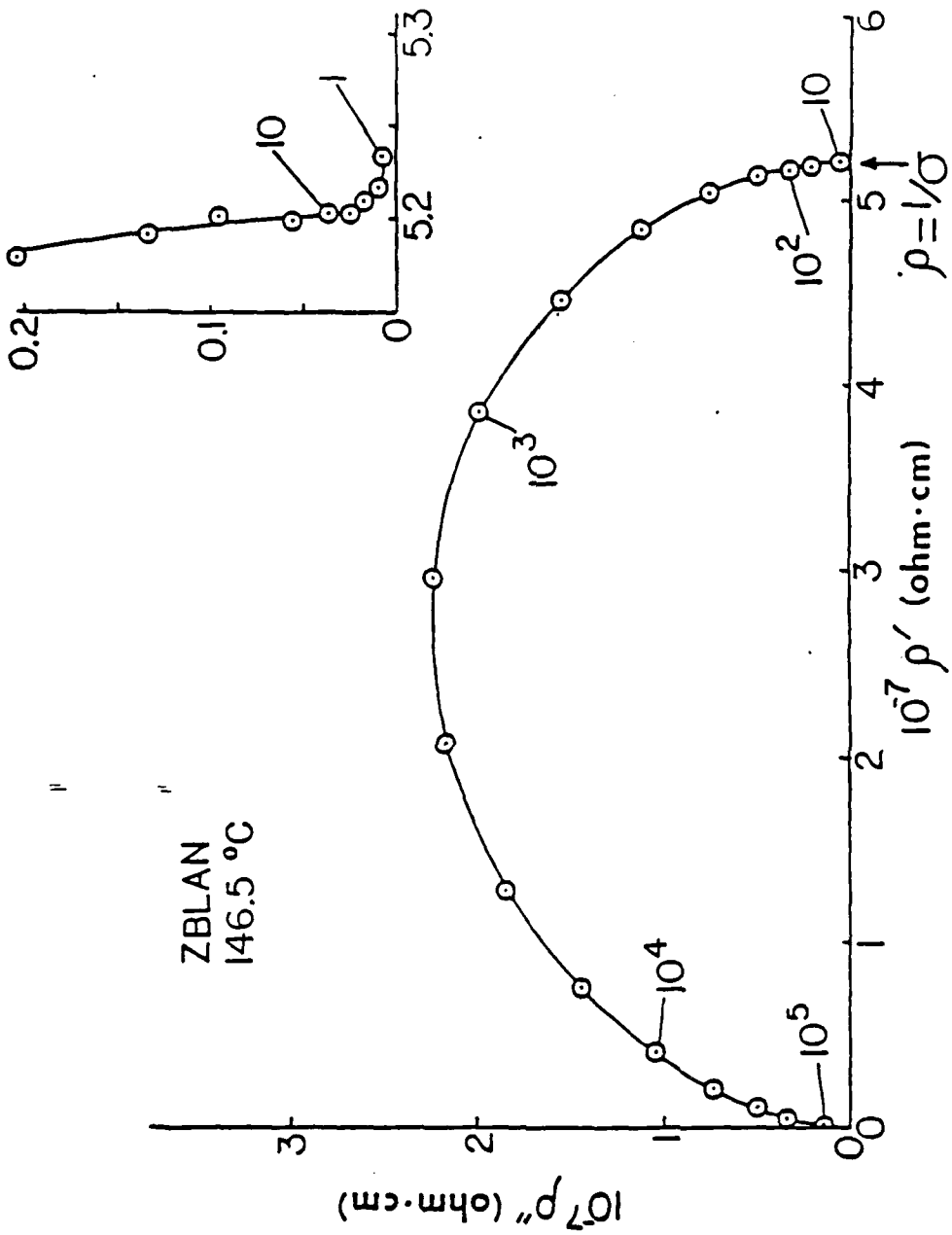

Figure 4. Complex plane plot of imaginary vs. real parts of complex resistivity of ZBLAN glass at 146.5°C. Numbers next to data points are measurement frequencies in Hz. Inset is enlargement of low frequency part of plot.

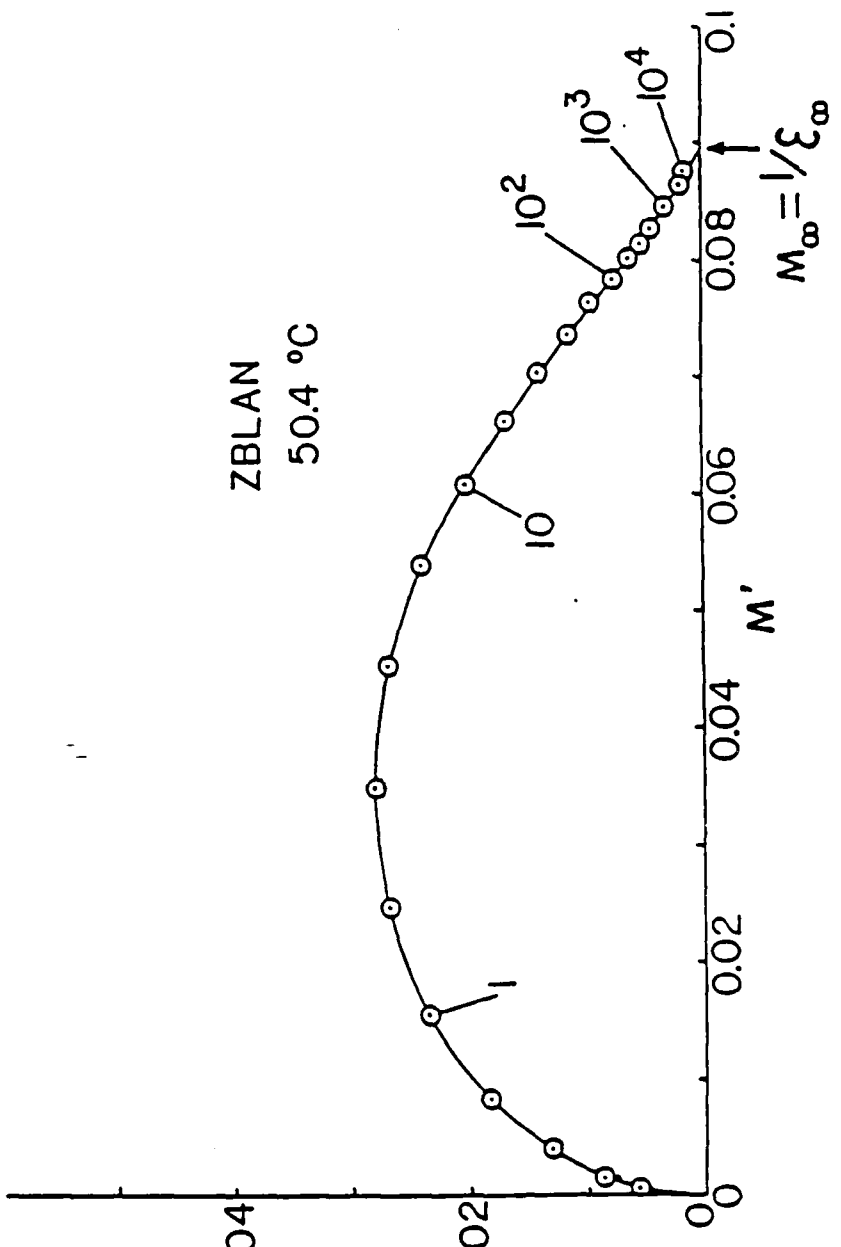

Figure 5. Complex plane plot of imaginary vs. real parts of electric modulus of ZBLAN glass at 50.4°C. Numbers next to data points are measurement frequencies in Hz.

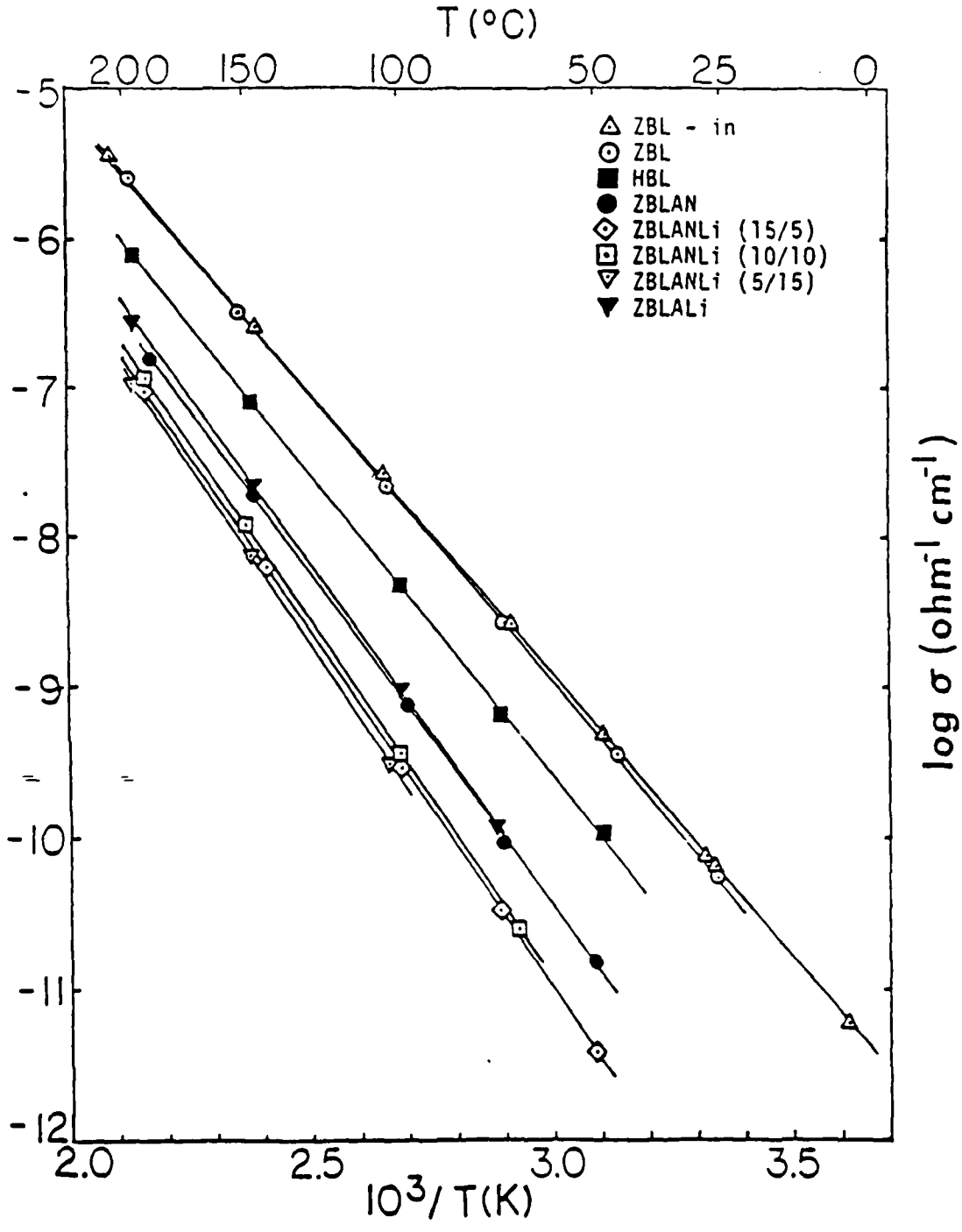

Figure 6. Arrhenius plots of fluorozirconate or fluorohafnate glass electrical conductivities.

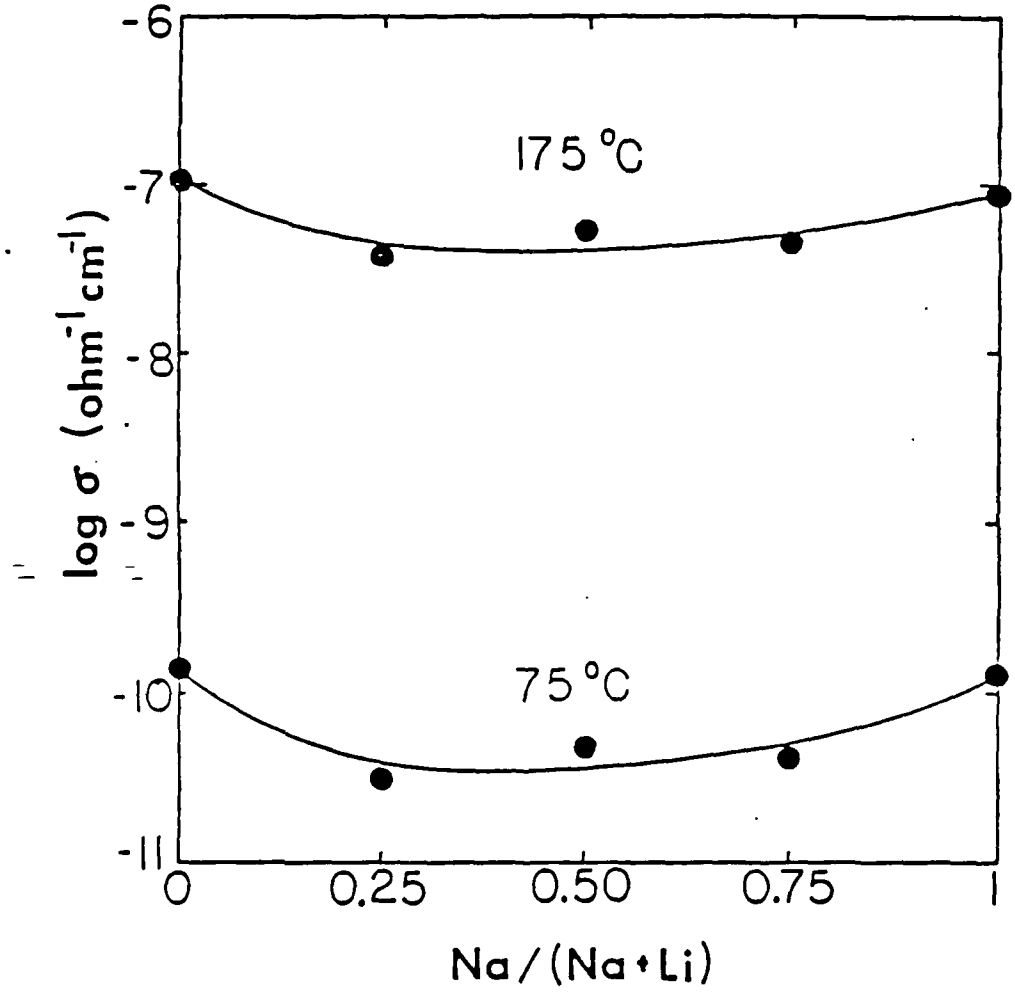

Figure 7. Electrical conductivity versus sodium cation fraction for mixed alkali $56ZrF_4$-$14BaF_2$-$6LaF_3$-$4AlF_3$-20(NaF+LiF) glasses.

PUBLICATIONS

Research supported partly (marked with an asterisk) or wholly by Contract No. F19628-83-C-0016.

1.* "Kinetics of Crystallization of ZrF_4-BaF_2-LaF_3 Glass by Differential Scanning Calorimetry". N.P. Bansal, R.H. Doremus, A.J. Bruce and C.T.Moynihan, J. Am. Ceram. Soc., 66 [4], 233-238 (1983).

2. "Viscous Flow Activation Energy and Devitrification of Heavy Metal Fluoride Glasses". C.T. Moynihan, D.L. Gavin, K.-H. Chung, A.J. Bruce, M.G. Drexhage and O.H. El-Bayoumi, Glastechn. Ber., 56K, 862-867 (1983).

3. "Physical Aging of Heavy Metal Fluoride Glasses. I. Sub-Tg Enthalpy Relaxation in a ZrF_4-BaF_2-LaF_3-AlF_3 Glass". C.T. Moynihan, A.J. Bruce, D.L. Gavin, S.R. Loehr, S.M. Opalka and M.G. Drexhage, Polymer Engineering and Science, 24 [14], 1117-1122 (1984).

4. "Crystallization of Heavy Metal Fluoride Glasses", N.P. Bansal, A.J. Bruce, R.H. Doremus, C.T. Moynihan, Proceedings SPIE, 484, 51-60 (1984).

5.* "Crystallization of Fluorozirconate Glasses". N.P. Bansal, R.H. Doremus, A.J. Bruce and C.T. Moynihan, Mat. Res. Bull., 19, 577-590 (1984).

6. "Heavy Metal Fluoride Glasses with Low Intrinsic Rayleigh Scattering". J. Schroeder, V. Tsoukala, C.O. Staller, M.A. Stiller, A.J. Bruce, C.T. Moynihan, J.J. Hutta, M.J. Suscavage and M.G. Drexhage, Electron. Lett., 20 [21], 860-862 (1984).

7. "Rayleigh and Brillouin Scattering in Heavy Metal Fluoride Glasses". J. Schroeder, M. Fox-Bilmont, B.G. Pazol, V. Tsoukala, M.G. Drexhage and O.H. El-Bayoumi, Opt. Engin., 24 [4], 697-703 (1985).

8.* "Intrinsic Instabilities of Heavy Metal Fluoride Glasses". A.J. Bruce, C.T. Moynihan, S.R. Loehr, S.M. Opalka, R. Mossadegh, N. Perazzo, N.P. Bansal, R.H. Doremus and M.G. Drexhage, Opt. Engin., 24 [3], 522-526 (1985).

9.* "Surface - OH Profile from Reaction of a Heavy Metal Fluoride Glass with Atmospheric Water". D. Tregoat, G. Fonteneau, C.T. Moynihan and J. Lucas, J. Am. Ceram. Soc., 68 [7], C171-C173 (1985).

10.* "Dry Box Melting of Heavy Metal Fluoride Glasses". M.J. Suscavage, J.J. Hutta, M.G. Drexhage, N. Perazzo, R. Mossadegh and C.T. Moynihan, Materials Science Forum, 5, 35-41 (1985).

11.* "Effect of Composition on the Crystallization Behavior of Heavy Metal Fluoride Glasses". N.P. Bansal, R.H. Doremus, C.T. Moynihan and A.J. Bruce, Materials Science Forum, 5, 211-218 (1985).

12. "IR Spectroscopy Studies of Attack of Liquid Water on ZrF_4-Based Glasses". S.R. Loehr, A.J. Bruce, R. Mossadegh, R.H. Doremus and C.T. Moynihan, Materials Science Forum, 5, 311-322 (1985).

13.* "Carbon Dioxide Absorption in Heavy Metal Fluoride Glasses". M.G. Drexhage, J.J. Hutta, M.J. Suscavage, R. Mossadegh and C.T. Moynihan, Materials Science Forum, 6, 509-524 (1985).

14.* "Vicosity Temperature Dependence and Crystallization of ZrF_4-Based Melts". C.T. Moynihan, R. Mossadegh, P.K. Gupta and M.G. Drexhage, Materials Science Forum, 6, 655-664 (1985).

15. "Mixed Alkali Effect and Effect of Substitution of HfF_4 for ZrF_4 on Heavy Metal Fluoride Glass Electrical Conductivities". N.L. Perazzo, R. Mossadegh and C.T. Moynihan, Materials Science Forum, 6, 775-791 (1985).

16.* "Composition and Structural Relaxation Effects on the Intrinsic Rayleigh Scattering of Halide Glasses: Annealing Studies". J. Schroeder, V. Tsoukala, A.J. Bruce, C.O. Staller, J.J. Hutta, M.J. Suscavage and M.G. Drexhage, Materials Science Forum, 6, 561-570 (1985).

17.* "Pockels' Elastooptic Coefficients and Brillouin Linewidths in Halide Glasses". J. Schroeder, G.A. Floudas, M.A. Stiller and M.G. Drexhage, Materials Science Forum, 6, 577-590 (1985).

18.* "Low Temperature Behavior of Potassium and Sodium Silicate Glasses". W.M. MacDonald, A.C. Anderson and J. Schroeder, Phys. Rev., B31 [2], 1090-1101 (1985).

19.* "Low Temperature Behavior of Potassium Borate Glasses". W.M. MacDonald, A.C. Anderson and J. Schroeder, Phys. Rev. B32 [2], 1208-1211 (1985).

20.* "Crystallization and Viscosity of Heavy Metal Fluoride Glasses". C.T. Moynihan, R. Mossadegh, S.N. Crichton, P.K. Gupta and M.G. Drexhage, Proceedings SPIE, 618, 178-183 (1986).

21.* "DSC Studies of Melting Behavior of Heavy Metal Fluoride Glasses". R. Mossadegh, C.T. Moynihan and A.J. Bruce, Mat. Res. Bull., 22, 593-600 (1987).

22.* "Structural Relaxation in Fluoride Glasses". C.T. Moynihan, S.M. Opalka, R. Mossadegh, S.N. Crichton and A.J. Bruce, in "Halide Glasses for Infrared Fiberoptics", R.M. Almeida, Ed., Martinus Nijhoff Publishers, Boston, 1987, pp. 163-178. (Also published in "Lecture Notes in Physics", Vol. 27, Th. Dorfmuller and G. Williams, Eds., Springer-Verlag, New York, 1987, pp. 16-26).

MISSION
of
Rome Air Development Center

RADC plans and executes research, development, test and selected acquisition programs in support of Command, Control, Communications and Intelligence (C^3I) activities. Technical and engineering support within areas of competence is provided to ESD Program Offices (POs) and other ESD elements to perform effective acquisition of C^3I systems. The areas of technical competence include communications, command and control, battle management, information processing, surveillance sensors, intelligence data collection and handling, solid state sciences, electromagnetics, and propagation, and electronic, maintainability, and compatibility.

END
DATE
FILMED
7-88
DTIC